Fall 10-18-2025

Enhanced Particle Interactions in Highly Curved Spacetime

Bradley Shapiro
Dartmouth College, bradley.e.shapiro.gr@dartmouth.edu

ENHANCED PARTICLE INTERACTIONS IN HIGHLY CURVED SPACETIME

A Thesis
Submitted to the Faculty
in partial fulfillment of the requirements for the
degree of

Doctor of Philosophy

in

Physics and Astronomy

by Bradley Shapiro

Guarini School of Graduate and Advanced Studies
Dartmouth College
Hanover, New Hampshire

September 2025

Examining Committee:

(chair) Devin Walker

Robert Caldwell

Marcelo Gleiser

Stephon Alexander

F. Jon Kull, Ph.D.
Dean of the Guarini School of Graduate and Advanced Studies

Abstract

Compact objects, such as black holes and neutron stars, are known to be surrounded by dense clouds of particles, including but not limited to photons, various plasmas, and potentially dark matter and gravitons. These environments are of immense research interest, not only for the purpose of understanding the compact objects they surround, but also in the search to identify new particles, especially dark matter. However, certain particle physics calculations are well developed in flat spacetime but intractable in curved spacetime. In this thesis, I present a formalism by which some of these calculations may be made tractable within a perturbative series. The formalism works by constructing small patches of locally flat spacetime, through which a particle travels; as a particle goes from one patch to another, the effective Lagrangian receives corrections for each patch. In this way we are able to construct comparators, analogous to a Wilson line, that "transport" the physics from one patch to another. These corrections can result in the enhancement of higher-dimensional, Planck-suppressed operators, enabling us to probe new physics.

This thesis also explores another topic in the area of particle behavior around a compact object, namely that of axion lasers produced by superradiance. Superradiance, a phenomenon through which energy and angular momentum may be extracted from a rotating black hole, can generate dense clouds of axions, which can then decay into photons; the number of photons produced by this decay can potentially stimulate further decay, creating a laser. This laser is powerful enough that the Schwinger

effect may become significant, producing an electron-positron plasma, which has the effect of slowing axion decay by imparting photons with an effective mass. In a simplified model consisting of a rotating primordial black hole devoid of any preexisting plasma, we find, depending on the system's parameters, that the equilibrium state of this laser may be mildly enhanced, or it may become unable to reach equilibrium, with the axion cloud continuing to grow superradiantly.

Preface

It would be an exaggeration to say that my PhD has been my entire life for the past five years, but it certainly feels that way, and not without reason. While I've had plenty of things beside my PhD occupying both my time and my thoughts, some of which have been deeply important to me, my PhD has been the center about which my life revolved. Everything always came back to it, with all its frustrations and joys (and there have certainly been plenty of both).

Because of the centrality of my PhD to my entire life, I could in all honesty thank every single person with whom I've had any sort of positive interaction in these past years, no matter how minor or how disconnected from my research and my classes. Every act of kindness, patience, friendship, support, interest, and human connection that I've enjoyed has, by making my life brighter, made my PhD that much more bearable. I say in full sincerity that there are more people than I can count whom I wish I could thank. However, since I cannot thank them all in this preface, I will reluctantly list only a small selection of people, without whom I could never have completed my PhD.

First and foremost, I need to thank my advisor, Devin Walker. From the moment I interviewed with him, I have never doubted his desire to support me, to advocate for me, to give me every possible opportunity, and to help me achieve all of my goals. He has been exceptionally patient with me when I struggled to understand the concepts central to our research, and ceaselessly empathetic towards the various

struggles I have faced throughout my PhD. I am grateful for the many, many ways he has helped me forward on this path.

I also need to extend my gratitude to the people I have worked with in Devin's research group. Nizar, Morgane, Charlie, Paola, Shadi, Ora, Kamal, Michael, and Dina have been constant sources of camaraderie and solidarity. Without them, this would have felt like one of the most isolating periods of my life; instead, I have had the deep pleasure of working with and befriending them.

I cannot put in strong enough words how lucky I am to have such a wonderful family supporting me, every step of the way. My mom's boundless empathy has helped me through the most emotionally difficult periods of my PhD. My dad has provided me with invaluable advice that has kept me grounded when I most needed it. Rob and Amanda have always been available for me to turn to them and rely on them. Reid, Henry, and Peter have given me much-needed moments of levity.

Last but by no means least, I want to thank two people who were not involved in my PhD directly, but who set me on this path. Carl Pennypacker gave me my first research opportunity, making sure I had a positive experience so that I could recognize that this is something I wanted to do for the rest of my life. He has always believed in me and has been an excellent mentor ever since. Stephon Alexander gave me an opportunity to continue in my career when I was at a very low point in my life; while he may not realize it, he played a big part in the process of getting me out of that low point.

My deepest thanks go to everyone mentioned here, and everyone that I could not include.

Contents

List of Figures

Chapter 1

Introduction

The vast majority of topics in astrophysics and cosmology, to greater or lesser extents, involve particles interacting in curved spacetime. For example, it has long been expected that regions of high dark matter density, known as dark matter spikes, will be found around supermassive black holes [1–6], and recent observational evidence seems to support this prediction [7, 8]. Similar predictions have been made for intermediate-mass black holes [9–12], primordial black holes [13–17], neutron stars [18–22], and white dwarfs [18, 23–26]. For a general review of the experimental prospects of dark matter around compact objects, see [27]. Besides dark matter, plasmas show unique behavior in curved spacetime [28, 29]. In cosmology, the expansion of spacetime directly produces particles [30–32].

Two specific examples of this, which are depicted in Fig 1.1 and which we will explore in detail in this thesis, are Primakoff-type bosonic mixing and axion lasers. Primakoff conversion [33–39] is to a phenomenon whereby an ingoing boson interacts with an insertion from a strong background field, producing an outgoing boson of a different species. The classic examples, from [36], are that of photon-axion and photon-gravitational wave mixing, both of which occur in a background magnetic field. Primakoff conversion underpins many efforts to identify for the axion, both

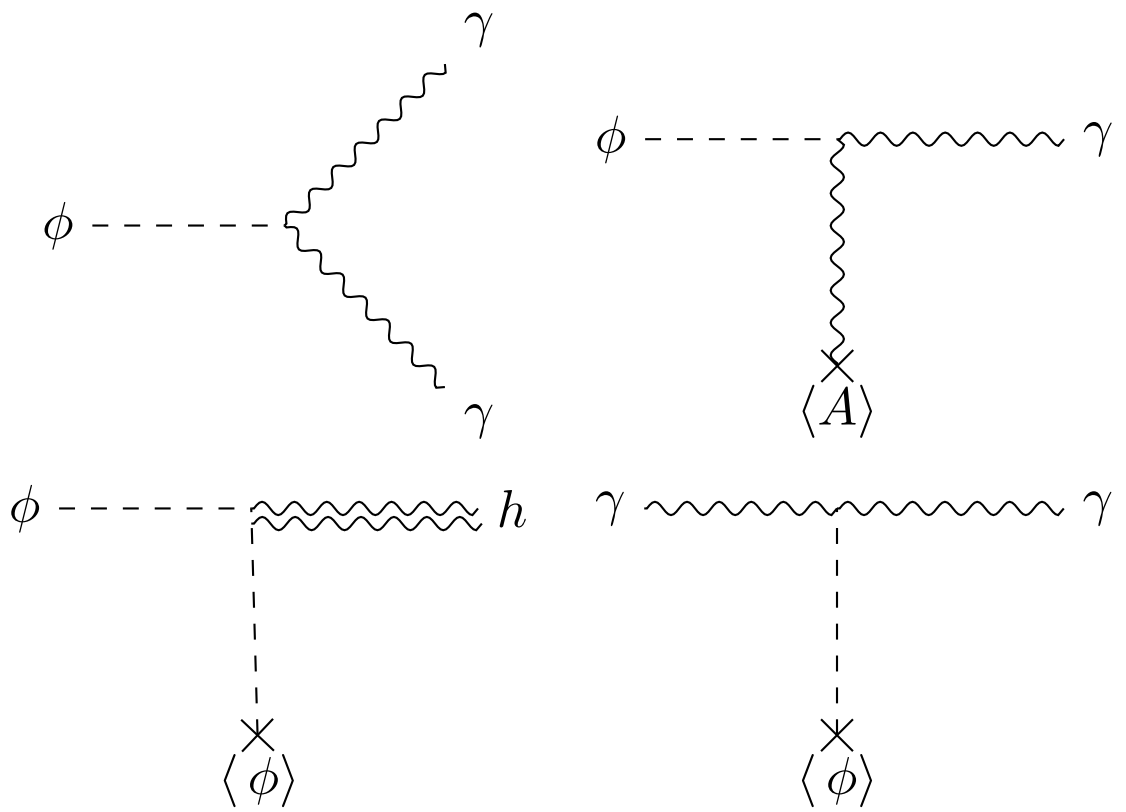

Figure 1.1: Feynman diagrams of the four most relevant interactions examined in this thesis. The top-left diagram shows the decay of an axion into two photons. It is this decay that, when stimulated, produces an axion laser, as will be discussed in more detail in chapter 2. The top-right and bottom-left diagrams depict Primakoff conversion: in the top-right, an axion transitions into a photon via a background electromagnetic field, and, in the bottom-left, an axion transitions into a graviton via a background axion field. The bottom-right diagram depicts the conversion of a photon of one polarization mode into a photon of another polarization mode, via a background axion field, which is analogous to Primakoff conversion. In all diagrams, time may go from left to right or right to left. As we will discuss in this thesis, all of these interactions are relevant in astrophysical circumstances as a means of potentially detecting axion dark matter, however it is important that the effects of curved spacetime be accounted for.

laboratory-based [40–43] and, more relevantly to us, astrophysical [44–57]. In these astrophysical searches, the basic concept is that, in a dense cloud of dark matter around a compact object, axions will mix with photons, resulting in either an excess or deficit of light emitted from the object.

Axion lasing [58–65] refers to the stimulated decay of axions into photons. Axions can spontaneously decay into photons, at an extremely low rate (in most axion models, the axion lifetime exceeds the present age of the universe). Nevertheless, in a cloud of axions of sufficient density, decay will still be expected to happen, simply as a consequence of the law of truly large numbers (although the amount of time for this decay will be inversely related with the axion-electromagnetic coupling constant). Crucially, the presence of these photons then enhances the rate of further axion decay, via Bose enhancement. Thus, shortly after reaching a certain critical number density, the axion cloud will begin decaying into photons at an enhanced rate, producing a light source of high luminosity. This is another means by which axion might be observed.

Returning from the specific to the general: Primakoff conversion and axion lasing represent two (though by no means the *only* two) situations in which there is research interest in particle interactions taking place around compact objects. However, analyzing the behavior of particles in curved spacetime presents unique challenges. While there exists a substantial body of work on the topic of quantum field theory (QFT) in curved spacetime, e.g. [66, 67], which allows one to calculate the behavior of particles in a non-dynamic curved spacetime, the fact that there exists no complete, consistent theory of quantum gravity means that it is impossible to use present QFT tools to calculate the backreaction of particles on spacetime. Instead, to calculate this backreaction, one may adopt a semiclassical approach, treating every field as quantum except for the metric, which is treated as a classical field; see [68] for a detailed treat-

ment. Importantly, both general relativity and semiclassical gravity may be viewed as effective field theories (EFTs) [69–72]. In other words, every tool that we currently have for describing the behavior of spacetime is an EFT, and, as we will see, EFTs offer us immense calculational power. See [73, 74] for a review of EFT methods.

Primakoff mixing provides an illustrative example of the calculational power of EFTs. Analogous to neutrino oscillations (for a review, see [75–77]), in Primakoff mixing the presence of a background field results in mass eigenstates that are linear combinations of the original polarization eigenstates, and it is these mass eigenstates that propagate independently of each other. However, unlike in neutrino oscillation, in Primakoff conversion the masses of these eigenstates depend on the background fields, which in turn depend on one's frame of reference. Thus, mixing is a frame-dependent phenomenon, which presents a problem for any attempt to describe mixing using QFT, as QFT in curved spacetime is fully covariant. EFT, in contrast, allows for mixing to be made tractable.

Nevertheless, this EFT approach has its own limitation, which is that all EFTs apply within a restricted range of energy and, analogously, a restricted region of spacetime. However, gravitational effects can be nonlocal, as the massless propagators allow for interactions across large lengthscales [78]. This is especially problematic in light of the infrared divergence of the metric. To see this infrared divergence, consider that, as a consequence of the equivalence principle, one may take any point in spacetime and construct coordinates such that the metric is locally flat about this point. The typical choice for this is Riemann normal coordinates, in which the metric is given by [79]

$$g_{\mu\nu}(x) = \eta_{\mu\nu} - \frac{1}{3}R_{\mu\rho\nu\sigma}(x_0)(x^\rho - x_0^\rho)(x^\sigma - x_0^\sigma) + \ldots, \tag{1.1}$$

where x_0 is the point about which the locally flat coordinates are defined. Higher-

order terms contain higher-order derivatives of the Riemann tensor. The magnitude of components of the n^{th}-order derivative of the Riemann tensor is given approximately by $\mathcal{R}_0^{-2-n}$, where $\mathcal{R}_0$ is the radius of curvature at x_0. Therefore, for sufficiently large displacement $x - x_0$, the expansion in (1.1) becomes divergent. Returning now to the nonlocal nature of gravity, we can see the problem: even if the local curvature at some point in spacetime is small, we should still see contributions from farther-away points, where components of the metric may be larger. Thus, an EFT of gravity must incorporate nonlocal corrections.

[78] proposed a means by which these nonlocal corrections could be incorporated into a local EFT. Independently of this proposal, with no knowledge of it until we had already completed our research, we pursued the exact approach described therein. It was only afterward that we learned our method had been anticipated. In light of its prescience, the statement from [78] is quoted in full:

> *Perhaps the issue could be addressed by combining patches using different coordinates and matching on the boundary. In each patch we can use the equivalence principle to make the coordinates nearly flat. Then matching at the boundaries would convey the information from one patch to another. However, this program has not yet been carried out.*

Later in this thesis, we will carry out this program.

Section 1.1

Structure of the thesis

This thesis is structured as follows. In chapter 2, we examine an issue specific to axion lasers, specifically taking place around a superradiant black hole. Superradiance refers to a process by which particles around a rotating black hole may extract energy and

angular momentum from the black hole [80–82], and it is expected that superradiance may result in the formation of a dense axion cloud. This axion cloud may then trigger lasing [61–65]. The resulting electromagnetic field is powerful enough to induce the Schwinger effect, by which electron and positron pairs are created. In chapter 2, we explore the effects of the resulting electron-positron plasma on the behavior of the axion laser.

In chapter 3, we present a mathematical background on Riemann normal coordinates, distinguishing between two forms, which we refer to as linear and nonlinear Riemann normal coordinates. The difference between these is the number of terms included in the definition of the coordinate system, and it should be emphasized that this terminology is novel. It is common to only consider the linear term in the coordinate system's definition (what we call linear Riemann normal coordinates), and the author is unaware of any detailed treatment on the impact of including higher-order terms in this definition. However, these higher-order terms will be of crucial importance in chapter 4, and thus it is important to understand the similarities and differences between them. In chapter 3, we derive important properties of linear Riemann normal coordinates, show that nonlinear Riemann normal coordinates do not satisfy these properties, and discuss the way in which quantities (such as the metric) may be calculated in nonlinear Riemann normal coordinates.

In chapter 4, we present a method for adding long-distance curvature corrections to standard gravitational wave effective field theory. As anticipated independently by [78], the method works by considering the motion of a particle along a geodesic and dividing spacetime into several locally flat patches, each of which is centered about a different point along the geodesic. The coordinates in each patch contain curvature corrections, and, by adding together the coordinates of the patches, one accumulates curvature corrections in the displacement four-vector between the first

and last patch along the geodesic. From these curvature corrections one is able to construct a comparator, with properties similar to a Wilson line, relating the fields in the first patch to those in the final patch. Through the use of this comparator, one may write a local EFT in the final patch that includes nonlocal corrections from the entire length of the geodesic.

In chapter 5, we analyze Primakoff-type bosonic mixing in curved spacetime, within a single patch of locally flat spacetime. We do not apply the technique established in chapter 4, instead considering a simplified model that includes no higher-dimensional operators (including those that would be introduced by nonlocal effects). We demonstrate how going from flat spacetime to curved spacetime introduces new mixing modes and changes the frequency of mixing. The techniques in this chapter can be elaborated upon to include nonlocal corrections, per chapter 4, and this is done in [83].

In chapter 6, we offer some brief concluding remarks and discuss potential future research directions.

Chapter 2 is reproduced from a paper written by the author, [84], which has been accepted for publication at Physical Review D at doi:10.1103/64sc-sg9n. Chapter 3 is also the author's original work, although two of the proofs presented in it are elaborations of proofs originally given in [79]; this chapter is planned to be adapted into a paper to be submitted for publication. Chapter 4 is drawn largely from a paper that the author and several coauthors have submitted for publication [85]. While the author participated in the production of this paper, little of its content is the author's original work. Sections 4.3.3 and 4.4 are the author's original work, although they do not appear in the final paper. The reasons for this are that section 4.3.3 neglects an important effect (discussed at the end of section 4.3.3), and section 4.4 was not completed until after the [85] was published. The author's only contributions that

remained in the final paper were the specific forms of eqs. 4.11 and 4.13 (which were originally written using a scalar rather than a tensor comparator) and the definitions of $\overline{\alpha}^{\rho\sigma}_{\alpha\beta}$ and $\overline{\beta}^{\alpha\beta}_{\rho\sigma}$ used therein. Chapter 5 is entirely the author's original work, except for the review of previous research in section 5.2.

Chapter 2

The Role of Schwinger Production in Superradiant Axion Lasers

Section 2.1

Introduction

The axion has emerged as a leading candidate for dark matter [86–92]. A topic of significant research interest is the idea that axions might be detected around rotating black holes [93–97], via superradiance, which allows for the extraction of energy and angular momentum from a rotating black hole [80–82]. Superradiance is often understood through the concept of a gravitational atom [98, 99], as, in Kerr spacetime, the Klein-Gordon equation permits quasi-bound state solutions, characterized by integer quantum numbers (n, ℓ, m), much like those around a hydrogen atom. For a massive scalar field, these quasi-bound states have energy [82]

$$E_{n,\ell} = \mathrm{Re}(\omega_{n,\ell}) = m_\phi \left(1 - \frac{\alpha^2}{2(n+\ell+1)^2}\right), \tag{2.1}$$

where m_ϕ is the scalar mass and the coupling parameter is

$$\alpha = \frac{G m_\phi M_{BH}}{\hbar c} = .037 \left(\frac{m_\phi}{10^{-5}\text{ eV}}\right)\left(\frac{M_{BH}}{10^{24}\text{ kg}}\right). \tag{2.2}$$

Importantly, unlike in hydrogen atoms, where the frequency is entirely real, the quasi-bound states around rotating black holes may have a complex frequency, $\text{Im}(\omega_{n,\ell}) \neq 0$. Depending on the sign of this imaginary frequency, the state will experience either exponential growth or exponential decay proportional to $e^{\text{Im}(\omega_{n,\ell})t}$. States with exponential growth are referred to as superradiant.

Conceptually, there are a number of ways to understand superradiance. [100] showed that, when a wave is incident on a rotating body, the second law of thermodynamics requires, under certain conditions, that the wave be reflected back with greater energy and angular momentum than it initially had. From a particle perspective, superradiance may be understood as a consequence of the Penrose process [101, 102], whereby an object passing through the ergosphere of a rotating black hole may extract energy and angular momentum from the black hole. In either picture, this energy extraction can only occur through the creation of new particles, because the quasi-bound nature of the aforementioned states means that individual particles cannot become more energetic. Consequently, superradiance increases the population of particles around the black hole. The aforementioned descriptions are classical in nature, i.e. the scalar field is not quantized, which is how superradiance is usually treated. However, there do exist some treatments of superradiance as a quantum phenomenon [103, 104]. These offer some additional insight into the exact mechanism in which superradiant particles are created around a black hole.

In models that include an axion, rotating black holes are therefore expected to produce a dense axion cloud via superradiance. It has been proposed [61–65] that, in certain regions of parameter space, these axions can undergo stimulated decay into

photons, creating a powerful laser, referred to in [61] as a BLAST (*Black hole Lasers powered by Axion SuperradianT instabilities*). It has been observed [61, 63] that these BLASTs are powerful enough that the Schwinger effect may become significant. The Schwinger effect refers to a quantum mechanical, nonperturbative process whereby a strong electromagnetic field produces electron-positron pairs. Plasma effects are significant in the dynamic of BLASTs [62, 63, 65], primarily because the plasma imparts photons with an effective mass, which eventually makes axion decay energetically impossible, thereby shutting off the laser. [61] speculated that plasma effects would result in the axion laser shutting off and then restarting in a periodic fashion, although they did not explore the underlying dynamics in detail. [63, 64] performed numerical simulations that seemed to validate the prediction of periodic bursts, whereas the simulations in [65] found that laser-like emission occurs not in bursts, but smoothly; however, all of these simulations assumed an electron-ion plasma acquired via accretion, as opposed to an electron-positron plasma acquired via the Schwinger effect. This paper therefore aims to explore the role of Schwinger production, specifically, in axion lasers.

This paper is structured as follows. In section 2.2, we review how BLASTs behave in the absence of the Schwinger effect. In section 2.3, we explore how an electron-positron plasma evolves in the superradiant axion cloud around a rotating black hole, and how that plasma affects the behavior of the photons and axions in that cloud. In section 2.4, we analyze the resulting Boltzmann equations. Section 2.5 is the conclusion.

Section 2.2

BLASTs without Schwinger Production

We begin by briefly summarizing the work of [61].* Importantly, this approach assumes a homogenous axion cloud in which decay happens uniformly; however, detailed simulations show that the substructure of the axion cloud does indeed play a role in the nature of the emitted lasers [65]. For example, lasers will include a beating pattern that is not predicted under the approach described herein, which results from photons produced inside the axion cloud traveling outward and interacting with the outer parts of the cloud. The simulations needed to predict such phenomena are beyond the scope of this paper, and we restrict ourselves to a simpler, analytic approach, which should be understood as a simplified model of a complicated system.

For scalar fields, the fastest-growing state is the $2p$-state ($n = 2$, $\ell = m = 1$). The $2p$-state is approximately toroidal in shape, with the following dimensions:

$$\text{Major radius:} \qquad \langle r \rangle = \frac{5\hbar}{c m_\phi \alpha} = 2.6 \left(\frac{\alpha}{0.037}\right)^{-1} \left(\frac{m_\phi}{10^{-5}\text{ eV}}\right)^{-1} \text{ m} \tag{2.3}$$

$$\text{Minor radius:} \qquad \Delta r = \frac{\sqrt{5}\hbar}{c m_\phi \alpha} = 1.2 \left(\frac{\alpha}{0.037}\right)^{-1} \left(\frac{m_\phi}{10^{-5}\text{ eV}}\right)^{-1} \text{ m} \tag{2.4}$$

$$\text{Volume:} \qquad V = 2\pi^2 \langle r \rangle \Delta r^2 = 71 \left(\frac{\alpha}{0.037}\right)^{-3} \left(\frac{m_\phi}{10^{-5}\text{ eV}}\right)^{-3} \text{ m}^3 \tag{2.5}$$

$$\text{Surface area:} \qquad A = 4\pi^2 \langle r \rangle \Delta r = 120 \left(\frac{\alpha}{0.037}\right)^{-2} \left(\frac{m_\phi}{10^{-5}\text{ eV}}\right)^{-2} \text{ m}^2. \tag{2.6}$$

In the $2p$-state, axions grow superradiantly at a rate

$$\Gamma_s = \frac{c^2 \tilde{a} \alpha^8 m_\phi}{24\hbar} = 2.2 * 10^{-3} \tilde{a} \left(\frac{\alpha}{0.037}\right)^{8} \left(\frac{m_\phi}{10^{-5}\text{ eV}}\right) \text{ s}^{-1}, \tag{2.7}$$

where $\tilde{a}$ is the black hole's spin parameter. At the same time, axions decay into

*Note that some numerical values differ from those given in [61], because we parameterize quantities in terms of $\frac{\alpha}{.037}$, whereas [61] parameterizes quantities in terms of $\frac{\alpha}{.03}$.

photons at a rate

$$\Gamma_\phi = 1.1 * 10^{-49} K^2 \left(\frac{m_\phi}{10^{-5}\text{ eV}}\right)^5 \text{ s}^{-1}, \tag{2.8}$$

where K is a model-dependent factor. For the more general axion-like particle, K is a free parameter, but for the QCD axion, which we examine in this paper, $K \sim \mathcal{O}(1)$. Due to the quasi-bound nature of the $2p$-state, axions will not leave the $2p$-cloud except when disturbed by outside forces. However, a photon produced inside the $2p$-cloud will naturally exit the $2p$-cloud at the speed of light, producing an escape rate of

$$\Gamma_\gamma = \frac{c}{\Delta r} = 2.5 * 10^8 \left(\frac{\alpha}{0.037}\right)\left(\frac{m_\phi}{10^{-5}\text{ eV}}\right) \text{ s}^{-1}. \tag{2.9}$$

[61] found that the Boltzmann equations for the total number of photons and axions in the $2p$-cloud to be

$$\frac{\mathrm{d}N_\phi}{\mathrm{d}t} = \Gamma_s N_\phi - \Gamma_\phi \left(N_\phi(1 + C_1 N_\gamma) - C_2 N_\gamma^2\right) \tag{2.10}$$

$$\frac{\mathrm{d}N_\gamma}{\mathrm{d}t} = -\Gamma_\gamma N_\gamma + 2\Gamma_\phi \left(N_\phi(1 + C_1 N_\gamma) - C_3 N_\gamma^2\right), \tag{2.11}$$

where

$$C_1 = \frac{8\alpha^2}{25} \qquad C_2 = \frac{2\alpha^4}{75} \qquad C_3 = C_2 + \alpha C_1. \tag{2.12}$$

$\Gamma_\gamma \gg \Gamma_s \gg \Gamma_\phi$, and so for low values of N_γ and N_ϕ photon production is negligible. In this regime, N_ϕ grows exponentially, $N_\phi \sim e^{\Gamma_s t}$, while $N_\gamma \sim \frac{2\Gamma_\phi}{\Gamma_\gamma} N_\phi$. However, when $N_\gamma \gtrsim \frac{1}{C_1}$, the $C_1 N_\gamma$ terms become significant, which increases the rate at which axions decay into photons; this marks the beginning of lasing. In this regime, N_γ

increases rapidly, while N_ϕ's growth slows, until both reach their equilibrium values:

$$N_\gamma^{\rm eq} = \frac{\Gamma_s}{C_1\Gamma_\phi} = 4.8 * 10^{49}\tilde{a}K^{-2}\left(\frac{\alpha}{0.037}\right)^6\left(\frac{m_\phi}{10^{-5}\text{ eV}}\right)^{-4} \tag{2.13}$$

$$N_\phi^{\rm eq} = \frac{\Gamma_\gamma}{2C_1\Gamma_\phi} = 2.7 * 10^{60}K^{-2}\left(\frac{\alpha}{0.037}\right)^{-1}\left(\frac{m_\phi}{10^{-5}\text{ eV}}\right)^{-4}. \tag{2.14}$$

One important consideration is that a BLAST is only possible if the black hole has enough spin to produce the requisite number of axions. Since the $2p$-state has magnetic quantum number $m = 1$, each axion produced by superradiance carries with it angular momentum $\hbar$, and therefore at the onset of lasing the axion cloud has angular momentum $\frac{\hbar\Gamma_\gamma}{2C_1\Gamma_\phi}$, whereas the black hole's angular momentum is given by $\tilde{a}\alpha\frac{M_{BH}}{m_\phi}$. This yields the requirement

$$\frac{0.06}{\tilde{a}\alpha^3K^2}\left(\frac{m_\phi}{10^{-8}\text{ eV}}\right)^{-2} \lesssim 1. \tag{2.15}$$

Superradiance requires $\alpha \lesssim .5$, and therefore we must have $m_\phi \gtrsim 10^{-8}$ eV and $M_{BH} \lesssim 10^{-2}M_\odot$. This constraint restricts BLASTs to occur only around primordial Kerr black holes. Primordial black holes are expected to form with some small initial spin [105–110], and they may spin up via a number of processes, including mergers [111], accretion [14, 112], hyperbolic encounters [113], and Hawking radiation [114]. Thus it is possible that the conditions for a BLAST might form in nature.

In the process of reaching the equilibrium values listed earlier, the photon number reaches a maximum value of

$$N_\gamma^{\rm max} \approx \frac{\Gamma_s}{C_1\Gamma_\phi}\ln\frac{\Gamma_s}{\Gamma_\phi} = 5.1 * 10^{51}\tilde{a}K^{-2}\left(\frac{\alpha}{0.037}\right)^6\left(\frac{m_\phi}{10^{-5}\text{ eV}}\right)^{-4}\left(\frac{\xi}{106}\right), \tag{2.16}$$

where

$$\xi = \ln \frac{\Gamma_s}{\Gamma_\phi} = 107 - 4 \ln \left(\frac{m_\phi}{10^{-5} \text{ eV}} \right) + 8 \ln \left(\frac{\alpha}{0.037} \right) + \ln \left(\frac{\tilde{a}}{K^2} \right). \tag{2.17}$$

This corresponds to a peak luminosity of

$$L^{\max} = \frac{m_\phi}{2} N_\gamma^{\max} \Gamma_\gamma = 1.0 * 10^{43} \tilde{a} K^{-2} \left(\frac{\alpha}{0.037} \right)^7 \left(\frac{m_\phi}{10^{-5} \text{ eV}} \right)^{-2} \left(\frac{\xi}{106} \right) \text{ erg/s}. \tag{2.18}$$

This luminosity is comparable to that of the entire Milky Way galaxy. These BLASTs, if they exist, are therefore of great experimental interest, as they should be observable and could provide insight into both primordial black holes and scalar dark matter.

Section 2.3

Electron-Positron Plasmas in BLASTs

[61, 63] showed that the number of photons generated by a BLAST is so great that the electric field inside the $2p$-cloud will approach the critical Schwinger field. It is expected that, in this limit, the production of electron-positron pairs via the Schwinger effect will be significant. In the resulting electron-positron plasma, the photon has an effective mass equal to the plasma frequency. For a sufficient density of electrons and positrons, this will result in axions being energetically incapable of decaying into photons. At the same time, the dynamics of the plasma are nontrivial. In this section, we explore the behavior of this plasma, and the effect it has on axion decay. From this point onward, we will work in natural units where $c = \hbar = \epsilon_0 = 1$.

2.3.1. Rate of Schwinger Production

The Schwinger effect [115, 116] is a nonperturbative effect caused by vacuum decay in the presence of an electromagnetic field. The Schwinger effect cannot occur when

$E^2 - B^2 = \vec{E} \cdot \vec{B} = 0$, and therefore a single beam of light cannot induce the Schwinger effect. However, when multiple beams of light intersect, the interference of the two electromagnetic fields may satisfy the requirements for Schwinger production [117, 118]; this is an area of significant research interest, as it is hoped that the Schwinger effect may be observable at the focus of two lasers (for a review, see [119]). In the same way, Schwinger production may occur inside the $2p$-cloud, where a large number of photons are traveling in different directions.

The Schwinger effect is driven not only by the electromagnetic field, but by the axion field as well [120, 121]. This is a consequence of the coupling between axions and electrons, which takes the form

$$\mathcal{L} \supset \frac{g_{ae}}{2m_e} \bar{\psi}_e \gamma^\mu \gamma^5 \psi_e \partial_\mu \phi, \tag{2.19}$$

where g_{ae} is the axion-electron coupling constant, m_e is the electron mass, ϕ is the axion field, and ψ_e is the electron bispinor. The presence of axions has the effect of enhancing the rate of pair production, compared to the Schwinger effect without axions; this is referred to as the axion-assisted Schwinger effect [120, 121]. This is an important consideration, however, for reasons that will be given momentarily, we do not include it in this paper, instead reserving it for future research. Therefore, the rate of Schwinger production given herein must be understood as a lower bound, as we are neglecting an effect that is known to enhance pair production. Put another way, the rate of Schwinger production that is used in this paper may be understood as the correct value only when $g_{ae} = 0$; for $g_{ae} > 0$, the rate of Schwinger production will be greater than what is used in this paper. Future research will be needed to determine the rate of Schwinger production when $g_{ae} > 0$.

In the following subsection, we discuss the rate of Schwinger production assuming no axion assistance; after that we will discuss the difficulties presented by axion

assistance. Finally, we present an alternative way in which the rate of pair production may be partially derived, in agreement with our result from the first subsection.

The Schwinger effect in Compton-volume patches. The Schwinger effect is typically calculated in the frame of reference in which the electric and magnetic field are parallel, which is guaranteed to exist except in the case where $E^2 - B^2 = \vec{E} \cdot \vec{B} = 0$. The strength of the electric and magnetic fields in this frame of reference can be found by taking advantage of the Lorentz invariance of $E^2 - B^2$ and $\vec{E} \cdot \vec{B}$:

$$E_\parallel = \sqrt{\frac{1}{2}\left(\sqrt{(E^2 - B^2)^2 + 4(\vec{E} \cdot \vec{B})^2} + (E^2 - B^2)\right)} \tag{2.20}$$

$$B_\parallel = \sqrt{\frac{1}{2}\left(\sqrt{(E^2 - B^2)^2 + 4(\vec{E} \cdot \vec{B})^2} - (E^2 - B^2)\right)}. \tag{2.21}$$

For a constant, homogenous electromagnetic field, the rate of Schwinger production is

$$\frac{\mathrm{d}n_{e^+e^-}}{\mathrm{d}t} = \frac{e^2 E_\parallel B_\parallel}{4\pi^2} \sum_{n=1}^{\infty} \frac{1}{n} \coth \frac{n\pi B_\parallel}{E_\parallel} e^{-n\pi \frac{E_c}{E_\parallel}}, \tag{2.22}$$

where $E_c = \frac{m_e^2}{e} = 1.3 * 10^{18}$ V/m is the critical Schwinger field. Note that this increases with $E_\parallel$ but decreases with $B_\parallel$. In general, the Schwinger effect is highly dependent on the space- and time-dependence of the electromagnetic field, i.e. a nonconstant and/or nonuniform field will produce electrons and positrons at a very different rate than the figure given above. However, the effects of nonconstancy and nonuniformity are most pronounced when the electromagnetic field varies on length- and time-scales less than the Compton wavelength of an electron, λ_C [122].

In our case, the random decay of axions into photons results in a superposition of an enormous number of electromagnetic fields, so that the total electromagnetic field within the $2p$-cloud will be highly inhomogeneous and impossible to predict. However, the length- and time-scales of these inhomogeneities will be the wavelength

of the light, which is $\frac{2}{m_\phi}$. For all axion masses that are of interest as a dark matter candidate, this is far greater than the Compton wavelength. Therefore we may divide the $2p$-cloud into a number of patches, each with volume equal to the Compton volume λ_C^3, and in each patch we may treat the electromagnetic field as uniform and constant. (It should be noted that most research on the Schwinger effect at the intersection of laser beams is done under the assumption of high-frequency light, typically X-rays, and in such cases this approximation does not hold. We are taking advantage of the fact that the light in a BLAST is at a much lower frequency than what would be practical in an earth-based experiment.) Therefore, the total rate of Schwinger pair production throughout the $2p$-cloud is

$$\frac{\mathrm{d}N_{e^+e^-}}{\mathrm{d}t} = \sum_{\text{patches}} \lambda_C^3 \frac{e^2 E_\parallel B_\parallel}{4\pi^2} \sum_{n=1}^{\infty} \frac{1}{n} \coth \frac{n\pi B_\parallel}{E_\parallel} e^{-n\pi \frac{E_c}{E_\parallel}}. \tag{2.23}$$

If one wished, one could now find the average value of $E_\parallel$ and $B_\parallel$ in the $2p$-cloud, and substitute these values into the above equation. However, this approach would not produce an accurate estimate of the rate of Schwinger production. This is because of the Schwinger effect's highly nonlinear nature, meaning that even slight increases to $E_\parallel$ or decreases to $B_\parallel$ may result in a dramatic increase to the rate of pair production. This is significant in our case, because we have an electromagnetic field that is, effectively, randomly varying, and as such there will be some patches where the electromagnetic field produces electron-positron pairs at a greater or lesser rate than would be predicted by the cloud-wide averages of $E_\parallel$ and $B_\parallel$. These "hotspots" and "coldspots" contribute more than average and less than average, respectively, to pair production. If the Schwinger effect were linear, the hotspots and coldspots would cancel out when averaging over the patches, and therefore they could be ignored. However, the Schwinger effect's nonlinear nature means that the surplus of pair production in the hotspots will be far greater than the deficit in pair production in the

coldspots. Consequently, if we were to use the average values of $E_\parallel$ and $B_\parallel$, we would significantly underestimate the rate of pair production. What we do instead is find the probability distribution of the electric and magnetic field strength throughout the $2p$-cloud, $f(E)$ and $f(B)$, and average over these. Our total rate of pair production will then be

$$\begin{aligned}\frac{\mathrm{d}N_{e^+e^-}}{\mathrm{d}t} &= V\int_0^\pi \frac{\mathrm{d}\theta\sin\theta}{2}\int_0^\infty\int_0^\infty \mathrm{d}E\mathrm{d}B f(E)f(B)\frac{e^2E_\parallel B_\parallel}{4\pi^2}\sum_{n=1}^\infty\frac{1}{n}\coth\frac{n\pi B_\parallel}{E_\parallel}e^{-n\pi\frac{E_c}{E_\parallel}}\\ &\equiv \Gamma_{\mathrm{Schw}},\end{aligned} \tag{2.24}$$

where θ is the angle between the electric and magnetic fields (assumed to be uniformly distributed between 0 and π), and $E_\parallel$ and $B_\parallel$ are functions of E, B, and θ. Note that E and B are the electric and magnetic field strengths in the axion cloud's zero-momentum frame, whereas $E_\parallel$ and $B_\parallel$ are the electric and magnetic field strengths in a different frame of reference (that being the one in which the electric and magnetic fields are parallel).

To find $f(E)$ and $f(B)$, we assume that the electromagnetic field components are normally distributed uncorrelated random variables with equal standard deviation, σ_{EM}. The electric field magnitude $E=\sqrt{E_x^2+E_y^2+E_z^2}$ then follows a chi distribution, with probability density

$$f(E)=\frac{\sqrt{2}}{\sqrt{\pi}\sigma_{\mathrm{EM}}^3}E^2e^{-\frac{E^2}{2\sigma_{\mathrm{EM}}^2}}. \tag{2.25}$$

An analogous expression for $f(B)$ may be found in the same way. σ_{EM} may be found from the energy density, which in terms of the electromagnetic field components is

$$u=\frac{1}{2}\left(E_x^2+E_y^2+E_z^2+B_x^2+B_y^2+B_z^2\right), \tag{2.26}$$

and therefore

$$\langle u \rangle = 3\sigma_{\rm EM}^2 = \frac{m_\phi N_\gamma}{2V}. \tag{2.27}$$

We perform the integral in eq. 2.24 in Appendix A and show that

$$\Gamma_{\rm Schw} \approx \frac{e^2 E_c^2 V}{8\sqrt{3}\pi} \sum_{n=1}^{\infty} e^{-3\left(\frac{N_\gamma}{n^2 N_\gamma^{\rm Schw}}\right)^{\frac{-1}{3}}} \left(\frac{N_\gamma}{n^2 N_\gamma^{\rm Schw}}\right)^{\frac{1}{3}} \tag{2.28}$$

where

$$N_\gamma^{\rm Schw} = \frac{3\pi^2 E_c^2 V}{4 m_\phi} = 4.9 * 10^{51} \left(\frac{\alpha}{0.037}\right)^{-3} \left(\frac{m_\phi}{10^{-5}\ {\rm eV}}\right)^{-4}. \tag{2.29}$$

This approximation holds for $N_\gamma \lesssim .1 N_\gamma^{\rm Schw}$. We will find that, for our purposes, this is always the case, so that we may freely use this approximation for $\Gamma_{\rm Schw}$.

The challenges of axion-assistance. In principle, the approach we've taken can easily be extended to account for axion-assistance. The axion field will vary in three ways with respect to time and space: it has a time-dependent phase factor $e^{-im_\phi t}$, its magnitude increases with time as a consequence of superradiant growth, and it is spatially inhomogeneous, which results from solving the Klein-Gordon equation in Kerr spacetime. These spatial inhomogeneities have lengthscale $\frac{2}{\alpha m_\phi}$ [80], and superradiant growth occurs over timescale $\frac{1}{2\Gamma_s}$. The shortest timescale is that which corresponds to the phase factor, $\frac{1}{m_\phi}$, and therefore this is the dominant form of axion assistance (since the axion couples to the electron via its derivative, $\partial_\mu \phi$). All of these length- and timescales are far larger than λ_C, and so, when we divide the axion cloud into Compton volumes, we may consider only the dominant term and approximate

$$\phi = e^{-im_\phi t}|\phi|. \tag{2.30}$$

In principle, all we need do is derive an analog to eq. 2.22 for the case of $\phi = e^{-im_\phi t}|\phi|$, i.e. find the rate of Schwinger production when the electric field, magnetic field, and magnitude of the axion field are all held constant. We may then repeat the same procedure as before, inserting this analog of eq. 2.22 into eq. 2.24.

The challenge here lies in finding this analog to eq. 2.22. To the author's knowledge, doing so analytically is not a solved problem in the literature; previous works on the axion-assisted Schwinger effect [120, 121] have been primarily numerical in nature. The prescription in these papers is to write a differential equation governing the time evolution of the Bogoliubov coefficients for the fermion, and then to numerically solve this differential equation. This yields the rate of pair production at a single point in momentum-space. To arrive at the total rate of pair production within a single Compton-volume patch (i.e., our analog to eq. 2.22), one would need to integrate over momentum space. Then, to find the total rate of pair production throughout the entire $2p$-cloud, one would need to integrate over E, B, and θ, analogous to eq. 2.24. This would yield the rate of pair production in the $2p$-cloud, but only for a single value of N_γ and N_ϕ. Because N_γ and N_ϕ will change over time, one would need to repeat this procedure as the axion laser evolves with time. The upshot is that numerically modeling the impact of the axion-assisted Schwinger effect on a superradiant axion laser would require an octuple integral (one integral to find the Bogoliubov coefficients, three over momentum space, three over the electric and magnetic fields, and one over time). As this is unlikely to be computationally feasible, it is necessary to determine an analytical expression to serve as our eq. 2.22-analog.

Deriving the rate of Schwinger production in the presence of both a constant electromagnetic field and an axion field that is constant up to a phase factor, is a sufficiently significant problem to deserve being a paper unto itself. For this paper, we defer that problem, neglecting axion assistance but noting that our expression for

Γ_{Schw} nevertheless has value as a lower bound. A more complete understanding of the Schwinger effect in BLASTs, applicable to the case of $g_{ae} > 0$, will only be possible when the aforementioned eq. 2.22-analog has been derived.

An alternate perspective on pair production. In the preceding subsections, we approached this problem from the perspective of the classical electromagnetic field; we showed that, for sufficiently large N_γ, the field is sufficient to induce pair production at a significant rate. There is an alternative way of considering the problem, which is to focus on the individual photons present in the $2p$-cloud, produced by axion decay. This is an attractive lens through which to view the situation, as we know to a good approximation the spectrum and distribution of these photons. At the level of the individual photons, the Schwinger effect is caused by interactions between photons and a single electron-positron loop. It is an interesting question to see if we can derive our earlier results from the perspective of these specific particle interactions.

[123] calculates the rate at which N photons, K of which have positive helicity, will undergo a scattering interaction involving a single loop. They find that, within an electromagnetic field defined by the tensor $F_{\mu\nu}$, such a scattering interaction will take place at the rate

$$\Gamma_{N,K} = -\frac{m_e^4}{8\pi^2}\left(\frac{2e}{m_e^2}\right)^N c\left(\frac{K}{2}, \frac{N-K}{2}\right)\chi_+^{\frac{K}{2}}\chi_-^{\frac{N-K}{2}}, \tag{2.31}$$

where c is a function defined in [123], and $\chi_\pm$ are related to the electromagnetic field:

$$\chi_\pm = \frac{1}{8}F_{\mu\nu}F^{\mu\nu} \pm \frac{i}{8}F_{\mu\nu}\tilde{F}^{\mu\nu}. \tag{2.32}$$

Without knowing the specific form of $F_{\mu\nu}$ (which will vary as a function of time and position), by considering the energy density of the electromagnetic field we may say

that, for a cloud of photons with angular frequency ω and number density n_γ, we will have

$$F_{\mu\nu} = \sqrt{n_\gamma \omega} f_{\mu\nu}(\vec{x}, t), \tag{2.33}$$

where $f_{\mu\nu}$ is a dimensionless function of time and space. The rate of scattering will therefore be

$$\Gamma_{N,K} \propto m_e^4 \left(\frac{e^2 \omega}{m_e^4} n_\gamma \right)^{\frac{N}{2}}, \tag{2.34}$$

where the constant of proportionality will depend on N and K, as well as time and position within the photon cloud. If $\frac{e^2\omega}{m_e^4} n_\gamma \ll 1$, $\Gamma_{N,K}$ will vanish for large N, and the rate of one-loop interaction will be negligible. Conversely, there exists some critical number density of photons above which pair production is significant, given by

$$n_\gamma^{\text{crit}} \sim \frac{m_e^4}{e^2 \omega}. \tag{2.35}$$

Bearing in mind that $E_c = \frac{m_e^2}{e}$ and $\omega = \frac{m_\phi}{2}$, this reproduces, up to a constant of proportionality, eq. 2.29.

2.3.2. Electron/Positron Escape Rate

Just as photons will exit the $2p$-cloud at a rate Γ_γ, we also must calculate the rate at which electrons and positrons will exit the $2p$-cloud. Schwinger pairs are created with some initial momentum, but we assume that this is negligible compared to the momentum imparted by radiation pressure. This radiation pressure is driven by an energy flux, which we assume to be constant throughout the $2p$-cloud and which is given by $F = \frac{L}{A} = \frac{3m_\phi}{4V} N_\gamma$. Let ρ be a coordinate defined as the distance from the ring running through the center of the $2p$-torus; we expect that radiation pressure will cause electrons and positrons to move predominantly in the $\hat{\rho}$ direction. Therefore

each electron and positron gains energy at a rate

$$\frac{3\sigma_T m_\phi}{4V} N_\gamma = \frac{\mathrm{d}}{\mathrm{d}t} g_{tt} p^t = \frac{\mathrm{d}}{\mathrm{d}t} \left(\left(1 - \frac{r_s r}{r^2 + \frac{1}{4} r_s^2 \tilde{a}^2 \cos^2\theta} \right) \frac{m_e}{\sqrt{1 - \left(\frac{\mathrm{d}\rho}{\mathrm{d}t}\right)^2}} \right), \tag{2.36}$$

where g is the Kerr metric, p is the four-momentum (related to the energy by $E = p_t$), r_s is the Schwarzschild radius of the black hole, and r and θ are Boyer-Lindquist coordinates. The factor of g_{tt} accounts for the curvature of Kerr spacetime; note that there could also be a $g_{t\phi} p^\phi$ term, corresponding to the electron or positron's azimuthal motion, except for the fact that, if the electron or positron is moving primarily in the $\hat{\rho}$ direction, then p^ϕ is negligible. The Schwarzschild radius may be written as

$$r_s = \frac{2GM}{c^2} = 1.5 * 10^{-3} \left(\frac{\alpha}{.037} \right) \left(\frac{m_\phi}{10^{-5}\ \mathrm{eV}} \right)^{-1}\ \mathrm{m}, \tag{2.37}$$

and therefore for all superradiant modes ($\alpha \lesssim .5$), $r \gg r_s$ at all points within the $2p$-cloud. We may therefore neglect this prefactor; put another way, the $2p$-cloud is far enough away from the black hole that we may treat spacetime as flat.

We assume that the timescale on which an individual electron or positron accelerates is much shorter than the timescale over which N_γ changes, and therefore we may treat N_γ as constant. From this we find that the time $T_{e^\pm}$ that it takes for the electron or positron to leave the $2p$-cloud is given by

$$\Delta r - \rho_0 = \sqrt{T_{e^\pm} \left(\frac{8V m_e}{3\sigma_T m_\phi N_\gamma} + T_{e^\pm} \right)} + \frac{4V m_e}{3\sigma_T m_\phi N_\gamma} \left(\frac{\pi}{3} - 2\tan^{-1} \frac{\sqrt{3}\left(\frac{4V m_e}{3\sigma_T m_\phi N_\gamma} + T_{e^\pm} \right) + 2\sqrt{T_{e^\pm} \left(\frac{8V m_e}{3\sigma_T m_\phi N_\gamma} + T_{e^\pm} \right)}}{\frac{4V m_e}{\sigma_T m_\phi N_\gamma} + T_{e^\pm}} \right). \tag{2.38}$$

where ρ_0 is the value of ρ where the electron or positron was created. While it is not possible to get an exact analytical expression for $T_{e^\pm}$ in terms of ρ_0, the above equation can be numerically inverted, so that in principal we may calculate the escape rate as

$$\Gamma_{e^\pm} = \frac{1}{\langle T_{e^\pm} \rangle} = \frac{\Delta r^2}{2\int_0^{\Delta r} T_{e^\pm} \rho_0 \mathrm{d}\rho_0}. \tag{2.39}$$

Notably, in the limit $\frac{3\sigma_T m_\phi}{4Vm_e}\Delta r N_\gamma \to \infty$, $\Gamma_{e^\pm} \to \Gamma_\gamma$; this represents the limit where the radiation pressure is so great that it immediately accelerates electrons and positrons to relativistic velocities. We may therefore use

$$\chi \equiv \frac{3\sigma_T m_\phi}{4Vm_e}\Delta r N_\gamma = \frac{N_\gamma}{6.2 * 10^{40}} \left(\frac{\alpha}{0.037}\right)^2 \left(\frac{m_\phi}{10^{-5}\text{ eV}}\right)^3 \tag{2.40}$$

as a dimensionless parameter for the behavior of $\Gamma_{e^\pm}$. $\Gamma_{e^\pm}$ increases monotonically as χ increases, asymptotically approaching Γ_γ. This behavior is analyzed in greater detail in Appendix B, and it is plotted in Fig. 2.1a.

2.3.3. Pair Annihilation

Within the electron-positron plasma, some number of electrons and positrons will annihilate and produce two photons. The cross-section of this annihilation is given by [124, 125]

$$\sigma(v_{\text{com}}) = \frac{3\sigma_T(1-v_{\text{com}})^2}{32 v_{\text{com}}} \left(\frac{3-v_{\text{com}}^4}{v_{\text{com}}} \ln\frac{1+v_{\text{com}}}{1-v_{\text{com}}} - 2(2-v_{\text{com}}^2)\right), \tag{2.41}$$

where v_{com} is the velocity of the electron and positron in the center-of-mass frame. Due to the effects of radiation pressure, described in the previous section, we expect the electrons and positrons are primarily moving in the $\hat{\rho}$ direction; we may therefore treat the electron-positron plasma as a series of beams, each pointed in the $\hat{\rho}$ direction.

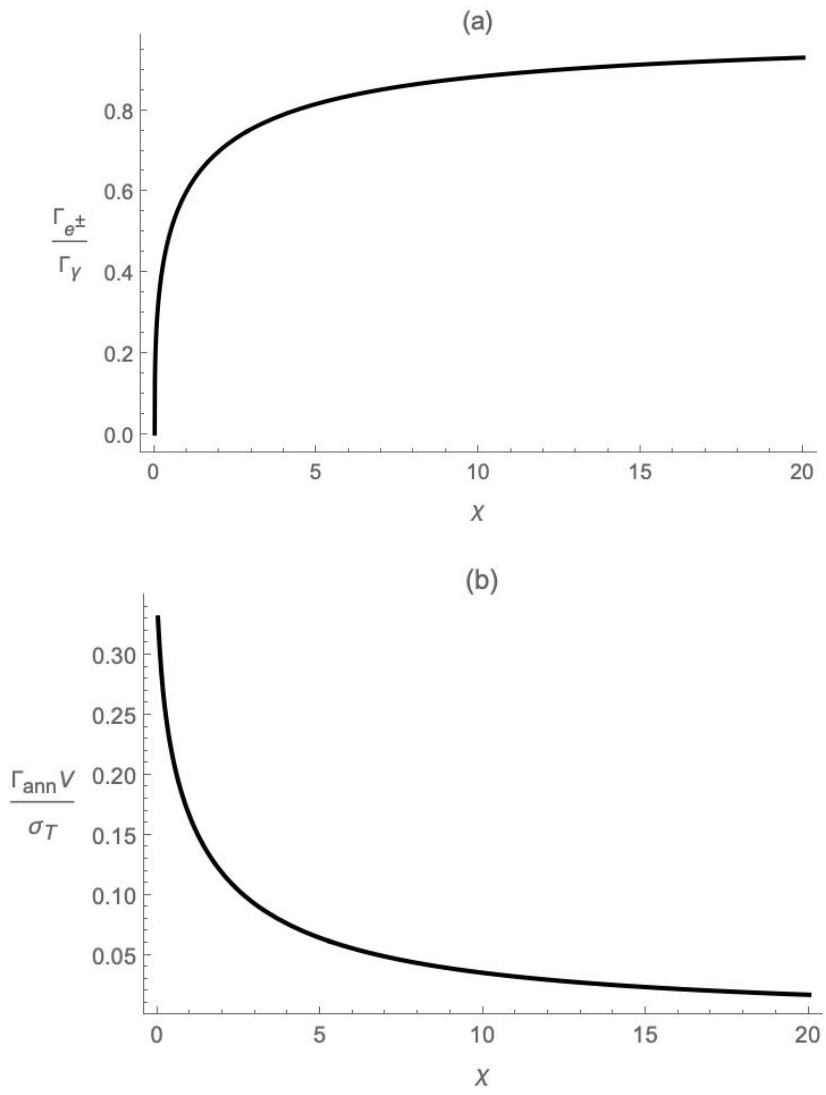

Figure 2.1 (continued on next page): Plot of functions of χ, which parameterizes how relativistic the electrons and positrons become as a result of radiation pressure. (a) demonstrates the behavior of $\Gamma_{e^\pm}$. At low χ, there is negligible radiation pressure driving electrons and positrons to exit the $2p$-cloud, and so $\Gamma_{e^\pm} \to 0$. For large χ the electrons and positrons are quickly accelerated to very close to the speed of light, causing them to exit the $2p$-cloud at roughly the same rate as the photons, and as a result $\Gamma_{e^\pm} \to \Gamma_\gamma$. (b) demonstrates the behavior of Γ_{ann}. Slower particles present a larger cross-section, and therefore pair annihilation occurs frequently for small χ but vanishes as $\chi \to \infty$. Note that Γ_{ann} is the rate of annihilation per number of pairs squared, not the total rate; in practice, large χ will correlate with large $N_{e^+e^-}$, so the total rate of annihilation will increase with χ.

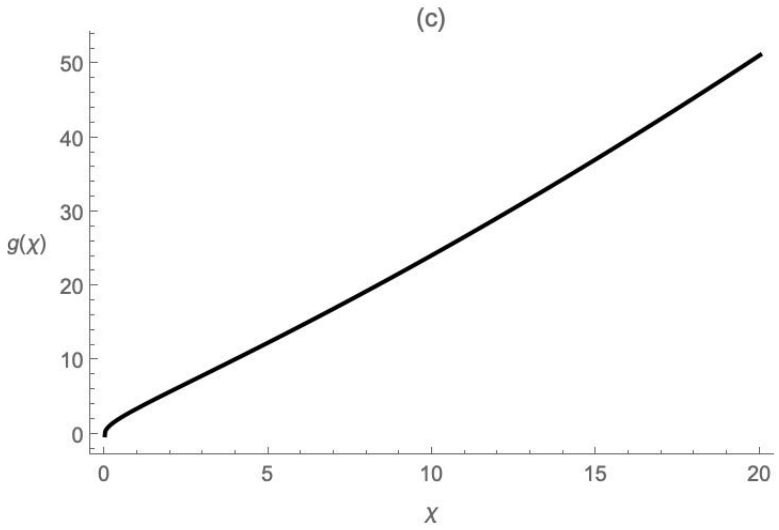

Figure 2.1 (continued from previous page): (c) demonstrates the behavior of $g(\chi)$, which scales the number of electron-positron pairs at which annihilation becomes relevant. We show in Appendix B that, for large χ, $g(\chi)$ grows as $\frac{\chi^2}{(\ln \chi)^2}$.

For a pure beam of positrons and a pure beam of electrons with velocities v_{e^+} and v_{e^-}, respectively, each of which is pointed in the same direction, the rate of annihilation is

$$\frac{\mathrm{d}n_{e^\pm}}{\mathrm{d}t} = -n_{e^+} n_{e^-} |v_{e^+} - v_{e^-}| \sigma(v_{\mathrm{com}}), \tag{2.42}$$

The center-of-mass velocity is related to the electron's and positron's velocities by

$$v_{\mathrm{com}} = \sqrt{\frac{\gamma_{e^+}\gamma_{e^-}(1 - v_{e^+}v_{e^-}) - 1}{\gamma_{e^+}\gamma_{e^-}(1 - v_{e^+}v_{e^-}) + 1}}, \tag{2.43}$$

where $\gamma_{e^\pm}$ are the Lorentz factors corresponding to $v_{e^\pm}$.

In our case, the electrons and positrons have a distribution of velocities, $f(v)$, and therefore the total rate of annihilation is

$$\frac{\mathrm{d}n_{e^\pm}}{\mathrm{d}t} = -n_{e^+} n_{e^-} \int dv_{e^+} dv_{e^-} f(v_{e^+}) f(v_{e^-}) |v_{e^+} - v_{e^-}| \sigma(v_{\mathrm{com}}). \tag{2.44}$$

Using the same approach as in the previous section, the velocity of an electron or

positron is directly related to the length of time it has existed, t:

$$t = \frac{1}{\sqrt{1-v^2}} \frac{4m_e V}{3\sigma_T m_\phi N_\gamma} = \frac{\Delta r}{\chi\sqrt{1-v^2}}, \tag{2.45}$$

and therefore we may relate the velocity of the electron or positron to the distance it has traveled since it was created, which we call $\Delta\rho$:

$$\Delta\rho = \frac{\Delta r}{\chi}\left(\frac{v}{\sqrt{1-v^2}} - \tan^{-1}\frac{v}{\sqrt{1-v^2}}\right). \tag{2.46}$$

As in the previous section, we cannot write an analytic expression for v in terms of $\Delta\rho$, but it is still possible in principle to express the former as a function of the latter, $v(\Delta\rho)$. We may therefore replace our integral over the velocities of the electron and positron with an integral over the locations at which the two particles are created and at which the annihilation occurs. Assuming that electrons and positrons are created uniformly throughout the $2p$-torus, and that annihilation occurs uniformly throughout the $2p$-torus, we get that the rate of annihilation is

$$\frac{\mathrm{d}n_{e^\pm}}{\mathrm{d}t} = -n_{e^+}n_{e^-}\int_0^{\Delta r}\mathrm{d}\rho\frac{2\rho}{\Delta r^2}\int_0^{\rho}\mathrm{d}\rho_{0e^+}\frac{2\rho_{0e^+}}{\rho^2}\int_0^{\rho}\mathrm{d}\rho_{0e^-}\frac{2\rho_{0e^-}}{\rho^2}|v_{e^+}-v_{e^-}|\sigma(v_{\mathrm{com}}), \tag{2.47}$$

where $v_{e^\pm}$ is a function of $\rho - \rho_{0e^\pm}$. In this integral, ρ represents the coordinate at which annihilation occurs, and $\rho_{0e^\pm}$ represents the coordinate at which the electron or positron was created. The factors of $\frac{2\rho}{\Delta r^2}$ and $\frac{2\rho_{0e^\pm}}{\rho^2}$ are the probability distributions for ρ and $\rho_{0e^\pm}$. Since the number of electrons and positrons is assumed to be equal, we may write this as

$$\begin{aligned}\frac{\mathrm{d}N_{e^+e^-}}{\mathrm{d}t} &= -\frac{8N_{e^+e^-}^2}{V\Delta r^2}\int_0^{\Delta r}\mathrm{d}\rho\int_0^{\rho}\int_0^{\rho}\mathrm{d}\rho_{0e^+}\mathrm{d}\rho_{0e^-}\frac{\rho_{0e^+}\rho_{0e^-}}{\rho^3}|v_{e^+}-v_{e^-}|\sigma(v_{\mathrm{com}}) \\ &\equiv -\Gamma_{\mathrm{ann}}N_{e^+e^-}^2.\end{aligned} \tag{2.48}$$

We show in Appendix B that $\Gamma_{\rm ann} V$ is a function only of χ, which is displayed in Fig. 2.1b. As χ increases, the electrons and positrons become more relativistic, and so both the cross section and the rate of annihilation decrease.

Each pair annihilation creates two photons, and therefore there ought to be a $\Gamma_{\rm ann} N_{e^+e^-}^2$ term in the photon Boltzmann equation. However, these photons will have energy of at least m_e, whereas the photons created by axion decay have energy $\frac{m_\phi}{2} \ll m_e$. A rigorous analysis will therefore require us to keep track of two separate photon populations, low-energy photons produced by axion decay and high-energy photons produced by pair annihilation; the $\Gamma_{\rm ann} N_{e^+e^-}^2$ term would appear in the Boltzmann equation of the latter, but not the former. However, as we will show later, pair annihilation does not occur at a significant rate, and therefore we may ignore these high-energy photons.

2.3.4. Suppression of Axion Decay

Lastly, we must account for the effects of the electron-positron plasma on axion decay. The plasma frequency is given by

$$\omega_p = \sqrt{\frac{2e^2 N_{e^+e^-}}{m_e V}}, \tag{2.49}$$

and this serves as the effective mass of photons in the $2p$-cloud. It is a straightforward exercise of QED to show that this scales the rate of axion decay by

$$\Gamma_\phi \to \Gamma_\phi \mathrm{Re}\sqrt{1 - \frac{8e^2}{m_e m_\phi^2 V} N_{e^+e^-}} \equiv \Gamma'_\phi. \tag{2.50}$$

Note that this has the effect of shutting down axion decay entirely when

$$N_{e^+e^-} \geq \frac{m_e m_\phi^2 V}{8e^2} = 6.5 * 10^{17} \left(\frac{\alpha}{0.037}\right)^{-3} \left(\frac{m_\phi}{10^{-5}\text{ eV}}\right)^{-1} \equiv N_{e^+e^-}^{\text{shutoff}}. \tag{2.51}$$

Another consequence of the photon's effective mass is that it permits the photon to grow superradiantly [28, 29, 126–128]. This effect is not considered in this paper, as accounting for it would require an understanding of the spatial distribution of the plasma, which is beyond our present scope. There is reason to believe it may not be significant, as numerical simulations have shown that this superradiant growth becomes significant only when $\omega_p > \frac{m_\phi}{2}$ [65], i.e. $N_{e^+e^-} > N_{e^+e^-}^{\text{shutoff}}$. We will show later that, to a good approximation, $N_{e^+e^-}$ increases monotonically with N_γ; therefore, because N_γ will not increase when $N_{e^+e^-} \geq N_{e^+e^-}^{\text{shutoff}}$, we do not expect $N_{e^+e^-}$ to exceed $N_{e^+e^-}^{\text{shutoff}}$. It must be acknowledged, however, that this is only an initial prediction, and a more detailed numerical model may reveal the superradiant growth of the photon to be significant.

Section 2.4

Boltzmann Equations and Parameter Space

We may now write the Boltzmann equations for the axion number, photon number, and Schwinger pair number:

$$\frac{\mathrm{d}N_\phi}{\mathrm{d}t} = \Gamma_s N_\phi - \Gamma'_\phi \left(N_\phi(1 + C_1 N_\gamma) - C_2 N_\gamma^2\right) \tag{2.52}$$

$$\frac{\mathrm{d}N_\gamma}{\mathrm{d}t} = -\Gamma_\gamma N_\gamma + 2\Gamma'_\phi \left(N_\phi(1 + C_1 N_\gamma) - C_3 N_\gamma^2\right) - \frac{4m_e}{m_\phi}\Gamma_{\text{Schw}} \tag{2.53}$$

$$\frac{\mathrm{d}N_{e^+e^-}}{\mathrm{d}t} = \Gamma_{\mathrm{Schw}} - \Gamma_{e^\pm} N_{e^+e^-} - \Gamma_{\mathrm{ann}} N_{e^+e^-}^2. \tag{2.54}$$

Note that, because we are modeling the total number of particles in the axion cloud, we have only included phenomena that can introduce or remove particles from the cloud. There are likely to be additional phenomena that alter the distribution of particles within the axion cloud (e.g. scattering between electrons and positrons), but these are not relevant to this paper.

Numerical solutions to these equations, for two different sets of parameters, are shown in Fig. 2.2. Initially, the rate of pair production is vanishingly small, so N_ϕ and N_γ behave identically to the description given in [61]. When N_γ gets within a few orders of magnitude of N_γ^{Schw} (roughly $10^{-4} N_\gamma^{\mathrm{Schw}}$), electron-positron pairs begin to be produced, and these electron-positron pairs impact the axion decay rate. Thus we need only consider the case when N_γ is approaching N_γ^{Schw}.

Let us first consider the behavior of $N_{e^+e^-}$. When $N_{e^+e^-}$ is small, the annihilation term is negligible, and so the number of electron-positron pairs is controlled only by the rate of production and the rate of escape. For all $N_\gamma < N_\gamma^{\mathrm{Schw}}$, $\Gamma_{e^\pm} \gg \frac{\Gamma_{\mathrm{Schw}}}{N_\gamma}$, and therefore we may approximate $N_{e^+e^-} \approx \frac{\Gamma_{\mathrm{Schw}}}{\Gamma_{e^\pm}}$. This approximation holds until either annihilation becomes significant, or until N_γ exceeds N_γ^{Schw}. We will show that, in what appears to be a remarkable coincidence, both of these conditions are met at roughly the same time. Examining first the matter of N_γ exceeding N_γ^{Schw}, we note that, when $N_\gamma = N_\gamma^{\mathrm{Schw}}$, χ is given by

$$\chi^{\mathrm{Schw}} = 7.8 * 10^{10} \left(\frac{\alpha}{0.037}\right)^{-1} \left(\frac{m_\phi}{10^{-5}\ \mathrm{eV}}\right)^{-1}, \tag{2.55}$$

and the number of electron-positron pairs is, provided the aforementioned approxi-

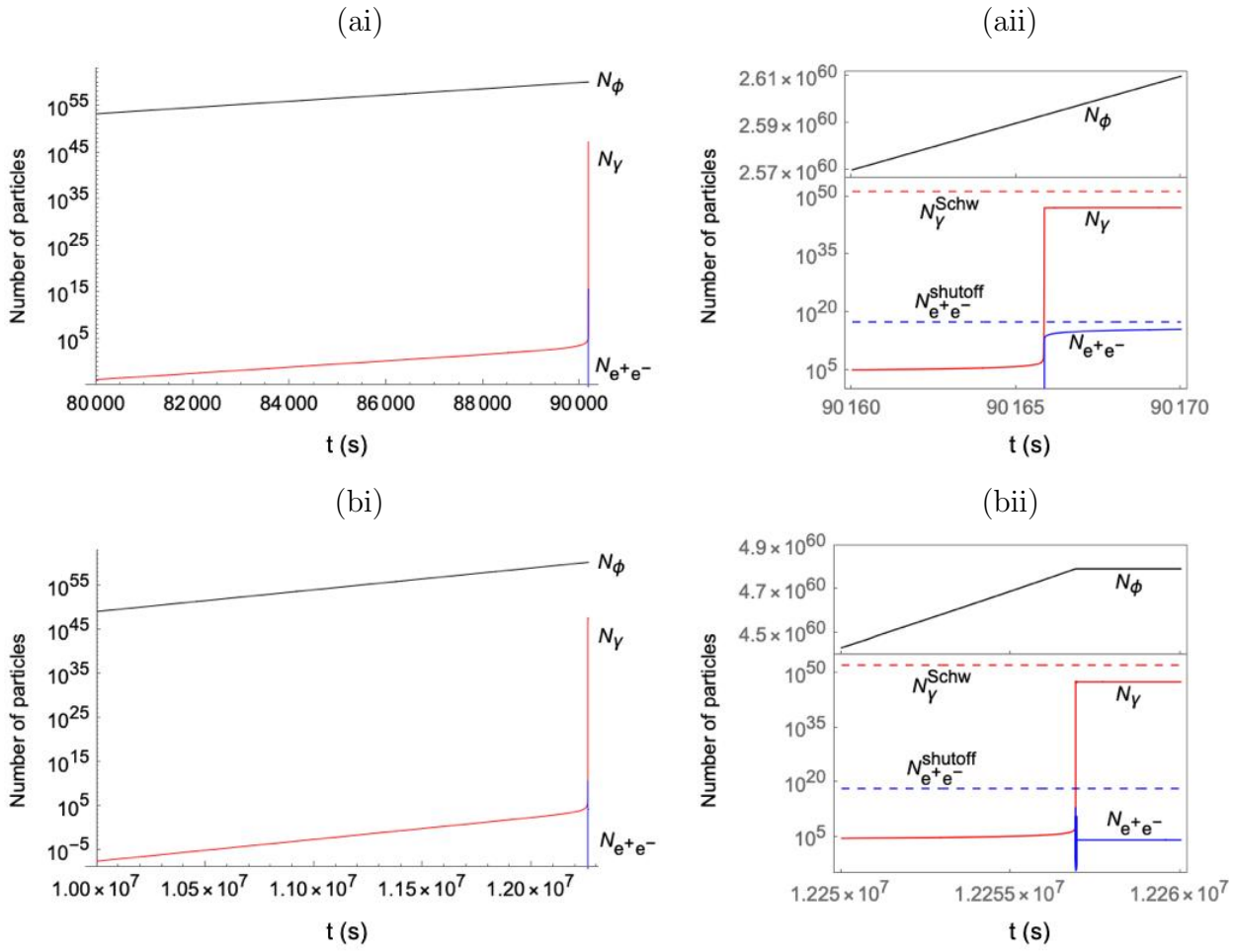

Figure 2.2: Numerical simulations of the growth of N_ϕ, N_γ, and $N_{e^+e^-}$. (a) is done with $\alpha = .037$ while (b) is done with $\alpha = .02$, with the other parameters set to $m_\phi = 10^{-5}$ eV, $\tilde{a} = .7$, and $K = 1$. (aii) and (bii) show zoomed-in views of the onset of lasing, when N_γ increases rapidly. In both cases, $N_{e^+e^-}$ increases alongside N_γ, matching with the approximation $N_{e^+e^-} \approx \frac{\Gamma_{\rm Schw}}{\Gamma_{e^\pm}}$. Prior to the onset of lasing, N_ϕ and N_γ increase exponentially, while $N_{e^+e^-}$ is negligible. In (a), $N_{e^+e^-}$ approaches $N_{e^+e^-}^{\rm shutoff}$, slowing axion decay, so that N_γ stops increasing while N_ϕ continues increasing. In (b), $N_{e^+e^-}$ is not large enough to significantly affect axion decay, and so N_γ and N_ϕ settle into their equilibrium values. (a) lies in the unstable region of parameter space, while (b) lies in the unenhanced region (see Figs. 2.3 and 2.4). Note that, in both plots, N_γ always remains multiple orders of magnitude below $N_\gamma^{\rm Schw}$, allowing for the approximation given in eq. 2.28.

mation still holds at this point,

$$N_{e^+e^-}^{\rm Schw} = 4 * 10^{48} \left(\frac{\alpha}{0.037}\right)^{-4} \left(\frac{m_\phi}{10^{-5}\ \text{eV}}\right)^{-4}. \tag{2.56}$$

As for pair annihilation, that becomes significant when $N_{e^+e^-} \sim \frac{\Gamma_{e^\pm}}{\Gamma_{\rm ann}} \equiv N_{e^+e^-}^{\rm ann}$, which may be written as

$$N_{e^+e^-}^{\rm ann} = \frac{\Gamma_\gamma V}{\sigma_T} g(\chi) = 2.7 * 10^{30} \left(\frac{\alpha}{0.037}\right)^{-2} \left(\frac{m_\phi}{10^{-5}\ \text{eV}}\right)^{-2} g(\chi), \tag{2.57}$$

where

$$g(\chi) = \frac{\chi^5}{48 \left(\int_0^\chi \hat{T}_{e^\pm} \hat{\rho}_0 \mathrm{d}\hat{\rho}_0\right) \left(\int_0^\chi \mathrm{d}\hat{\rho} \int_0^{\hat{\rho}} \mathrm{d}\hat{\rho}_{0e^+} \int_0^{\hat{\rho}} \mathrm{d}\hat{\rho}_{0e^-} \frac{\hat{\rho}_{0e^+}\hat{\rho}_{0e^-}}{\hat{\rho}^3} |v_{e^+} - v_{e^-}| \frac{\sigma(v_{\rm com})}{\sigma_T}\right)}, \tag{2.58}$$

which uses the hat notation defined in Appendix B. $g(\chi)$ is plotted in Fig. 2.1c, and we show in Appendix B that its asymptotic form is

$$g(\chi) \xrightarrow[\chi\to\infty]{} \frac{2\chi^2}{3(\ln\chi)^2}. \tag{2.59}$$

This means that, at $\chi = \chi^{\rm Schw}$, $N_{e^+e^-}^{\rm ann} \sim N_{e^+e^-}^{\rm Schw}$. In other words, pair annihilation only becomes relevant right as N_γ reaches $N_\gamma^{\rm Schw}$. Thus, in the $N_\gamma < N_\gamma^{\rm Schw}$ regime, we may ignore annihilation, and the approximation $N_{e^+e^-} \approx \frac{\Gamma_{\rm Schw}}{\Gamma_{e^\pm}}$ holds.

We now examine the assumption that $N_\gamma < N_\gamma^{\rm Schw}$. The only positive term in the Boltzmann equation vanishes when $N_{e^+e^-} \geq N_{e^+e^-}^{\rm shutoff}$. If this happens when $N_\gamma < N_\gamma^{\rm Schw}$, then the photon number will have a ceiling, which we refer to as $N_\gamma^{\rm ceiling}$ and which may be found by solving $\frac{\Gamma_{\rm Schw}}{\Gamma_{e^\pm}} = N_{e^+e^-}^{\rm shutoff}$ for N_γ. Note that N_γ might never reach $N_\gamma^{\rm ceiling}$. This inversion is easy to do numerically, but it is impossible analytically, and therefore it is unclear how $N_\gamma^{\rm ceiling}$ depends on α and m_ϕ. However, it

is straightforward to show that, for any reasonable values of α and m_ϕ, $\frac{\Gamma_{\rm Schw}}{\Gamma_{e^\pm}} \gg N^{\rm shutoff}_{e^+e^-}$ when $N_\gamma = N^{\rm Schw}_\gamma$. From this we conclude that $N^{\rm ceiling}_\gamma \ll N^{\rm Schw}_\gamma$, and we may therefore assume, throughout this analysis, that $N_\gamma < N^{\rm Schw}_\gamma$, and we may use the approximations derived from this assumption.

Let us next turn to the effects of $N_{e^+e^-}$ on N_ϕ and N_γ. There are two conditions under which the electron-positron plasma may become significant to the dynamics of the photon number and the axion number. The first way is that, as $N_{e^+e^-}$ approaches $N^{\rm shutoff}_{e^+e^-}$, the rate of axion decay Γ'_ϕ vanishes. This happens when $\frac{\Gamma_{\rm Schw}}{\Gamma_{e^\pm} N^{\rm shutoff}_{e^+e^-}} \sim 1$. The second way is that, for sufficiently large N_γ, the rate of photon loss from the Schwinger effect will become significant. This happens when $\frac{4m_e\Gamma_{\rm Schw}}{m_\phi \Gamma_\gamma N_\gamma} \sim 1$. For all values of N_γ, $\frac{\Gamma_{\rm Schw}}{\Gamma_{e^\pm} N^{\rm shutoff}_{e^+e^-}} \gg \frac{4m_e\Gamma_{\rm Schw}}{m_\phi \Gamma_\gamma N_\gamma}$, and therefore the former condition will be met before the latter. Once the number of electron-positron pairs reaches $N^{\rm shutoff}_{e^+e^-}$, N_γ ceases to increase, and consequently it will never become large enough for the second condition to be fulfilled. We may therefore neglect the $\frac{4m_e}{m_\phi}\Gamma_{\rm Schw}$ term in the N_γ Boltzmann equation.

The buildup of Schwinger pairs suppresses the decay of axions into photons, resulting in a lower equilibrium value for the photon number. The equilibrium value may be found by taking the expression from [61] and substituting $\Gamma_\phi \to \Gamma'_\phi$, which yields the expression

$$N^{\rm eq2}_\gamma \left(1 - \frac{8e^2\Gamma^{\rm eq}_{\rm Schw}}{m_e m_\phi^2 V \Gamma^{\rm eq}_{e^\pm}}\right) = N^{\rm eq,w/o2}_\gamma, \tag{2.60}$$

where $\Gamma^{\rm eq}_{\rm Schw}$ and $\Gamma^{\rm eq}_{e^\pm}$ represent $\Gamma_{\rm Schw}$ and $\Gamma_{e^\pm}$ evaluated at $N^{\rm eq}_\gamma$, and $N^{\rm eq,w/o}_\gamma = \frac{\Gamma_s}{C_1\Gamma_\phi}$ is the expression for $N^{\rm eq}_\gamma$ calculated without accounting for the Schwinger effect. This equation does not have a solution for all regions of parameter space; for some values of m_ϕ and α, it is simply impossible for the system to reach equilibrium. This represents the case where the suppression of axion decay is so great that the photons will never build up to the point where they come into equilibrium with the axions. While the

number of photons will reach or approach $N_\gamma^{\text{ceiling}}$, the number of axions will continue growing unbounded. This is reflected mathematically by the fact that $C_1\Gamma'_\phi N_\gamma$ has some maximum attainable value, and, if this maximum value is less than Γ_s, then N_ϕ will increase without bound. This will eventually result in the black hole spinning down to the point where superradiance ceases. These regions of parameter space where the system is unstable are shown in Fig. 2.3.

It should be noted that, while this paper has focused on axion decay, which cannot happen when the plasma frequency exceeds $\frac{m_\phi}{2}$, it has been shown that axion clouds may still emit light after exceeding this limit, via axion annihilation, i.e. $\phi+\phi \to \gamma+\gamma$ [62, 65]. Indeed, it is possible to have any number of photons annihilate to produce two photons, $n\phi \to \gamma + \gamma$, with each individual annihilation process shutting off when $\omega_p > n\frac{m_\phi}{2}$. These higher-order processes will become more relevant in the unstable case, as the axion cloud is expected to reach greater densities than is possible outside of the unstable case, and these processes may in fact allow the system to reach equilibrium (making the term "unstable case" something of a misnomer; it is only unstable in this particular analysis, which ignores higher-level processes). This, however, is beyond the scope of this paper.

In regions of parameter space where the system is stable, the equilibrium photon number is enhanced by a factor of $\frac{\Gamma_\phi}{\Gamma'_\phi}$. This enhancement is plotted in Fig. 2.4. It is somewhat counterintuitive that the Schwinger effect, which has the consequence of suppressing axion decay, enhances the equilibrium luminosity of axion lasers; the reason for this enhancement is that, with the Schwinger effect reducing the axion decay rate, a greater number of photons are needed to stimulate axion decay to the point where equilibrium is reached. Thus, when the enhancement is large, we would expect N_γ to grow, as a function of time, more slowly than when the enhancement is small; however, it will take a longer time and more photons to reach equilibrium.

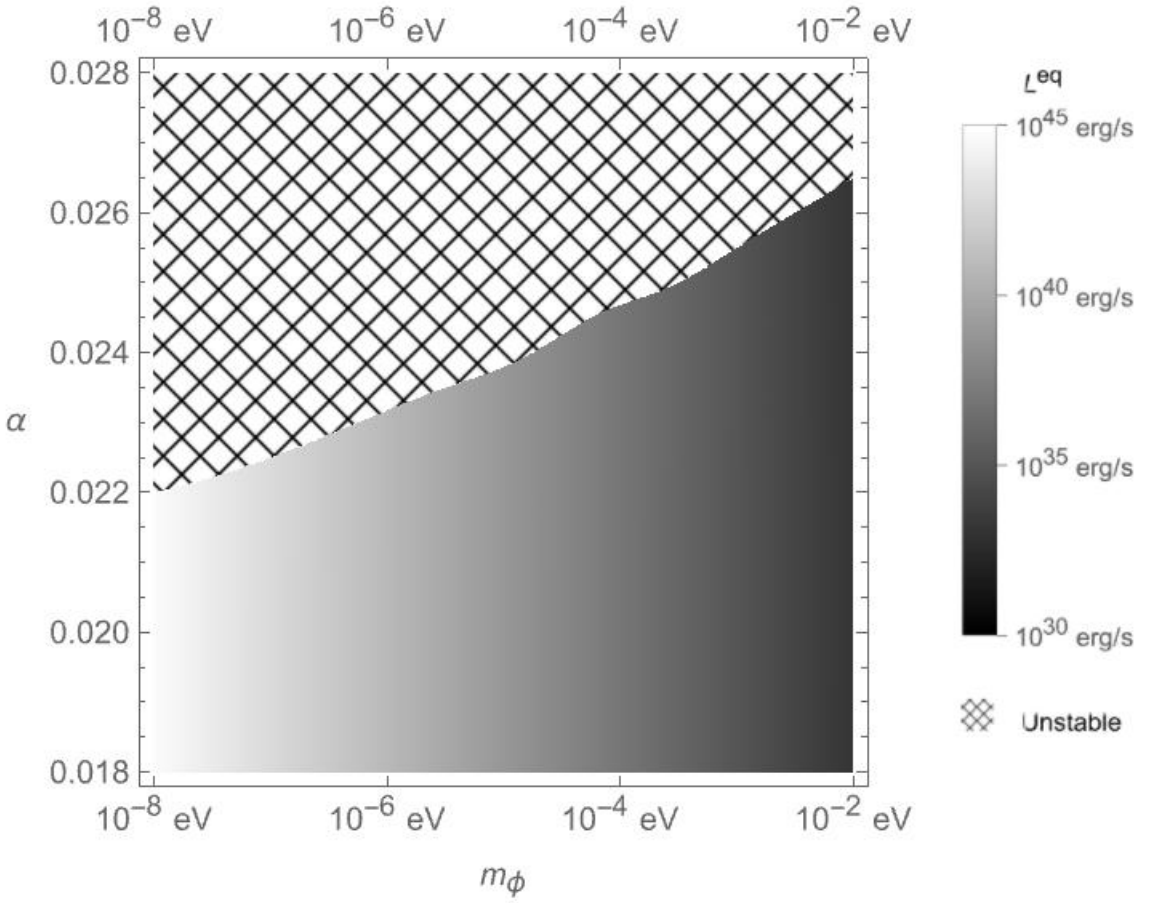

Figure 2.3: Plot of the αm_ϕ plane of parameter space. The other parameters were taken to be $\tilde{a} = .7$ and $K = 1$. For larger values of α and smaller values of m_ϕ, the system is unstable, represented by the black-colored region of parameter space. In this region, the electron-positron plasma suppresses the axion decay so much that the photon number never becomes large enough to halt the growth of the axion number. The axion number therefore continues to grow superradiantly, causing the black hole to spin down until it is no longer superradiant. In the colored regions of parameter space, it is possible for the system to reach equilibrium, and the equilibrium luminosity is plotted. Especially for light axions, these luminosities are extremely high, making BLASTs potentially significant for future experiments. In the shaded region of parameter space, L^{eq} depends on both α and m_ϕ, but the dependence on α is too small to see on this plot.

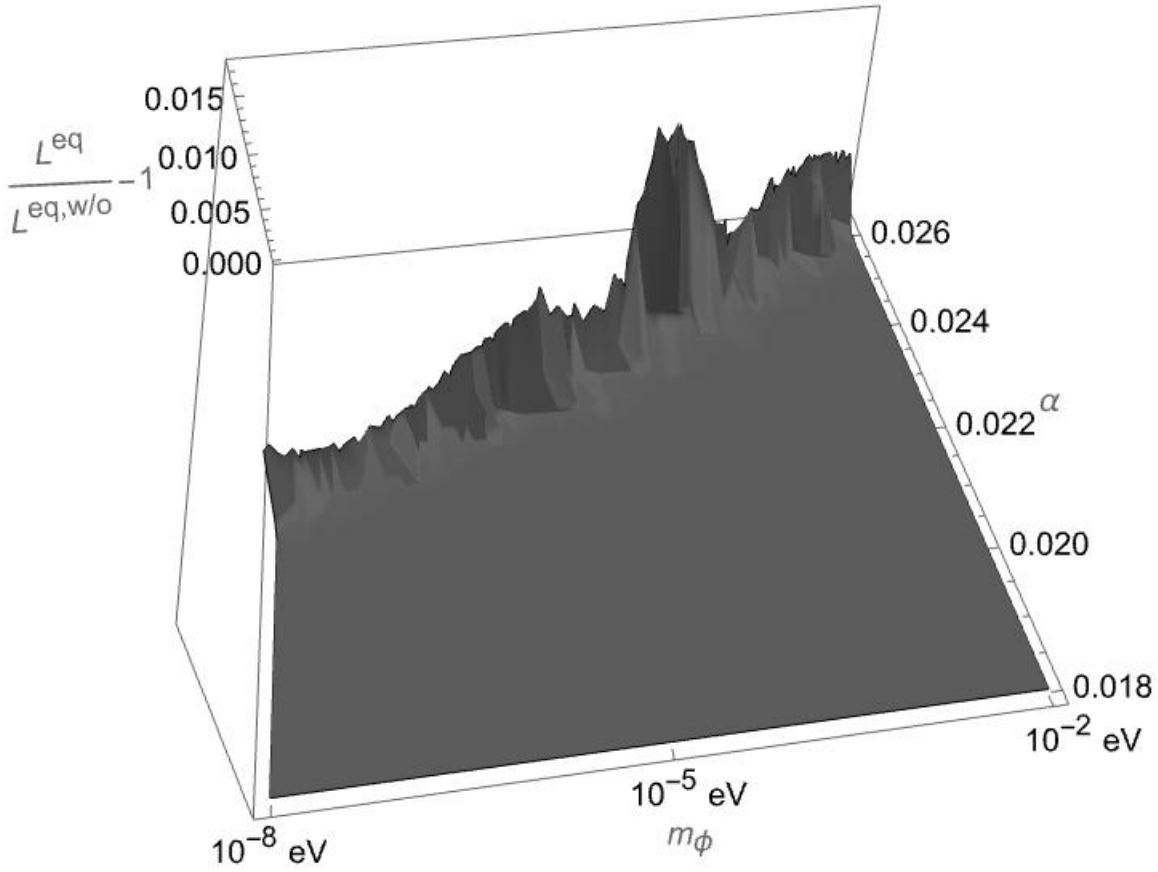

Figure 2.4: Plot of the enhancement of the equilibrium luminosity against α and m_ϕ. $L^{\rm eq}$ is the equilibrium luminosity, while $L^{\rm eq,w/o}$ is the equilibrium luminosity found in [61], i.e. ignoring the effects of Schwinger pairs. The same unstable region shown in Fig. 2.2 is also visible here. In the part of parameter space where an equilibrium state exists, we can see that the equilibrium luminosity is hardly enhanced at all, which means that the role of Schwinger production is negligible to the final state of the BLAST. However, close to the unstable region, there is a region where the enhancement becomes more significant. Note that computational constraints limit the resolution of the section of the plot with the greatest enhancement. This means that, even though the largest enhancement displayed on this plot is .02, it is likely that even greater enhancements can be achieved.

For the majority of parameter space (where equilibrium is possible), this enhancement is negligible, as can be seen in Fig. 2.4. In regions where the enhancement is negligible, the behavior of the BLAST may be modeled without considering the impact of the Schwinger effect. However, we can see that the enhancement to the photon number (and, consequently, the luminosity) increases somewhat as one approaches the region of parameter space where the system becomes unstable. The result is that there is a small region of parameter space, located right next to the region where BLASTs become unstable, where the BLASTS are stable but enhanced. It is in this region where we would expect to find the strongest stable BLASTs.

Section 2.5

Conclusion

When an axion laser, such as a BLAST, becomes sufficiently strong, it can produce an electric field close to the critical Schwinger limit, resulting in the creation of electron-positron pairs. This has three effects on the dynamics of the photon and axion number: photons are lost as their energy is converted into electrons and positrons; electrons and positrons annihilate into photons, but with a higher energy than the photons produced by axion decay; and the buildup of an electron-positron plasma imparts an effective mass on the photon, slowing the rate of axion decay. We found that the third is the dominant phenomenon. How this alters the behavior of a BLAST depends on its parameters, specifically the values of α and m_ϕ.

To summarize, the parameter space of a BLAST may be divided into three regions:

- **Unenhanced:** In this region, the electron-positron plasma produced by the Schwinger effect has a negligible impact on the dynamics of the BLAST, and the analysis from [61] applies.

- **Unstable:** In this region, the system never reaches equilibrium. While the photon number N_γ will increase after the onset of lasing, the buildup of an electron-positron plasma suppresses the axion decay rate, so that the axion number N_ϕ continues to rise. The annihilation of multiple axions into two photons may eventually bring the system to equilibrium; otherwise, the unbounded growth continues until the black hole spins down, at which point the axion no longer experiences superradiant growth.

- **Enhanced:** In between the previous two regions, the BLAST has an equilibrium state, but its equilibrium luminosity is enhanced compared to what is predicted in [61]. The BLAST will take a longer time to reach this equilibrium state, compared to in the unenhanced case.

It is important to note that, in the first and third cases, the system will eventually reach its equilibrium state (likely undergoing damped oscillations about said equilibrium state). This is in contrast to what was predicted in [61], which speculated that the Schwinger effect would "restart" the system periodically. We therefore should only expect a BLAST to exhibit periodic behavior if we happen to observe it in its initial stages, before it has reached its equilibrium state.

This work has focused on the role of the Schwinger effect, and the resulting electron-positron plasma, in the behavior of BLASTs, but this is not the only means by which a plasma may come to interact with the axion cloud. Black holes are expected to be surrounded by a plasma, acquired via accretion, and the role of this plasma in the behavior of BLASTs is nontrivial [62, 63, 65]. More study is needed to see how the Schwinger-produced electron-positron plasma interacts with this preexisting, accreted plasma.

The equilibrium luminosities we have calculated are quite large in comparison to the mass of a primordial black hole. For example, if $m_\phi = 10^{-5}$ eV, then the

largest a black hole can be while remaining in the stable region of parameter space is $6.5 * 10^{28}$ kg, and, if such a black hole were to remain in that equilibrium state continuously, it would evaporate after $7 * 10^5$ years. In practice, such a black hole would undergo spin-down before this happened. Since the $2p$-state has magnetic quantum number $m = 1$, each axion produced by superradiance carries with it angular momentum $\hbar$, and therefore the black hole's spin changes at a rate of $\frac{d\tilde{a}}{dt} = -\frac{\Gamma_s m_\phi}{\alpha M_{BH}} N_\phi$. As the black hole spins down, the superradiant growth of axions slows and eventually stops. Thus, BLASTS represent a potentially important aspect of the spin evolution of rotating black holes.

This paper has focused on the role of the Schwinger effect in one type of axion lasing system, namely, BLASTs. However, there are many other axion lasers that are of research interest (see [60] for a recent review). It is conceivable that the Schwinger effect may play a significant role in these axion lasers as well. Axion lasers are a promising method by which we might probe the existence of scalar dark matter. Understanding the role of the Schwinger effect in these processes may be necessary in order to develop accurate models of axion lasers.

An important caveat to these results is that our calculation of the rate of pair production ignored the phenomenon of axion assistance to the Schwinger effect [120, 121]. Because a BLAST occurs in an axion field, we should expect the rate of pair production to be greater than what is calculated using the standard Schwinger effect (i.e., based only on the electromagnetic field, without considering the axion field). The rate of Schwinger production used in this paper therefore serves as a lower bound. The closeness this lower bound to reality will depend on the axion-electron coupling, g_{ae}, with the true rate of pair production approaching the rate used in this paper only in the limit $g_{ae} \to 0$. We may predict that increasing g_{ae} will have the effect of expanding the unbounded region of parameter space, as it becomes easier for the

Schwinger effect to create a plasma of sufficient density that axion decay is shut off. However, future research is needed to examine, in greater detail, the behavior of BLASTs in the case of $g_{ae} > 0$.

It is also worth noting that we have assumed that all particles are uniformly distributed throughout the $2p$-cloud; however, the simulations conducted in [65] have demonstrated that this approximation can fail to predict significant phenomena. It is therefore necessary to do away with this assumption as well, which will entail replacing the analytical calculations in this paper with numerical simulations.

Chapter 3

Linear and Nonlinear Riemann Normal Coordinates

Section 3.1

Introduction

There exist problems in particle physics that are well developed in flat spacetime but intractable in curved spacetime. Indeed, the notion of a particle is not even well-defined in all spacetimes [129, 130]. Therefore, despite the existence of a substantial body of research devoted to the topic of quantum field theory in curved spacetime, e.g. [66, 67], any phenomenon in which the notion of an individual particle is essential becomes much more challenging in a generic curved spacetime. Examples of such phenomena include all types of mixing, e.g. Primakoff mixing [33–36] and neutrino mixing [131–133]. In order to handle such problems, an attractive approach is to choose a coordinate system such that spacetime is locally flat about a given point; this is always possible, as a consequence of the equivalence principle. In such a coordinate system, the metric acquires corrections as one moves away from this central point. Denoting these coordinates as ξ^μ and the point about which they are defined as ξ^μ_0,

the metric in these coordinates is given by

$$g_{\mu\nu} = \eta_{\mu\nu} + O\left((\xi - \xi_0)^2\right). \tag{3.1}$$

Within a certain radius of ξ_0, such that the corrections to the metric are small, one may treat spacetime as flat with perturbative corrections, and in this spacetime one may construct an effective field theory (EFT).

It should be noted that the process of constructing this EFT is not straightforward, as the graviton's massless propagator introduces nonlocal corrections [78]. Treating these nonlocal corrections is the topic of the following chapter. In this chapter, we provide a mathematical exposition on the construction of the aforementioned coordinate system and the properties of the metric in that coordinate system.

The most common example of a locally flat coordinate system is Riemann normal coordinates (see [79] for a review). In general, Riemann normal coordinates will have the form

$$\xi^\mu = \xi_0^\mu + a^\mu s + \frac{1}{3!}A^\mu_{\alpha_1\alpha_2\alpha_3}a^{\alpha_1}a^{\alpha_2}a^{\alpha_3}s^3 + \frac{1}{4!}A^\mu_{\alpha_1\alpha_2\alpha_3\alpha_4}a^{\alpha_1}a^{\alpha_2}a^{\alpha_3}a^{\alpha_4}s^4 + \cdots, \tag{3.2}$$

where a^μ is a vector tangent at ξ_0 to the geodesic connecting ξ_0 with ξ, s is an affine parameter, and $A^\mu_{\alpha_1\ldots\alpha_n}$ are constant tensors that are totally symmetric in their lower indices. The choice of the values for $A^\mu_{\alpha_1\ldots\alpha_n}$ is a gauge choice; any values of $A^\mu_{\alpha_1\ldots\alpha_n}$ represent a valid coordinate definition, and thus there exist multiple Riemann normal coordinates [134]. In practice, it is common to consider only the lowest-order term:

$$\xi^\mu = \xi_0^\mu + a^\mu s. \tag{3.3}$$

This may be viewed as an approximation of eq. 3.2, or as a coordinate definition in

its own right.

Both eqs. 3.2 and 3.3 define Riemann normal coordinates, in that in both coordinates the metric will satisfy eq. 3.1. To distinguish between the two, we refer to eq. 3.3 as linear Riemann normal coordinates (LRNC) and eq. 3.2 as nonlinear Riemann normal coordinates (NRNC). An equivalent way of defining LRNC and NRNC is that LRNC are an approximation of eq. 3.2 in which all higher-order terms are neglected, whereas NRNC indicates the preservation of these higher-order terms. We stress that the distinction between LRNC and NRNC is not common in the literature, and the terms LRNC and NRNC are novel to this thesis. The distinction is important insofar as including the additional terms in eq. 3.2 will cause NRNC to have different properties than LRNC. Most relevantly, the derivatives of the metric evaluated at the origin will have different values in NRNC than in LRNC. The vast majority of literature concerns LRNC (i.e., neglecting higher-order terms in the definition of ξ^μ), and the author is unaware of any systematic exposition on the properties of NRNC. The following chapter will make use of the higher-order terms in eq. 3.2, and therefore it is valuable to discuss the properties of NRNC, highlighting the ways in which it is both similar to and distinct from the more commonly-used LRNC.

One important caveat is that the definitions of both LRNC and NRNC assume a unique geodesic connecting ξ_0 and ξ, but this is not the case for all pairs of points in spacetime. For example, consider two particles traveling along the ISCO of a Schwarzschild black hole in opposite directions, beginning at the same point. The point in spacetime at which the particles' paths re-intersect is connected to the starting point by two distinct geodesics. A more famous example of this phenomenon would be gravitational lensing. Thus Riemann normal coordinates are only defined within the normal neighborhood of ξ_0, i.e. the region of spacetime in which all points are connected to ξ_0 by a unique geodesic. See [135] for details on the determination

of normal neighborhoods in an arbitrary spacetime. In practice, normal neighborhoods are often large enough that, at their edge, the deviation of the metric from the Minkowski metric is significant. Riemann normal coordinates (both LRNC and NRNC) are typically convenient only insofar as the metric is an approximation of the Minkowski metric, and therefore one typically restricts the use of Riemann normal coordinates to a patch of spacetime wherein this approximation holds. If this patch of spacetime is contained within the normal neighborhood of ξ_0, then the restriction on the definition of Riemann normal coordinates is of no practical concern.

We discuss LRNC, which is more commonly used in the literature than NRNC, in the following section. We will prove several important properties. The section after that discusses NRNC, comparing it with LRNC. Following that, we discuss the treatment of gravitational waves in Riemann normal coordinates. Throughout this chapter, we work in a metric with $(+---)$ signature. Before proceeding, we will define some useful notation.

3.1.1. Notation

We use brackets to indicate symmetrization in the standard way, e.g.

$$T_{(\mu\nu\rho)} = \frac{1}{6}\left(T_{\mu\nu\rho} + T_{\mu\rho\nu} + T_{\nu\mu\rho} + T_{\nu\rho\mu} + T_{\rho\mu\nu} + T_{\rho\nu\mu}\right). \tag{3.4}$$

However, we will often find it necessary to exclude an index from symmetrization. Whenever we place a dot over an index, it indicates that that index is exempt from any symmetrization brackets surrounding it. For example, in contrast with eq. 3.4,

$$T_{(\mu\dot{\nu}\rho)} = \frac{1}{2}\left(T_{\mu\nu\rho} + T_{\rho\nu\mu}\right). \tag{3.5}$$

We define the generalized connection, for $n \geq 3$, as

$$\Gamma^{\mu}_{\alpha_1 \ldots \alpha_n} = \Gamma^{\mu}_{(\alpha_1 \ldots \alpha_{n-1}, \alpha_n)} - (n-1)\Gamma^{\mu}_{\nu(\alpha_1 \ldots \alpha_{n-2}}\Gamma^{\nu}_{\alpha_{n-1}\alpha_n)}. \tag{3.6}$$

Note that the generalized connection is totally symmetric in its lower indices. It should be emphasized that, when we wish to refer to $\Gamma^{\mu}_{\alpha_1 \ldots \alpha_n}$ for $n \geq 3$, we will *always* use the term "generalized connection"; if the word "connection" appears without being preceded by the word "generalized," then we are referring to $\Gamma^{\mu}_{\alpha_1 \alpha_2}$ (i.e., the $n = 2$ case).

Section 3.2

Linear Coordinates

We begin by noting two gauge choices we are free to make within LRNC. The first is to contract ξ^{μ} with a tetrad, e^{α}_{μ}:

$$\xi'^{\alpha} = e^{\alpha}_{\mu}\xi^{\mu} \qquad \xi'^{\alpha}_0 = e^{\alpha}_{\mu}\xi^{\mu}_0 \qquad a'^{\alpha} = e^{\alpha}_{\mu}a^{\mu}, \tag{3.7}$$

resulting in new coordinates

$$\xi'^{\alpha} = \xi'^{\alpha}_0 + a'^{\alpha}s \tag{3.8}$$

Because s has retained its meaning as an affine parameter along a geodesic, a'^{α} is tangent at ξ'_0 to the geodesic connecting ξ'_0 with ξ'; in other words, eq. 3.8 defines a LRNC. This means we may freely choose whichever e^{α}_{μ} is convenient, and this corresponds to defining the axes of our coordinate system. Under the choice of e^{α}_{μ}, the metric transforms as

$$g'^{\alpha\beta} = e^{\alpha}_{\mu}e^{\beta}_{\nu}g^{\mu\nu}, \tag{3.9}$$

and thus we may freely choose our axes such that $g_{\mu\nu}\Big|_{\xi_0} = \eta_{\mu\nu}$.

As we will show later, $g_{\mu\nu,\alpha}\Big|_{s=0} = 0$, and therefore we arrive at

$$g_{\mu\nu} = \eta_{\mu\nu} + O\left((\xi - \xi_0)^2\right), \tag{3.10}$$

characterizing the rate at which the metric in LRNC deviates from Minkowski metric.

The second choice we may make is rescaling,

$$a^\mu \to \alpha\, a^\mu \qquad\qquad s \to \alpha^{-1}\, s, \tag{3.11}$$

under which eq. 3.3 is plainly invariant. A particularly useful rescaling (valid only when a^μ is not tangent to a null geodesic) is to make a^μ a unit vector, i.e. $\eta_{\mu\nu}a^\mu a^\nu = \pm 1$, with $+$ corresponding to a timelike geodesic and $-$ corresponding to a spacelike geodesic. In this case, the proper distance L along the geodesic from ξ_0 to ξ has a useful relationship with s. To show this, we note that, because s is an affine parameter of the geodesic, $\frac{\mathrm{d}L}{\mathrm{d}s}$ is constant along a geodesic (this is a general property of any affine parameter of a geodesic [136]). Therefore

$$\begin{aligned} L &= \int \frac{\mathrm{d}L}{\mathrm{d}s}\mathrm{d}s = \frac{\mathrm{d}L}{\mathrm{d}s}\bigg|_{s=0}\int \mathrm{d}s = \sqrt{-g_{\mu\nu}\frac{\mathrm{d}\xi^\mu}{\mathrm{d}s}\frac{\mathrm{d}\xi^\nu}{\mathrm{d}s}}\bigg|_{s=0} s = \sqrt{-\eta_{\mu\nu}a^\mu a^\nu}\, s \\ &= \begin{cases} is & a^\mu \text{ timelike} \\ s & a^\mu \text{ spacelike} \end{cases}. \end{aligned} \tag{3.12}$$

Going forward, we will assume a^μ is a unit vector.

3.2.1. Important Properties of LRNC

There are two important properties of LRNC. The first is that, in LRNC, all partial derivatives of the connection, when symmetrized over the lower indices, vanish when

evaluated at the origin:

$$\Gamma^{\mu}_{(\alpha_1\alpha_2,\alpha_3\ldots\alpha_n)}\Big|_{s=0} = 0, \tag{3.13}$$

for all $n \geq 2$. The second is that the partial derivatives of the metric, evaluated at the origin, may be expressed in terms of the Riemann tensor and its covariant derivatives, in a specific form. Specifically, any partial derivative of the metric is a linear combination of terms of the following form, written in shorthand:

$$g_{--,\cdots}\Big|_{s=0} \supset R_{\cdots}\, R^{-}{}_{\cdots} \cdots R^{-}{}_{\cdots}\Big|_{s=0}, \tag{3.14}$$

where where dashes indicate a single index, and dots indicate some number of indices (which may include indices corresponding to covariant derivatives). Necessarily, some of these indices will be dummy indices, while others will correspond to the indices of $g_{--,\cdots}$. As a concrete example [79]:

$$g_{\mu\nu,\alpha\beta\gamma\delta}\Big|_{s=0} = \frac{2}{15}\left(8R_{\mu(\alpha\beta\dot{\rho}}R^{\rho}{}_{\gamma\delta)\nu} + 9R_{\mu(\alpha\beta\dot{\nu};\gamma\delta)}\right)\Big|_{s=0}, \tag{3.15}$$

which uses the dot notation defined earlier, and a semicolon indicates the covariant derivative.

In this subsection, we will first prove that LRNC necessarily satisfy these two properties (i.e., eqs 3.13 and 3.14). These proofs are adapted from [79]. We will then show that if either of these properties are satisfied, then our coordinates must be LRNC; we will do this by showing that eqs. 3.13 and 3.14 each (separately) imply eq. 3.3. That is, if one knows that eq. 3.13 holds *or* that all derivatives of the metric evaluated at the origin have the form given by eq. 3.14, then one immediately knows that one is working in LRNC. In other words, we will show that eqs. 3.3, 3.13, and 3.14 are logically equivalent. This latter set of proofs is original work.

Lemma 1. *In any coordinate system, the coordinates x^μ as one moves along a geodesic are given by*

$$x^\mu = x_0^\mu + b^\mu s - \sum_{n=2}^{\infty} \frac{1}{n!} \Gamma^\mu_{\alpha_1 \dots \alpha_n}\Big|_{s=0} b^{\alpha_1} \cdots b^{\alpha_n} s^n, \tag{3.16}$$

where $b^\mu = \frac{dx^\mu}{ds}\Big|_{s=0}$.

Proof. Because s is an affine parameter, we may describe x^μ as one moves along the geodesic by the geodesic equation:

$$\frac{\mathrm{d}^2 x^\mu}{\mathrm{d}s^2} = -\Gamma^\mu_{\alpha\beta} \frac{\mathrm{d}x^\alpha}{\mathrm{d}s} \frac{\mathrm{d}x^\beta}{\mathrm{d}s}. \tag{3.17}$$

More generally, for $n \geq 2$,

$$\frac{\mathrm{d}^n x^\mu}{\mathrm{d}s^n} = -\Gamma^\mu_{\alpha_1 \dots \alpha_n} \frac{\mathrm{d}x^{\alpha_1}}{\mathrm{d}s} \cdots \frac{\mathrm{d}x^{\alpha_n}}{\mathrm{d}s}, \tag{3.18}$$

which may be shown by induction:

$$\begin{aligned}
\frac{\mathrm{d}^{n+1} x^\mu}{\mathrm{d}s^{n+1}} &= \frac{\mathrm{d}}{\mathrm{d}s} \left(-\Gamma^\mu_{\alpha_1 \dots \alpha_n} \frac{\mathrm{d}x^{\alpha_1}}{\mathrm{d}s} \cdots \frac{\mathrm{d}x^{\alpha_n}}{\mathrm{d}s} \right) \\
&= -\left(\frac{\mathrm{d}}{\mathrm{d}s} \Gamma^\mu_{\alpha_1 \dots \alpha_n} \right) \frac{\mathrm{d}x^{\alpha_1}}{\mathrm{d}s} \cdots \frac{\mathrm{d}x^{\alpha_n}}{\mathrm{d}s} - n \Gamma^\mu_{\alpha_1 \dots \alpha_n} \frac{\mathrm{d}x^{\alpha_1}}{\mathrm{d}s} \cdots \frac{\mathrm{d}x^{\alpha_{n-1}}}{\mathrm{d}s} \frac{\mathrm{d}^2 x^{\alpha_n}}{\mathrm{d}s^2} \\
&= -\Gamma^\mu_{\alpha_1 \dots \alpha_n, \alpha_{n+1}} \frac{\mathrm{d}x^{\alpha_1}}{\mathrm{d}s} \cdots \frac{\mathrm{d}x^{\alpha_{n+1}}}{\mathrm{d}s} \\
&\quad + n \Gamma^\mu_{\alpha_1 \dots \alpha_n} \Gamma^{\alpha_n}_{\alpha_{n+1} \alpha_{n+2}} \frac{\mathrm{d}x^{\alpha_1}}{\mathrm{d}s} \cdots \frac{\mathrm{d}x^{\alpha_{n-1}}}{\mathrm{d}s} \frac{\mathrm{d}x^{\alpha_{n+1}}}{\mathrm{d}s} \frac{\mathrm{d}x^{\alpha_{n+2}}}{\mathrm{d}s} \\
&= -\Gamma^\mu_{\alpha_1 \dots \alpha_{n+1}} \frac{\mathrm{d}x^{\alpha_1}}{\mathrm{d}s} \cdots \frac{\mathrm{d}x^{\alpha_{n+1}}}{\mathrm{d}s}.
\end{aligned} \tag{3.19}$$

Evaluating at the origin:

$$\frac{\mathrm{d}^n x^\mu}{\mathrm{d}s^n}\Big|_{s=0} = -\Gamma^\mu_{\alpha_1 \dots \alpha_n}\Big|_{s=0} a^{\alpha_1} \cdots a^{\alpha_n}. \tag{3.20}$$

Performing a Taylor expansion of x^μ yields eq. 3.16. □

Theorem 1. *In any LRNC defined by eq. 3.3, eq. 3.13 holds.*

Proof. Comparing eq. 3.16 with eq. 3.3, we see that we must have

$$\Gamma^\mu_{\alpha_1\ldots\alpha_n}\Big|_{s=0} a^{\alpha_1}\cdots a^{\alpha_n} = 0 \tag{3.21}$$

for all $n \geq 2$. Because lemma 1 applies for any geodesic, eq. 3.21 must hold for any value of a^μ. The only way for this to be possible is if

$$\Gamma^\mu_{\alpha_1\ldots\alpha_n}\Big|_{s=0} = 0 \tag{3.22}$$

for all $n \geq 2$.

From eq. 3.6, the generalized connection may clearly be written in terms of only the connection and its partial derivatives, where the highest-order derivative within the expression for $\Gamma^\mu_{\alpha_1\ldots\alpha_n}$ is $(n-2)^{\text{th}}$-order (this may easily be shown by induction). A general term in this expression will have the form

$$\Gamma^\mu_{\alpha_1\ldots\alpha_n} \supset \Gamma^-_{--,\cdots}\,\Gamma^-_{--,\cdots}\cdots\Gamma^-_{--,\cdots}, \tag{3.23}$$

using the same shorthand defined earlier. If this term contains m factors of the connection (or a partial derivative of it), then there are m upper indices, of which $m-1$ must be dummy indices. This of course means that there must be $m-1$ dummy indices among the lower indices, with the rest being $\alpha_1,\ldots,\alpha_n$. By the pigeonhole principle,* there must be at least one Γ in each term whose lower indices are only drawn from $\alpha_1,\ldots,\alpha_n$. Because $\Gamma^\mu_{\alpha_1\ldots\alpha_n}$ is totally symmetric in its lower indices, we

*The pigeonhole principles that if more than n items are being sorted into n categories, then there must be at least one category containing multiple items. Similarly, if fewer than n items are being sorted into n categories, then there must be at least one category that remains empty.

may freely symmetrize the α's in the right-hand side of eq. 3.23, and thus we see that each term in the expression for $\Gamma^{\mu}_{\alpha_1\ldots\alpha_n}$ will contain either a connection or a partial derivative of the connection wherein all lower indices are symmetrized. A corollary of this is that the highest-order term in $\Gamma^{\mu}_{\alpha_1\ldots\alpha_n}$ is $\Gamma^{\mu}_{(\alpha_1\alpha_2,\alpha_3\ldots\alpha_n)}$.

We may now prove our theorem by induction. Eq. 3.22 clearly implies that eq. 3.13 holds for $n = 2$. To prove the theorem for greater n, consider $\Gamma^{\mu}_{\alpha_1\ldots\alpha_{n+1}}\Big|_{s=0}$. We have established that this may be written in terms of the connection and its partial derivatives, with each term containing at least one connection (or a partial derivative thereof) that is symmetrized over all lower indices. Thus, if eq. 3.13 holds up to some value of n, then all terms in the expression for $\Gamma^{\mu}_{\alpha_1\ldots\alpha_{n+1}}\Big|_{s=0}$ will vanish except for the highest-order term:

$$\Gamma^{\mu}_{\alpha_1\ldots\alpha_{n+1}}\Big|_{s=0} = \Gamma^{\mu}_{(\alpha_1\alpha_2,\alpha_3\ldots\alpha_{n+1})}\Big|_{s=0}. \tag{3.24}$$

From eq. 3.22, it follows that eq. 3.13 holds up to $n+1$. □

A special case worth noting is

$$\Gamma^{\mu}_{\alpha\beta}\Big|_{s=0} = 0, \tag{3.25}$$

which implies that $g_{\mu\nu,\alpha}\Big|_{s=0} = 0$.

Lemma 2. *In any LRNC defined by eq. 3.3,* $R^{\rho}{}_{(\sigma\mu\dot{\nu},\alpha_1\ldots\alpha_n)}\Big|_{s=0}$ *may be expressed in terms of the Riemann tensor and its covariant derivatives evaluated at the origin, and the connection and its partial derivatives of the form* $\Gamma^{\tau}_{\kappa(\lambda,\beta_1\ldots\beta_m)}\Big|_{s=0}$*, where* $\{\lambda,\beta_1,\ldots,\beta_m\} \subseteq \{\alpha_1,\ldots,\alpha_n\}$.

Proof. In general, the partial derivatives of a tensor may be expressed in terms of the covariant derivative along with some Christoffel symbols. Thus, by repeatedly

expanding partial derivatives of the Riemann tensor in this way, it is possible to write

$$R^{\rho}{}_{\sigma\mu\nu,\alpha_1\ldots\alpha_n} = R^{\rho}{}_{\sigma\mu\nu;\alpha_1\ldots\alpha_n} + Q^{\rho}{}_{\sigma\mu\nu\alpha_1\ldots\alpha_n}, \tag{3.26}$$

where Q may be expressed in terms of the Riemann tensor and its covariant derivatives and the connection and its partial derivatives. From the expression for the covariant derivative of an arbitrary tensor, in terms of the partial derivative and the connection, we see that all connections will be of the form $\Gamma^{\tau}_{\kappa\lambda,\beta_1\ldots\beta_m}$, where $\{\lambda,\beta_1,\ldots,\beta_m\} \subseteq \{\alpha_1,\ldots,\alpha_n\}$ and κ either is an element of $\{\sigma,\mu,\nu\}$ or is a dummy index internal to Q. Therefore, if we symmetrize over σ, μ, and $\alpha_1,\ldots,\alpha_n$, all connections will have the form $\Gamma^{\tau}_{(\kappa\lambda,\beta_1\ldots\beta_m)}$ (if $\kappa \in \{\sigma,\mu\}$) or $\Gamma^{\tau}_{\kappa(\lambda,\beta_1\ldots\beta_m)}$ (if not). When we evaluate at the origin, the former vanishes by theorem 1. Thus,

$$R^{\rho}{}_{(\sigma\mu\dot{\nu},\alpha_1\ldots\alpha_n)}\Big|_{s=0} = R^{\rho}{}_{(\sigma\mu\dot{\nu};\alpha_1\ldots\alpha_n)}\Big|_{s=0} + Q^{\rho}{}_{(\sigma\mu\dot{\nu}\alpha_1\ldots\alpha_n)}\Big|_{s=0}, \tag{3.27}$$

and the latter term contains only the Riemann tensor and its covariant derivatives evaluated at the origin and the connection and its partial derivatives of the form $\Gamma^{\tau}_{\kappa(\lambda,\beta_1\ldots\beta_m)}\Big|_{s=0}$. □

Lemma 3. *In any LRNC defined by eq. 3.3,* $\Gamma^{\rho}_{\sigma(\alpha_1,\alpha_2\ldots\alpha_n)}\Big|_{s=0}$ *may be expressed in terms of the Riemann tensor and its covariant derivatives evaluated at the origin.*

Proof. Considering a (higher-order) partial derivative of the Riemann tensor, symmetrized over most of its indices and evaluated at the origin:

$$\begin{aligned} R^{\rho}{}_{(\sigma\mu\dot{\nu},\alpha_1\ldots\alpha_n)}\Big|_{s=0} &= \Bigg(\Gamma^{\rho}_{\nu(\sigma,\mu\alpha_1\ldots\alpha_n)} - \Gamma^{\rho}_{(\mu\sigma,\alpha_1\ldots\alpha_n)\nu} \\ &\qquad + \left(\Gamma^{\rho}_{\lambda(\mu}\Gamma^{\lambda}_{\dot{\nu}\sigma}\right)_{,\alpha_1\ldots\alpha_n)} - \left(\Gamma^{\rho}_{\lambda\nu}\Gamma^{\lambda}_{(\mu\sigma)}\right)_{,\alpha_1\ldots\alpha_n)}\Bigg)\Bigg|_{s=0} \\ &= \left(\Gamma^{\rho}_{\nu(\sigma,\mu\alpha_1\ldots\alpha_n)} - \Gamma^{\rho}_{(\mu\sigma,\alpha_1\ldots\alpha_n)\nu} + \left(\Gamma^{\rho}_{\lambda(\mu}\Gamma^{\lambda}_{\dot{\nu}\sigma}\right)_{,\alpha_1\ldots\alpha_n)}\right)\Bigg|_{s=0}, \end{aligned} \tag{3.28}$$

where the last term in the first line vanishes as a result of theorem 1. Next, we consider all the terms in $\Gamma^{\rho}_{(\mu\sigma,\alpha_1\ldots\alpha_n\nu)}$, and divide them into two categories: terms in which ν appears in the first two indices, and terms in which ν appears in the last $n+1$ indices. Because $\Gamma^{\rho}_{(\mu\sigma,\alpha_1\ldots\alpha_n\nu)}$ is separately symmetrized over these two sets of indices, doing so gives us the expression

$$(n+3)!\Gamma^{\rho}_{(\mu\sigma,\alpha_1\ldots\alpha_n\nu)} = 2(n+2)!\Gamma^{\rho}_{\nu(\sigma,\mu\alpha_1\ldots\alpha_n)} + (n+1)(n+2)!\Gamma^{\rho}_{(\mu\sigma,\alpha_1\ldots\alpha_n)\nu}. \tag{3.29}$$

Evaluating at the origin gives

$$\Gamma^{\rho}_{(\mu\sigma,\alpha_1\ldots\alpha_n)\nu}\Big|_{s=0} = \frac{-2}{n+1}\,\Gamma^{\rho}_{\nu(\sigma,\mu\alpha_1\ldots\alpha_n)}\Big|_{s=0}. \tag{3.30}$$

Substituting this into eq. 3.28 gives

$$\Gamma^{\rho}_{\nu(\sigma,\mu\alpha_1\ldots\alpha_n)}\Big|_{s=0} = \frac{n+1}{n+3}\left(R^{\rho}{}_{(\sigma\mu\dot{\nu},\alpha_1\ldots\alpha_n)}\Big|_{s=0} - \left(\Gamma^{\rho}_{\lambda(\mu}\Gamma^{\lambda}_{\dot{\nu}\sigma}\right)_{,\alpha_1\ldots\alpha_n)}\Big|_{s=0}\right). \tag{3.31}$$

By lemma 2, the first term may be expressed in terms of the Riemann tensor and its covariant derivatives evaluated at the origin, and partial derivatives of the connection of the form $\Gamma^{\tau}_{\kappa(\lambda,\beta_1\ldots\beta_m)}\Big|_{s=0}$, where $\{\lambda,\beta_1,\ldots,\beta_m\}\subseteq\{\alpha_1,\ldots,\alpha_n\}$. Therefore, all derivatives of the connection appearing within $R^{\rho}{}_{(\sigma\mu\dot{\nu},\alpha_1\ldots\alpha_n)}\Big|_{s=0}$ are at most order $n-1$. When the second term in eq. 3.31 is expanded via the product rule, all terms in which the first connection is not differentiated will vanish, as a result of eq. 3.25. Thus, all partial derivatives of the connection appearing within $\left(\Gamma^{\rho}_{\lambda(\mu}\Gamma^{\lambda}_{\dot{\nu}\sigma}\right)_{,\alpha_1\ldots\alpha_n)}\Big|_{s=0}$ are at most order $n-1$. Furthermore, all partial derivatives of the connection appearing within $\left(\Gamma^{\rho}_{\lambda(\mu}\Gamma^{\lambda}_{\dot{\nu}\sigma}\right)_{,\alpha_1\ldots\alpha_n)}\Big|_{s=0}$ will be of the form $\Gamma^{\tau}_{\kappa(\lambda,\beta_1\ldots\beta_m)}\Big|_{s=0}$. Thus, we may apply eq. 3.31 recursively, successively removing derivatives of the connection. Since each application of eq. 3.31 is guaranteed to decrease the highest order within the

expression for $\Gamma^{\rho}_{\nu(\sigma,\mu\alpha_1\ldots\alpha_n)}\Big|_{s=0}$, this process is guaranteed to terminate when all connections are undifferentiated (and therefore vanish per eq. 3.25). At this point, one is left with an expression for $\Gamma^{\rho}_{\nu(\sigma,\mu\alpha_1\ldots\alpha_n)}\Big|_{s=0}$ solely in terms of the Riemann tensor and its covariant derivatives evaluated at the origin. □

Theorem 2. *In any LRNC defined by eq. 3.3, eq. 3.14 holds.*

Proof. Consider the Taylor expansion of the metric:

$$g_{\mu\nu} = \eta_{\mu\nu} + \sum_{n=1}^{\infty} \frac{1}{n!}\, g_{\mu\nu,\alpha_1\ldots\alpha_n}\Big|_{s=0} (\xi^{\alpha_1} - \xi_0^{\alpha_1}) \cdots (\xi^{\alpha_n} - \xi_0^{\alpha_n})\,. \tag{3.32}$$

The partial derivatives of the metric can be calculated using the identity

$$g_{\mu\nu,\alpha} = g_{\mu\rho}\Gamma^{\rho}_{\nu\alpha} + g_{\nu\rho}\Gamma^{\rho}_{\mu\alpha}, \tag{3.33}$$

and therefore

$$\begin{aligned} g_{\mu\nu,\alpha_1\ldots\alpha_n} &= \left(g_{\mu\rho}\Gamma^{\rho}_{\nu\alpha_1}\right)_{,\alpha_2\ldots\alpha_n} + \left(g_{\nu\rho}\Gamma^{\rho}_{\mu\alpha_1}\right)_{,\alpha_2\ldots\alpha_n} \\ &= \left(g_{\mu\rho}\Gamma^{\rho}_{\nu(\alpha_1}\right)_{,\alpha_2\ldots\alpha_n)} + \left(g_{\nu\rho}\Gamma^{\rho}_{\mu(\alpha_1}\right)_{,\alpha_2\ldots\alpha_n)}, \end{aligned} \tag{3.34}$$

where we arrived at the second line by noting that $g_{\mu\nu,\alpha_1\ldots\alpha_n}$ is symmetric over $\alpha_1 \ldots \alpha_n$. By repeatedly applying eq. 3.34, one can express $g_{\mu\nu,\alpha_1\ldots\alpha_n}$ in terms of $\Gamma^{\rho}_{\sigma(\beta_1,\beta_2\ldots\beta_m)}$, where $m \leq n$. From lemma 3, it follows that $g_{\mu\nu,\alpha_1\ldots\alpha_n}\Big|_{s=0}$ may be expressed in terms of only the Riemann tensor and its covariant derivatives evaluated at the origin.

The Riemann tensor and its covariant derivatives, as introduces into the expression for $g_{\mu\nu,\alpha_1\ldots\alpha_n}\Big|_{s=0}$, are of the form $R^{\rho}{}_{\sigma\mu\nu,\beta_1\ldots\beta_m}$. At no point in lemmas 2 and 3 did we introduce a contravariant metric, and thus we cannot have any upper indices besides the first index of each Riemann tensor. In contrast, the recursive application

of eq. 3.34 inevitable terminates with one factor of the covariant metric in each term. Thus, one (and only one) of the upper indices in each term of the expression for $g_{\mu\nu,\alpha_1\ldots\alpha_n}\Big|_{s=0}$ may be lowered. Thus every term in the expression for $g_{\mu\nu,\alpha_1\ldots\alpha_n}\Big|_{s=0}$ has the form given in eq. 3.14. □

The significance of theorem 2 may easily be seen by noting that the covariant derivative of the Riemann tensor is itself a tensor. If one knows the value of the Riemann tensor in some arbitrary coordinate system x^μ, and one also knows the tetrad that converts between x^μ and ξ^μ at the origin (and, as noted earlier, the choice for this tetrad is totally arbitrary), then one may contract the Riemann tensor (and its covariant derivatives) with these tetrads in order to find the value of the Riemann tensor and its covariant derivatives, in LRNC, evaluated at the origin. Thus, given any arbitrary coordinate system, we have an easy prescription for finding an expression for the metric in LRNC.

We now reverse the direction of implication:

Theorem 3. *If eq. 3.13 holds, then so too must eq. 3.3.*

Proof. From eq. 3.6, the generalized connection may clearly be written in terms of only the connection and its partial derivatives. A general term in this expression will have the form

$$\Gamma^\mu_{\alpha_1\ldots\alpha_n} \supset \Gamma^-_{--,\cdots}\,\Gamma^-_{--,\cdots}\cdots\Gamma^-_{--,\cdots}. \tag{3.35}$$

If this term contains m factors of the connection (or a partial derivative of it), then there are m upper indices, of which $m-1$ must be dummy indices. This of course means that there must be $m-1$ dummy indices among the lower indices, with the rest being $\alpha_1,\ldots,\alpha_n$. By the pigeonhole principle, there must be at least one Γ in each term whose lower indices are only drawn from $\alpha_1,\ldots,\alpha_n$. Because $\Gamma^\mu_{\alpha_1\ldots\alpha_n}$ is totally symmetric in its lower indices, we may freely symmetrize the α's in the right-hand

side of eq. 3.35, and thus we see that each term in the expression for $\Gamma^{\mu}_{\alpha_1\ldots\alpha_n}$ will contain either a connection or a partial derivative of the connection wherein all lower indices are symmetrized. Thus, by eq. 3.13, all terms will vanish, and we see that

$$\Gamma^{\mu}_{\alpha_1\ldots\alpha_n}\Big|_{s=0} = 0 \tag{3.36}$$

for all $n \geq 2$. Substituting this into lemma 1, we see that the coordinates as one moves along a geodesic from the point x_0^μ to x^μ are given by

$$x^\mu = x_0^\mu + b^\mu s, \tag{3.37}$$

which is the definition for a LRNC. □

Theorem 4. *If eq. 3.14 holds, then so too must eq. 3.3.*

Proof. Consider some term in eq. 3.14 containing m Riemann tensors (or covariant derivatives of the Riemann tensor). This term will have $m-1$ upper indices, which must all be dummy indices, as $g_{--,\ldots}\Big|_{s=0}$ has no upper indices. This obviously means there must be $m-1$ dummy indices among the lower indices. The Riemann tensor with a raised index, $R^{-}{}_{\ldots}$, contains one pair of antisymmetric indices, while the Riemann tensor with no raised indices, $R_{\ldots}$, contains two pairs of antisymmetric indices. Thus each term in $g_{--,\ldots}\Big|_{s=0}$ contains $m+1$ pairs of antisymmetric indices. By the pigeonhole principle, there must be at least two pairs of antisymmetric indices that do not contain any dummy indices. Thus, if we symmetrize all but one of the non-dummy indices, then we are guaranteed to symmetrize over at least one antisymmetric pair, causing the entire term to vanish. Therefore, for all $n \geq 1$,

$$g_{\mu(\nu,\alpha_1\ldots\alpha_n)}\Big|_{s=0} = 0 = g_{(\mu\nu,\alpha_1\ldots\alpha_{n-1})\alpha_n}\Big|_{s=0}. \tag{3.38}$$

Next consider the partial derivative of the connection, symmetrized over all lower indices and evaluated at the origin:

$$\Gamma^{\rho}_{(\mu\nu,\alpha_1\ldots\alpha_n)}\Big|_{s=0} = \frac{1}{2}\left(g^{\rho\lambda}\left(g_{\sigma(\mu,\nu} + g_{\sigma(\nu,\mu} - g_{(\mu\nu,\dot{\sigma}}\right)\right)_{,\alpha_1\ldots\alpha_n)}\Big|_{s=0}. \tag{3.39}$$

Expanding out the derivatives, we find that every term in $\Gamma^{\rho}_{(\mu\nu,\alpha_1\ldots\alpha_n)}\Big|_{s=0}$ contains a derivative of the metric of either of the forms in eq. 3.38, and therefore $\Gamma^{\rho}_{(\mu\nu,\alpha_1\ldots\alpha_n)}\Big|_{s=0}$ vanishes for all $n \geq 0$. Thus we see that eq. 3.14 implies eq. 3.13. From theorem 3, we know that eq. 3.13 implies eq. 3.3. □

Thus we see that eqs. 3.3, 3.13, and 3.14 may all serve as definitions of LRNC, as each one is logically equivalent to the other two.

Section 3.3

Nonlinear Riemann Normal Coordinates

We now turn to NRNC. Much of what was said about LRNC applies to NRNC. We may freely transform our basis with the use of tetrads, so that we may set $g_{\mu\nu}\Big|_{s=0} = \eta_{\mu\nu}$. We may freely rescale a^{μ} and s, making a^{μ} a unit vector. Our derivation of eq. 3.12 only relies on s being an affine parameter, so it holds for the case of NRNC.

Comparing eq. 3.16 with eq. 3.2 yields

$$\Gamma^{\mu}_{\alpha_1\ldots\alpha_n}\Big|_{s=0} = -A^{\mu}_{\alpha_1\ldots\alpha_n} \tag{3.40}$$

for $n \geq 3$, which serves as the NRNC analog to eq. 3.22. Similarly, we may see that $\Gamma^{\mu}_{\alpha\beta}\Big|_{s=0} = 0$, and thus we get that 3.10 holds for NRNC. However, the coefficients in the Taylor expansion of $g_{\mu\nu}$ will be different from what we found in LRNC. This is necessarily true as a consequence of eqs. 3.13 and 3.14 not holding in the case of

NRNC, which is the most important difference between LRNC and NRNC.

Indeed, despite having eq. 3.40 as an analog to eq. 3.22, there is no clear way to generalize the proofs in the previous section to NRNC. The reason for this relates to one particular step in the proof of theorem 1. As part of that proof, we established that each term in the expression for $\Gamma^{\mu}_{\alpha_1\ldots\alpha_n}$ will contain either a connection or a partial derivative of the connection wherein all lower indices are symmetrized. Note however that we could not guarantee that *all* partial derivatives of the connection appearing in the expression for $\Gamma^{\mu}_{\alpha_1\ldots\alpha_n}$ will have all of their lower indices symmetrized. When proving theorem 1, this was not an issue, as our inductive step caused the entire term to vanish; that is to say, making an assumption about $\Gamma^{\mu}_{(\alpha_1\alpha_2,\alpha_3\ldots\alpha_n)}\Big|_{s=0}$ allowed us to treat all Γ's, whether or not they were symmetrized over all of the lower indices. However, in the case of NRNC, we know that $\Gamma^{\mu}_{(\alpha_1\alpha_2,\alpha_3\ldots\alpha_n)}\Big|_{s=0}$ is generally nonzero, and therefore we cannot remove these terms in their entirety. Thus the expression for $\Gamma^{\mu}_{\alpha_1\ldots\alpha_n}$ will contain partial derivatives of the connection that are not symmetrized over all lower indices, and we do not have an obvious way to deal with these. Thus our proof of theorem 1 cannot be adapted to NRNC. Because theorem 1 was used in our proof of theorem 2, this also prevents us from generalizing theorem 2 to NRNC.

Instead, to calculate derivatives of the metric in NRNC, the most expedient option is to begin by calculating the derivatives in LRNC, and then performing a coordinate transformation to NRNC. Defining $v^{\mu} = a^{\mu}s$, we see that

$$\begin{aligned}
\frac{\partial\xi^{\mu}_{\text{NRNC}}}{\partial\xi^{\rho}_{\text{LRNC}}} &= \frac{\partial\xi^{\mu}_{\text{NRNC}}}{\partial v^{\rho}} \\
&= \delta^{\mu}_{\rho} + \frac{1}{2!}A^{\mu}_{\alpha_1\alpha_2\rho}v^{\alpha_1}v^{\alpha_2} + \frac{1}{3!}A^{\mu}_{\alpha_1\alpha_2\alpha_3\rho}v^{\alpha_1}v^{\alpha_2}v^{\alpha_3} + \cdots \qquad (3.41) \\
\frac{\partial\xi^{\rho}_{\text{LRNC}}}{\partial\xi^{\mu}_{\text{NRNC}}} &= \frac{\partial v^{\rho}}{\partial\xi^{\mu}_{\text{NRNC}}} \\
&= \delta^{\rho}_{\mu} + \frac{1}{2!}B^{\rho}_{\alpha_1\alpha_2\mu}v^{\alpha_1}v^{\alpha_2} + \frac{1}{3!}B^{\rho}_{\alpha_1\alpha_2\alpha_3\mu}v^{\alpha_1}v^{\alpha_2}v^{\alpha_3} + \cdots , \qquad (3.42)
\end{aligned}$$

where the coefficients $B^{\rho}_{\alpha_1\ldots\alpha_n\mu}$ may be found by recognizing $\frac{\partial\xi^{\mu}_{\text{NRNC}}}{\partial\xi^{\rho}_{\text{LRNC}}}\frac{\partial\xi^{\rho}_{\text{LRNC}}}{\partial\xi^{\nu}_{\text{NRNC}}} = \delta^{\mu}_{\nu}$, contracting eqs. 3.41 and 3.42, and going order-by-order. Note that the lowest-order terms in the coordinate transformations are Kronecker deltas, meaning that any tensor evaluated at the origin will have the same value in both LRNC and NRNC. Importantly, this applies to the Riemann tensor and its covariant derivatives.

Thus, given the derivatives of the metric in LRNC, calculated using the techniques in the previous section, we may calculate the metric in NRNC:

$$g^{\text{NRNC}}_{\mu\nu} = g^{\text{LRNC}}_{\rho\sigma}\frac{\partial\xi^{\rho}_{\text{LRNC}}}{\partial\xi^{\mu}_{\text{NRNC}}}\frac{\partial\xi^{\sigma}_{\text{LRNC}}}{\partial\xi^{\nu}_{\text{NRNC}}}, \tag{3.43}$$

where the coefficients in the Taylor expansion for $\frac{\partial\xi^{\rho}_{\text{LRNC}}}{\partial\xi^{\mu}_{\text{NRNC}}}$ may be expressed in terms of $A^{\mu}_{\alpha_1\ldots\alpha_n}$. The coefficients in the Taylor expansion for $g^{\text{LRNC}}_{\rho\mu}$ may be expressed in terms of the Riemann tensor and its covariant derivatives evaluated at the origin, as proven in the previous section, and the Riemann tensor (and its covariant derivatives) evaluated at the origin are the same in both LRNC and NRNC. Thus we arrive at our key result for NRNC:

Theorem 5. *In any NRNC defined by eq. 3.2, any derivative of the metric evaluated at the origin may be written in terms of the Riemann tensor and its covariant derivatives evaluated at the origin and the coefficients* $A^{\mu}_{\alpha_1\ldots\alpha_n}$.

For example, we find that the metric out to fourth order in s is given by

$$\begin{aligned} g_{\mu\nu} = \eta_{\mu\nu} &+ \left(\frac{1}{3}\, \overline{R}_{\alpha_1\mu\nu\alpha_2}\Big|_{s=0} - \eta_{\rho(\mu} A^{\rho}_{\nu)\alpha_1\alpha_2} \right) a^{\alpha_1} a^{\alpha_2} s^2 \\ &+ \left(\frac{1}{6}\, \overline{R}_{\alpha_1\mu\nu\alpha_2;\alpha_3}\Big|_{s=0} - \frac{1}{3} \eta_{\rho(\mu} A^{\rho}_{\nu)\alpha_1\alpha_2\alpha_3} \right) a^{\alpha_1} a^{\alpha_2} a^{\alpha_3} s^3 \\ &+ \left(\frac{1}{20}\, \overline{R}_{\alpha_1\mu\nu\alpha_2;\alpha_3\alpha_4}\Big|_{s=0} + \frac{2}{45}\, \overline{R}_{\rho\alpha_1\alpha_2\mu}\Big|_{s=0}\, \overline{R}^{\rho}{}_{\alpha_3\alpha_4\nu}\Big|_{s=0} \right. \\ &\quad - \frac{1}{3}\, \overline{R}_{\rho\alpha_1\alpha_2(\mu}\Big|_{s=0} A^{\rho}_{\nu)\alpha_3\alpha_4} + \frac{1}{4} \eta_{\rho\sigma} A^{\rho}_{\alpha_1\alpha_2\mu} A^{\sigma}_{\alpha_3\alpha_4\nu} \\ &\quad \left. - \frac{1}{12} \eta_{\rho(\mu} A^{\rho}_{\nu)\alpha_1\alpha_2\alpha_3\alpha_4} + \frac{1}{2} \eta_{\rho(\mu} A^{\sigma}_{\nu)\alpha_1\alpha_2} A^{\rho}_{\alpha_3\alpha_4\sigma} \right) a^{\alpha_1} a^{\alpha_2} a^{\alpha_3} a^{\alpha_4} s^4 \\ &+ O(s^5). \end{aligned} \tag{3.44}$$

Similarly, the Taylor series for the contravariant metric may be found using

$$g^{\mu\nu}_{\mathrm{NRNC}} = g^{\rho\sigma}_{\mathrm{LRNC}} \frac{\partial \xi^{\mu}_{\mathrm{NRNC}}}{\partial \xi^{\rho}_{\mathrm{LRNC}}} \frac{\partial \xi^{\nu}_{\mathrm{NRNC}}}{\partial \xi^{\sigma}_{\mathrm{LRNC}}}, \tag{3.45}$$

which yields

$$\begin{aligned} g^{\mu\nu} = \eta^{\mu\nu} &- \left(\frac{1}{3}\, \overline{R}_{\alpha_1}{}^{\mu\nu}{}_{\alpha_2}\Big|_{s=0} - \eta^{\rho(\mu} A^{\nu)}_{\alpha_1\alpha_2\rho} \right) a^{\alpha_1} a^{\alpha_2} s^2 \\ &- \left(\frac{1}{6}\, \overline{R}_{\alpha_1}{}^{\mu\nu}{}_{\alpha_2;\alpha_3}\Big|_{s=0} - \frac{1}{3} \eta^{\rho(\mu} A^{\nu)}_{\alpha_1\alpha_2\alpha_3\rho} \right) a^{\alpha_1} a^{\alpha_2} a^{\alpha_3} s^3 \\ &- \left(\frac{1}{20}\, \overline{R}_{\alpha_1}{}^{\mu\nu}{}_{\alpha_2;\alpha_3\alpha_4}\Big|_{s=0} - \frac{1}{15}\, \overline{R}^{\rho}{}_{\alpha_1\alpha_2}{}^{\mu}\Big|_{s=0}\, \overline{R}^{\nu}{}_{\alpha_3\alpha_4\rho}\Big|_{s=0} \right. \\ &\quad + \frac{1}{3}\, \overline{R}^{\rho}{}_{\alpha_1\alpha_2}{}^{(\mu}\Big|_{s=0} A^{\nu)}_{\alpha_3\alpha_4\rho} - \frac{1}{4} \eta^{\rho\sigma} A^{\mu}_{\alpha_1\alpha_2\rho} A^{\nu}_{\alpha_3\alpha_4\sigma} \\ &\quad \left. - \frac{1}{12} \eta^{\rho(\mu} A^{\nu)}_{\alpha_1\alpha_2\alpha_3\alpha_4\rho} \right) a^{\alpha_1} a^{\alpha_2} a^{\alpha_3} a^{\alpha_4} s^4 \\ &+ O(s^5). \end{aligned} \tag{3.46}$$

It is straightforward to check that this satisfies $g^{\mu\rho} g_{\rho\nu} = \delta^{\mu}_{\nu}$. All other quantities, e.g. the connection and its partial derivatives, may be calculated using eqs. 3.44 and 3.46.

3.3.1. N^{th}-order NRNC

To better understand how the introduction of the coefficients $A^{\mu}_{\alpha_1\ldots\alpha_n}$ causes NRNC to differ from LRNC, we define the order N of a NRNC as the largest value such that $n < N \implies A^{\mu}_{\alpha_1\ldots\alpha_n} = 0$. In other words, all coefficients in eq. 3.2 vanish until one reaches the $A^{\mu}_{\alpha_1\ldots\alpha_N}$ term. LRNC may be viewed as an ∞^{th}-order NRNC, and the order of a NRNC may be understood as describing how far one has to go from the origin before one deviates from LRNC. Note that, by our definition of NRNC (eq. 3.2), a NRNC necessarily has an order of at least 3.

From eq. 3.40, we may see that, in an N^{th}-order NRNC, eq. 3.22 holds for all $n < N$. It is then easy to see that we may apply our proof of theorem 1 for all $n < N$:

Corollary 1. *In an N^{th}-order NRNC, eq. 3.13 holds for all $n < N$.*

The proofs for lemmas 2 and 3 may also be extended to an N^{th}-order NRNC, although in this case the restriction is $n < N - 1$. This allows us to partially extend theorem 2 to NRNC:

Corollary 2. *In an N^{th}-order NRNC, all n^{th}-order partial derivatives of the metric, evaluated at the origin, are the same as those calculated in LRNC, if $n \leq N - 2$.*

For example, in the lowest-order NRNC, $N = 3$, only the first-order derivative of the metric has the same value at the origin as in LRNC, which is another way of stating that eq. 3.10 holds for both LRNC and NRNC. At $N = 4$, we get that the second-order derivative of the metric at the origin will also have the same value in NRNC as in LRNC, and so on, so forth. Put another way, introducing an $O(s^N)$ term to the right-hand side of eq. 3.3 results in a change to the metric at order $O(s^{N-1})$.

As with LRNC, the converse of these statements is also true.

Corollary 3. *If in a NRNC eq. 3.13 holds for $n \leq N - 1$, then the NRNC's order is at least N.*

Proof. The proof is very similar to that for theorem 3, except that we only have

$$\Gamma^{\mu}_{\alpha_1\ldots\alpha_n}\Big|_{s=0} = 0 \tag{3.47}$$

for $n \leq N-1$. By eq. 3.40, this means that $A^{\mu}_{\alpha_1\ldots\alpha_n}$ for $n \leq N-1$. Thus the lowest-order coefficient that may be nonzero is $A^{\mu}_{\alpha_1\ldots\alpha_N}$. □

Corollary 4. *If the metric in a NRNC is equal to the metric in LRNC up to order $N-2$ in s, then the NRNC's order is at least N.*

Proof. $\Gamma^{\mu}_{\alpha_1\ldots\alpha_n}\Big|_{s=0}$ depends on the first $n-1$ derivatives of the metric, evaluated at the origin. Since the first $N-2$ derivatives are the same in our NRNC as they are in LRNC, it follows that $\Gamma^{\mu}_{(\alpha_1\ldots\alpha_n)}\Big|_{s=0} = 0$ for $n \leq N-1$. By eq. 3.40, we will therefore have $A^{\mu}_{\alpha_1\ldots\alpha_n} = 0$ for all $n < N$, and thus the NRNC is at least order N. □

Section 3.4

Gravitational Waves in Riemann Normal Coordinates

Gravitational waves are readily studied in flat spacetime, where they are defined as perturbations on the Minkowski metric:

$$g_{\mu\nu} = \eta_{\mu\nu} + \varepsilon h_{\mu\nu}, \tag{3.48}$$

where ϵ is a bookkeeping variable to distinguish between background terms and small perturbations. More challenging is the case of gravitational waves in a curved background spacetime:

$$g_{\mu\nu} = \overline{g}_{\mu\nu} + \varepsilon h_{\mu\nu}, \tag{3.49}$$

where the separation of g into $\overline{g}$ and h must be carried out via a scale separation; see [134, 137, 138] for a detailed treatment on the subject. It is reasonable to hope that, by using Riemann normal coordinates, we might be able to treat gravitational waves in a curved spacetime, while retaining some of the simplicity of flat spacetime. In this section, we examine the extent to which this is possible.

The metric perturbation is gauge fixed by performing coordinate transformations,

$$x^\mu \to x'^\mu = x^\mu + \varepsilon f^\mu, \tag{3.50}$$

under which the metric perturbation transforms as

$$h_{\mu\nu} \to h'_{\mu\nu} = h_{ab} - 2\overline{\nabla}_{(\mu} f_{\nu)}, \tag{3.51}$$

where $\overline{\nabla}$ indicates the covariant derivative taken with respect to the background metric ($\overline{g}$ for curved spacetime or η for flat spacetime). In flat spacetime, a common choice of gauge is the transverse traceless (TT) gauge, in which $h = \partial^\mu h_{\mu\nu} = h_{0\nu} = 0$, where $h = \eta^{\mu\nu} h_{\mu\nu}$ is the trace of the metric perturbation. If the gravitational wave is propagating in the 3 direction, then the metric perturbation may be written in this gauge as

$$h_{\mu\nu} = \begin{bmatrix} 0 & 0 & 0 & 0 \\ 0 & h_+ & h_\times & 0 \\ 0 & h_\times & -h_+ & 0 \\ 0 & 0 & 0 & 0 \end{bmatrix} = h_+ e^+_{\mu\nu} + h_\times e^\times_{\mu\nu}, \tag{3.52}$$

where

$$e^+_{\mu\nu} = \begin{bmatrix} 0 & 0 & 0 & 0 \\ 0 & 1 & 0 & 0 \\ 0 & 0 & -1 & 0 \\ 0 & 0 & 0 & 0 \end{bmatrix} \qquad e^\times_{\mu\nu} = \begin{bmatrix} 0 & 0 & 0 & 0 \\ 0 & 0 & 1 & 0 \\ 0 & 1 & 0 & 0 \\ 0 & 0 & 0 & 0 \end{bmatrix}. \tag{3.53}$$

h_+ and $h_\times$ are then the two degrees of freedom of the graviton in flat spacetime. However, in curved spacetime, the graviton acquires an effective mass and has five degrees of freedom, so that the gravitational wave will have the form

$$h_{\mu\nu} = h_+ e^+_{\mu\nu} + h_\times e^\times_{\mu\nu} + h_3 e^3_{\mu\nu} + h_4 e^4_{\mu\nu} + h_5 e^5_{\mu\nu}, \tag{3.54}$$

where $e^3_{\mu\nu}$, $e^4_{\mu\nu}$, and $e^5_{\mu\nu}$ are the extra polarization modes. Note that $e^+_{\mu\nu}$ and $e^\times_{\mu\nu}$ may not have the same form as they do in flat spacetime (they need not be constant).

Mathematically, the reason why we have eq. 3.54 instead of 3.52 in curved spacetime is because we cannot necessarily force the gauge condition $h_{0\nu} = 0$ in curved spacetime. However, in this section, we will prove that, in LRNC or in NRNC of at least order 4, it is possible to choose our gauge such that $h_{0\nu} = O\left((\xi - \xi_0)^2\right)$. The result of this is that all new degrees of freedom and all corrections to the old degrees of freedom are quadratic in displacement from the origin,

$$\begin{aligned}
e^+_{\mu\nu} &= \begin{bmatrix} 0 & 0 & 0 & 0 \\ 0 & 1 & 0 & 0 \\ 0 & 0 & -1 & 0 \\ 0 & 0 & 0 & 0 \end{bmatrix} + O\left((\xi - \xi_0)^2\right) \\
e^\times_{\mu\nu} &= \begin{bmatrix} 0 & 0 & 0 & 0 \\ 0 & 0 & 1 & 0 \\ 0 & 1 & 0 & 0 \\ 0 & 0 & 0 & 0 \end{bmatrix} + O\left((\xi - \xi_0)^2\right) \\
e^3_{\mu\nu} &= e^4_{\mu\nu} = e^5_{\mu\nu} = O\left((\xi - \xi_0)^2\right).
\end{aligned} \tag{3.55}$$

Thus, if we only work in a region of spacetime small enough that we may neglect all terms of order $(\xi - \xi_0)^2$ or higher, then we may use eq. 3.52 as a valid approximation for gravitational waves.

To prove this, we will work in a vacuum, i.e. we will set $\overline{R}_{\mu\nu} = 0$, where $\overline{R}_{\mu\nu}$ is the Ricci tensor calculated using the background metric. The reason for this is that, in

the presence of a stress-energy tensor, the metric perturbation may be divided into a radiating component in the TT gauge, which corresponds to the gravitational wave, and a non-radiating component, which is not in the TT gauge [137]. In a vacuum spacetime, we only have the radiating component. We may therefore examine the case of a vacuum spacetime to determine what mathematical form that radiating component will have.

We will be performing a series of coordinate transformations, i.e.

$$\begin{aligned} \xi^\mu &\longrightarrow \xi'^\mu = \xi^\mu + \varepsilon f^\mu \\ &\longrightarrow \xi''^\mu = \xi'^\mu + \tau\kappa f'^\mu \\ &\longrightarrow \ldots, \end{aligned} \tag{3.56}$$

which corresponds to a series of transformations to $h_{\alpha\beta}$:

$$\begin{aligned} h_{\mu\nu} &\longrightarrow h'_{\mu\nu} = h_{\mu\nu} - 2\overline{\nabla}_{(\mu} f_{\nu)} \\ &\longrightarrow h''_{\mu\nu} = h'_{\mu\nu} - 2\overline{\nabla}_{(\mu} f'_{\nu)} \\ &\longrightarrow \ldots. \end{aligned} \tag{3.57}$$

Each coordinate transformation is chosen so as to give $h_{\mu\nu}$ an additional gauge property. However, we must take care that one coordinate transformation does not undo the gauge condition imposed by the previous coordinate transformation. Therefore, each coordinate transformation will impose a condition that all future coordinate transformations must obey, in order to preserve the gauge condition imposed by the former coordinate transformation. Our first coordinate transformation is chosen such that

$$\overline{\nabla}^\mu \overline{\nabla}_\mu f_\nu = \overline{\nabla}^\mu h_{\mu\nu} - \frac{1}{2}\overline{\nabla}_\nu h, \tag{3.58}$$

which imposes the gauge condition

$$\overline{\nabla}^{\mu} h'_{\mu\nu} = \frac{1}{2}\overline{\nabla}_{\nu} h' \tag{3.59}$$

and forces all future coordinate transformations to obey

$$\overline{\nabla}^{\mu}\overline{\nabla}_{\mu} f'_{\nu} = 0. \tag{3.60}$$

It can be shown that, if we have chosen our coordinates such that $\xi^0 = \xi^0_0$ is a spacelike surface, then it is possible to choose an f' that satisfies eq. 3.60 as well as

$$2\overline{\nabla}_{\mu} f'^{\mu}\big|_{\xi^0=\xi^0_0} = -h'\big|_{\xi^0=\xi^0_0} \tag{3.61}$$

and

$$2\partial_0\overline{\nabla}_{\mu} f'^{\mu}\big|_{\xi^0=\xi^0_0} = -\partial_0 h'\big|_{\xi^0=\xi^0_0}, \tag{3.62}$$

and that such a choice of f' causes $h'' = 0$ [139]. Therefore, we have as our gauge conditions $\overline{\nabla}^{\mu} h''_{\mu\nu} = h'' = 0$, and future coordinate transformations must obey

$$\begin{aligned} \overline{\nabla}^{\mu}\overline{\nabla}_{\mu} f''_{\nu} &= 0, \\ \overline{\nabla}_{\mu} f''^{\mu}\big|_{\xi^0=\xi^0_0} &= 0, \\ \text{and} \quad \partial_0\overline{\nabla}_{\mu} f''^{\mu}\big|_{\xi^0=\xi^0_0} &= 0. \end{aligned} \tag{3.63}$$

Because our metric is locally Minkowskian at $\xi = \xi_0$, there must exist a gauge in which $h''' = \partial^{\mu} h_{\mu\nu} = h_{0\nu} = 0$ at $\xi = \xi_0$ [134], and therefore it must be possible to choose some f'' that satisfies eq. 3.63 while also satisfying

$$\overline{\nabla}_{(0} f''_{\nu)}\big|_{\xi=\xi_0} = \frac{1}{2} h''_{0\nu}\bigg|_{\xi=\xi_0}, \tag{3.64}$$

which causes $h'''_{0\nu}\big|_{\xi=\xi_0} = 0$.

We will now perform one last coordinate transformation, with the goal of setting $\partial_\mu h''''_{0\nu}\big|_{\xi=\xi_0}$. To summarize, we have already forced the gauge conditions

$$\begin{aligned} \overline{\nabla}^\mu h'''_{\mu\nu} &= 0, \\ h''' &= 0, \\ \text{and} \quad h'''_{0\nu}\big|_{\xi=\xi_0} &= 0, \end{aligned} \tag{3.65}$$

and our final coordinate transformation must satisfy

$$\begin{aligned} \overline{\nabla}^\mu \overline{\nabla}_\mu f'''_\nu &= 0, \\ \overline{\nabla}_\mu f'''^\mu\big|_{\xi^0=\xi_0^0} &= 0 \\ \partial_0 \overline{\nabla}_\mu f'''^\mu\big|_{\xi^0=\xi_0^0} &= 0 \\ \overline{\nabla}_{(0} f'''_{\nu)}\big|_{\xi=\xi_0} &= 0 \\ \text{and} \quad \partial_\mu \overline{\nabla}_{(0} f'''_{\nu)}\big|_{\xi=\xi_0} &= \frac{1}{2}\partial_\mu h'''_{0\nu}\bigg|_{\xi=\xi_0}, \end{aligned} \tag{3.66}$$

where the first four equations are necessary to maintain the gauge conditions in eq. 3.66, and the last equation is to force the gauge condition $\partial_\mu h''''_{0\nu}\big|_{\xi=\xi_0}$. We may simplify eq. 3.66 to first order in $(\xi - \xi_0)$, by making use of the fact that, in our coordinate system,

$$\overline{\Gamma}^\rho_{\mu\nu} = -\frac{2}{3}\overline{R}^\rho{}_{(\mu\nu)\alpha} a^\alpha s + O\left(s^2\right), \tag{3.67}$$

where $\overline{\Gamma}^\rho_{\mu\nu}$ and $\overline{R}^\rho{}_{\sigma\mu\nu}$ are the Christoffel symbol and Riemann tensor, respectively, calculated using the background metric. (The reason this proof does not work for third-order NRNC is that, in third-order NRNC, $\overline{\Gamma}^\rho_{\mu\nu}$ has an additional term at first order in s, proportional to $A^\rho_{\mu\nu\alpha}$.) Dropping the primes, we find that we may rewrite

eq. 3.66 as

$$\begin{aligned}
\partial^\mu \partial_\mu f_\nu &= O\left(\xi - \xi_0\right) \\
\partial_\mu f^\mu\big|_{\xi^0=\xi_0^0} &= O\left(\left(\xi - \xi_0\right)^2\right) \\
\partial_0 \partial_\mu f^\mu\big|_{\xi^0=\xi_0^0} &= O\left(\xi - \xi_0\right) \\
\partial_{(0} f_{\mu)}\big|_{\xi=\xi_0} &= 0 \\
\left(\partial_\mu \partial_{(0} f_{\nu)} + \frac{2}{3}\overline{R}^\rho{}_{(0\nu)\mu} f_\rho\right)\Big|_{\xi=\xi_0} &= \frac{1}{2}\partial_\mu h_{0\nu}\Big|_{\xi=\xi_0}.
\end{aligned} \tag{3.68}$$

It is easy to check that the first three of these equations are satisfied by

$$f_\mu = \int \mathrm{d}^4 k' \delta\left(k'^\rho k'_\rho\right) F_\mu(k') e^{i k'_\rho \left(\xi^\rho - \xi_0^\rho\right)} + O\left(\left(\xi - \xi_0\right)^3\right), \tag{3.69}$$

where $F_\mu(k')$ is some function satisfying $F_\mu k'^\mu = 0$. The $O\left(\left(\xi - \xi_0\right)^3\right)$ is necessary to satisfy the right-hand sides of the first three equations. The remaining two equations become

$$\int \mathrm{d}^4 k' \delta\left(k'^\rho k'_\rho\right) k'_{(0} F_{\mu)}(k') = 0 \tag{3.70}$$

$$\int \mathrm{d}^4 k' \delta\left(k'^\rho k'_\rho\right) \left(\frac{2}{3}\,\overline{R}^\rho{}_{(0\nu)\mu}\Big|_{s=0} F_\rho(k') - k'_\mu k'_{(0} F_{\nu)}(k')\right) = \frac{1}{2}\partial_\mu h_{0\nu}\Big|_{\xi=\xi_0}, \tag{3.71}$$

which can easily be solved by letting $F_\mu(k')$ be a sum of Dirac deltas. Therefore it is possible to choose a gauge in which

$$\begin{aligned}
\overline{\nabla}^\mu h_{\mu\nu} &= 0 \\
h &= 0 \\
h_{0\nu}\big|_{\xi=\xi_0} &= 0 \\
\partial_\mu h_{0\nu}\big|_{\xi=\xi_0} &= 0,
\end{aligned} \tag{3.72}$$

which means that

$$h_{0\nu} = O\left((\xi - \xi_0)^2\right). \tag{3.73}$$

We can show the same thing for $h_{3\nu}$ by considering the gauge condition $\overline{\nabla}^\mu h_{\mu\nu} = 0$:

$$\begin{aligned} 0 &= \overline{g}^{\mu\rho}\partial_\rho h_{\mu\nu} - \overline{g}^{\mu\rho}\overline{\Gamma}^\sigma_{\rho\mu} h_{\sigma\nu} - \overline{g}^{\mu\rho}\overline{\Gamma}^\sigma_{\rho\nu} h_{\mu\sigma} \\ &= \partial^3 h_{3\nu} + \partial^0 h_{0\nu} + O\left(\xi - \xi_0\right). \end{aligned} \tag{3.74}$$

We have used the fact that, since we are examining a wave propagating in the 0 and 3 directions, $\partial_1 = \partial_2 = 0$. $\partial^0 h_{0\nu}$ is at least order $\xi - \xi_0$, so it follows that $h_{3\nu} = O\left((\xi - \xi_0)^2\right)$. Lastly, we note that

$$\begin{aligned} 0 = h &= \overline{g}^{\mu\nu} h_{\mu\nu} = \eta^{\mu\nu} h_{\mu\nu} + O\left((\xi - \xi_0)^2\right) \\ &= h_{11} + h_{22} + O\left((\xi - \xi_0)^2\right), \end{aligned} \tag{3.75}$$

so

$$h_{22} = -h_{11} + O\left((\xi - \xi_0)^2\right). \tag{3.76}$$

Therefore, defining $h_+ = h_{11}$ and $h_\times = h_{12}$, we get

$$h_{\mu\nu} = \begin{bmatrix} 0 & 0 & 0 & 0 \\ 0 & h_+ & h_\times & 0 \\ 0 & h_\times & -h_+ & 0 \\ 0 & 0 & 0 & 0 \end{bmatrix} + O\left((\xi - \xi_0)^2\right). \tag{3.77}$$

We have thus proved that, to our order of approximation, we may use eq. 3.52 as our expression for $h_{\mu\nu}$, in all Riemann normal coordinates except for third-order NRNC.

As an aside, it is instructive to examine why we are only requiring the first derivative of $h_{0\nu}$ to be 0 at $\xi = \xi_0$, i.e., would it be possible to require higher-order derivatives to also be 0? While it is possible that there may exist a gauge in which a higher-order

derivative of $h_{0\nu}$ is 0 at $\xi = \xi_0$, the proof above cannot be used to demonstrate this. The reason for this is that one of the equations f_ν would have to satisfy (analogous to eq. 3.68) would involve a derivative of at least third order (as opposed to the proof above, which only involved at most second-order derivatives), and this would cause the $O\left((\xi - \xi_0)^3\right)$ correction in eq. 3.69 to become relevant at $\xi = \xi_0$. As a result, eq. 3.69 would no longer satisfy all of the constraints on f_ν.

Section 3.5

Conclusion

Linear and nonlinear Riemann normal coordinates are both means of defining a locally flat patch of spacetime. Historically, studies of Riemann normal coordinates have considered only LRNC, whereas in the next chapter we will use NRNC, hence the necessity of understanding the differences between them. In both coordinates, there exists some point ξ_0 where $g_{\mu\nu}\Big|_{\xi_0} = \eta_{\mu\nu}$ and $\Gamma^\rho_{\mu\nu}\Big|_{\xi_0} = 0$. As one moves away from ξ_0, spacetime becomes curved, proportionally to $(\xi - \xi_0)^2$:

$$g_{\mu\nu} = \eta_{\mu\nu} + O\left((\xi - \xi_0)^2\right). \tag{3.78}$$

However, the coefficients in this expansion will be different in LRNC and NRNC. We have demonstrated how these coefficients may be calculated. In LRNC, the derivatives of the metric evaluated at ξ_0 may be written in terms of the Riemann tensor and its covariant derivatives evaluated at ξ_0. In NRNC, the derivatives of the metric evaluated at ξ_0 depend on both the Riemann tensor and its covariant derivatives evaluated at ξ_0, and the coefficients used to define the NRNC, $A^\mu_{\alpha_1\ldots\alpha_n}$. It is impossible to find some nonzero choice of $A^\mu_{\alpha_1\ldots\alpha_n}$ such that the dependence on $A^\mu_{\alpha_1\ldots\alpha_n}$ cancels out for all n. However, if all $A^\mu_{\alpha_1\ldots\alpha_n}$ are zero for $n < N$, then the

coefficients in the Taylor series of the metric will be the same as in LRNC up to order $N-2$ in s. Thus, it is possible for a NRNC to approximate LRNC arbitrarily well.

LRNC and NRNCs of at least order 4 are particularly useful in the treatment of gravitational waves, as in these coordinates gravitational waves may be treated as having their flat-spacetime forms out to order $(\xi - \xi_0)^2$. Thus, within a certain radius of ξ_0, Riemann normal coordinates allow us to analyze gravitational waves in curved spacetime without accounting for the effects of curved spacetime on the gravitational wave's form. This is an example of a more general concept, which is that Riemann normal coordinates are useful insofar as they allow us to treat the curvature of spacetime as corrections to a flat spacetime, with these corrections dependent on the displacement. It is in this way that we will utilize both LRNC and NRNC in the following two chapters.

Chapter 4

Gravitational Wave Effective Theory with Curvature Corrections

Section 4.1

Introduction

In the previous chapter, we established how, with the right choice of coordinates, one may describe spacetime within a certain region as locally flat. Such a locally flat patch of spacetime is a natural choice for constructing an effective field theory (EFT). The premise of EFT is to describe physics primarily using low-energy degrees of freedom, with only a small number of high-energy degrees of freedom. Careful examination of relevant energy scales reveals that many terms involving high-energy degrees of freedom will be suppressed at low energies, so that they may be ignored. This produces a tractable theory capable of producing accurate predictions. See [73, 74] for a review of EFT methods.

The problem of constructing an EFT of gravity has been well-studied [69–72, 78], but one challenge that remains arises from the infrared divergence of gravity. This infrared divergence may be seen in the series expansion of the metric in linear Riemann

normal coordinates. We saw in the previous chapter that the derivatives of the metric evaluated at $s = 0$ may be represented in terms of the Riemann tensor and its covariant derivatives, also evaluated at the origin. The magnitude of components of the n^{th}-order derivative of the Riemann tensor is given approximately by $\mathcal{R}_0^{-2-n}$, where $\mathcal{R}_0$ is the radius of curvature of the metric at $s = 0$ [134]. Thus, as an order of magnitude estimate, we may write

$$\underbrace{\partial \cdots \partial g}_{n^{\text{th}} \text{ derivative}}\Big|_{s=0} \sim \mathcal{R}_0^{-n}. \tag{4.1}$$

From this, we see that each term in the Taylor expansion of the metric will have magnitude of $(s/\mathcal{R}_0)^n$. Thus, at lengthscales greater than $\mathcal{R}_0$, the series expansion for the metric becomes divergent.

This infrared divergence is not cured by going to nonlinear Riemann normal coordinates. The derivatives of the metric in NRNC, evaluated at $s = 0$, may be expressed as their value in LRNC plus some terms involving the coefficients $A^{\mu}_{\alpha_1 \ldots \alpha_n}$. Consequently, the scale of these derivatives will be at least the scale of the derivatives in LRNC:

$$\begin{aligned} \partial \cdots \partial g_{\text{NRNC}}\Big|_{s=0} &= \partial \cdots \partial g_{\text{LRNC}}\Big|_{s=0} + \left(\text{additional terms involving } A^{\mu}_{\alpha_1 \ldots \alpha_n}\right) \\ &\gtrsim \mathcal{R}_0^{-n}, \end{aligned} \tag{4.2}$$

with this scale increasing as the various $A^{\mu}_{\alpha_1 \ldots \alpha_n}$ increase. Thus the terms in the Taylor expansion of the metric will increase at least as fast in NRNC as they do in LRNC.

This infrared divergence presents a problem for EFTs in curved spacetime because of the nonlocal nature of gravity. Even if we restrict our EFT to a patch of spacetime in which $s \lesssim \mathcal{R}_0$, so that the metric remains convergent within the patch, the graviton's massless propagator will import physics from beyond that patch, where

the metric is divergent. Thus, an EFT constructed solely within a local patch, ignoring physics outside the patch, may fail to match with reality. To prevent this, it is necessary that we add nonlocal corrections to our EFT.

[78] proposed (but did not meaningfully explore the proposal) that one method for introducing these nonlocal corrections would be by chaining together patches of Riemann normal coordinates, within each of which spacetime is locally flat and the EFT is well-defined. As a particle goes from one patch to another, the curvature corrections from each patch accrue, thus introducing nonlocal corrections into the EFT of the final patch. This is the method we develop in this chapter.

This chapter is divided is follows. In section 4.2, we discuss how coordinates defining locally flat patches of spacetime may be chained together in order to define long-distance coordinates, which incorporate the curvature of spacetime. In section 4.3, we show how these coordinates naturally allow for the construction of comparators linking quantities between two distant patches. These comparators may be used to introduce nonlocal corrections into the Lagrangian defined in a single patch, and in section 4.4 we use naive dimensional analysis to estimate the size of the resulting operators. Section 4.5 is the conclusion.

Section 4.2

Long-Distance Curvature Corrections

The method in this chapter builds on gravitational wave effective field theory. Within areas where the local lengthscale of spacetime curvature is large (i.e., spacetime is not highly curved), there exists a rigorous framework for gravitational waves [134, 137, 138]. This involves a introducing a new lengthscale, $\mathcal{L}$, which is the lengthscale over which the metric changes significantly, and separating the metric into high- and low-frequency components based on this lengthscale. We may then express the metric

a low-frequency background plus a high-frequency perturbation,

$$g_{\mu\nu} = \overline{g}_{\mu\nu} + \epsilon\kappa h_{\mu\nu}, \tag{4.3}$$

where $\kappa = 4\sqrt{\pi}/m_{\rm Pl}$, and $m_{\rm Pl}$ is the Planck mass; this factor is included so that the gravitational wave will have units of mass. $\epsilon \sim O\left(\frac{\lambda\!\!\!^{-}}{\mathcal{L}}\right)$ is a dimensionless parameter, where $\lambda\!\!\!^{-} = \lambda/2\pi$ is the reduced wavelength of the gravitational wave. The gravitational wave will vary over lengthscale $\lambda\!\!\!^{-}$, while the background metric will vary over lengthscale $\mathcal{L}$. The study of gravitational waves is well-developed, *provided* that $\lambda\!\!\!^{-} \ll \mathcal{L}$.

This exposes both the utility and the limitations of Riemann normal coordinates, within a single patch. Out to a suitably chosen radius, the curvature of spacetime in Riemann normal coordinates is small enough that preexisting tools for examining gravitational waves in curved spacetime are sufficient. However, as one moves away from ξ_0, the metric diverges (as already discussed) and $\mathcal{L}$ shrinks, until we no longer have $\lambda\!\!\!^{-} \ll \mathcal{L}$.

4.2.1. Multiple Locally Flat Patches

In light of this limitation on Riemann normal coordinates, rather than attempting to describe curved spacetime using a single large patch, we use multiple patches of appropriate size (i.e. $s < \mathcal{R}_0$ at all points in the patch). Let us consider a particle that moves along a geodesic from a point ξ_0 to a point ξ_f. Defining around ξ_f a NRNC, we may trace backwards along the geodesic from ξ_f, until we reach a point

$$v_0^\mu = \xi_f^\mu - a_1^\mu s_1 + \frac{1}{3!}\,\overline{\Gamma}^\mu_{\rho\sigma\tau}\big|_{\xi_0}\, a_1^\rho a_1^\sigma a_1^\tau s_1^3 + \ldots, \tag{4.4}$$

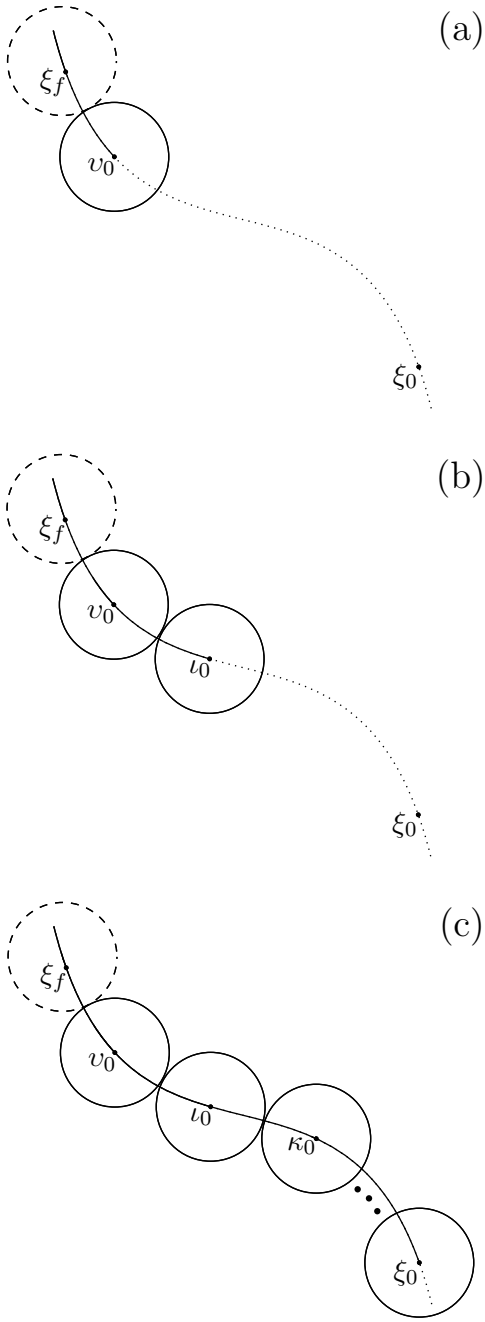

Figure 4.1: A demonstration of the process by which locally flat patches may be joined along a geodesic. Circles represent patches of spacetime in which a locally flat coordinate system is well-defined. (a) We trace backwards along the geodesic from ξ_f to υ_0, a point outside ξ_f's patch. ξ_f and υ_0 are related by eq. 4.4. We then define a new set of locally flat coordinates in a patch about υ_0. (b) We continue backwards along the geodesic to reach a new point, ι_0, related to υ_0 by eq. 4.5, and define locally flat coordinates in a patch about ι_0. (c) We iterate this process across a total of N patches until we reach ξ_0, related to ξ_f by eq. 4.6. A particle traveling along the geodesic from ξ_0 to ξ_f may thus always be described in terms of locally flat coordinates.

where a_1 is a vector parallel to the geodesic at ξ_f, s_1 is is the value of s at the edge of the patch, and $\overline{\Gamma}^{\mu}_{\rho\sigma\tau}$ is the generalized connection defined in the previous chapter (calculated in terms of the background metric $g_{\mu\nu}$). We choose υ_0 to be outside ξ_f's patch, and we may now define a new NRNC in a patch centered about υ_0. We may then continue traveling along the geodesic until we again reach a point at the edge of that patch:

$$\iota^{\mu}_0 = \upsilon^{\mu}_0 - a^{\mu}_2 s_2 + \frac{1}{3!}\,\overline{\Gamma}^{\mu}_{\rho\sigma\tau}\big|_{\upsilon_0}\, a^{\rho}_2 a^{\sigma}_2 a^{\tau}_2 s^3_2 + \dots . \tag{4.5}$$

In this way, we may traverse a total of N locally flat patches until we reach ξ_0, as depicted in Fig. 4.1. Through this process, we obtain an expression for ξ_0 in terms of ξ_f:

$$\xi^{\mu}_0 = \xi^{\mu}_f - \sum_{i=1}^{N} a^{\mu}_i s_i + \frac{1}{3!}\sum_{i=1}^{N} \overline{\Gamma}^{\mu}_{\rho\sigma\tau}\big|_{s_i=0}\, a^{\rho}_i a^{\sigma}_i a^{\tau}_i s^3_i + \dots . \tag{4.6}$$

As in the first patch, the values of s_i must be small enough that each patch may be approximated as flat, i.e. $s_i < \mathcal{R}_i$, where $\mathcal{R}_i$ is the metric's radius of curvature at the center of the i^{th} patch. $\overline{\Gamma}^{\mu}_{\alpha_1\alpha_2\alpha_3\cdots\alpha_n}\big|_{s_i=0} \sim \mathcal{R}_i^{1-n}$, which ensures that the sum will converge. However, as the number of patches N increases, the higher-order terms in eq. 4.6 may become significant.

4.2.2. Uniform Patch Approximation

As a particle travels along a geodesic, it accumulates curvature corrections, represented by the higher-order terms in eq. 4.6. A useful simplification is to assume that

the geometry of each patch is identical, so that we may approximate

$$s_1 = s_2 = \cdots = s_N \equiv s \tag{4.7}$$

$$a_1^\mu = a_2^\mu = \cdots = a_N^\mu \equiv a^\mu \tag{4.8}$$

$$\overline{\Gamma}^\mu_{\alpha_1\ldots\alpha_n}\big|_{s_1=0} = \cdots = \overline{\Gamma}^\mu_{\alpha_1\ldots\alpha_n}\big|_{s_N=0} \equiv \overline{\Gamma}^\mu_{\alpha_1\ldots\alpha_n}\big|_{s=0}\,. \tag{4.9}$$

Eq. 4.6 then takes the form

$$\xi_0^\mu = \xi_f^\mu - Na^\mu + \frac{N}{3!}\,\overline{\Gamma}^\mu_{\rho\sigma\tau}\Big|_{s=0} a^\rho a^\sigma a^\tau s^3 + \ldots. \tag{4.10}$$

The factor of N in front of the higher-order terms represents the enhancement received from traversing multiple patches.

Section 4.3

Comparators

Using eq. 4.6, we may relate quantities at ξ_0 with those at ξ_f. This acts analogously to a Wilson line, transporting quantities along the geodesic.

4.3.1. Comparators of the metric

We begin with the metric. As before, we begin by traveling backward, from the final patch at ξ_f to the patch at υ_0. The metric at υ_0 is given by

$$\begin{aligned}\overline{g}_{\mu\nu}(\upsilon_0) &= \overline{g}_{\mu\nu}(\xi_f) + \frac{1}{2!}\overline{g}_{\mu\nu,\alpha_1\alpha_2}(\xi_f)\left(\upsilon_0^{\alpha_1} - \xi_f^{\alpha_1}\right)\left(\upsilon_0^{\alpha_2} - \xi_f^{\alpha_2}\right) + \ldots \\ &= \left(\delta_\mu^\rho\delta_\nu^\sigma + \frac{1}{4}\overline{\alpha}^{\rho\sigma}_{\mu\nu}(\upsilon_0,\xi_f)\right) g_{\rho\sigma}(\xi_f),\end{aligned} \tag{4.11}$$

where $\overline{\alpha}^{\rho\sigma}_{\mu\nu}(\upsilon_0, \xi_f) \equiv \overline{g}^{\rho\sigma}(\xi_f)\overline{\alpha}_{\mu\nu}(\upsilon_0, \xi_f)$, and

$$\overline{\alpha}_{\mu\nu}(\upsilon_0, \xi_f) = \sum_{n=2}^{\infty} \frac{1}{n!} \overline{g}_{\mu\nu,\alpha_1\ldots\alpha_n}(\xi_f) \left(\upsilon_0^{\alpha_1} - \xi_f^{\alpha_1}\right) \cdots \left(\upsilon_0^{\alpha_n} - \xi_f^{\alpha_n}\right). \tag{4.12}$$

Note that there is no first derivative of the metric because, in Riemann normal coordinates, the derivative of the metric vanishes at the origin.

Similarly, the comparator for the contravariant metric is

$$\overline{g}^{\mu\nu}(\upsilon_0) = \left(\delta^\mu_\rho \delta^\nu_\sigma + \frac{1}{4}\overline{\beta}^{\mu\nu}_{\rho\sigma}(\upsilon_0, \xi_f)\right) g^{\rho\sigma}(\xi_f), \tag{4.13}$$

where $\overline{\beta}^{\rho\sigma}_{\mu\nu}(\upsilon_0, \xi_f) \equiv \overline{g}_{\rho\sigma}(\xi_f)\overline{\beta}^{\mu\nu}(\upsilon_0, \xi_f)$, and

$$\overline{\beta}^{\mu\nu}(\upsilon_0, \xi_f) = \sum_{n=2}^{\infty} \frac{1}{n!} \overline{g}^{\mu\nu}{}_{,\alpha_1\ldots\alpha_n}(\xi_f) \left(\upsilon_0^{\alpha_1} - \xi_f^{\alpha_1}\right) \cdots \left(\upsilon_0^{\alpha_n} - \xi_f^{\alpha_n}\right). \tag{4.14}$$

Comparing eqs. 4.11 and 4.13, we see that these two comparators may be related by

$$\overline{\beta}^{\mu\nu}(\upsilon_0, \xi_f) = \overline{g}^{\mu\rho}(\upsilon_0)\overline{g}^{\nu\sigma}(\upsilon_0)\alpha_{\rho\sigma}(\upsilon_0, \xi_f). \tag{4.15}$$

Additionally, we know that $g^{\mu\alpha}(\upsilon_0)g_{\alpha\nu}(\upsilon_0) = \delta^\mu_\nu$, and from this we get

$$\overline{\beta}^{\mu\alpha}(\upsilon_0, \xi_f)\left(\delta^\nu_\alpha + \overline{\alpha}_{\alpha\beta}(\upsilon_0, \xi_f)\overline{g}^{\nu\beta}(\xi_f)\right) = -\overline{\alpha}_{\alpha\beta}(\upsilon_0, \xi_f)\overline{g}^{\mu\alpha}(\xi_f)\overline{g}^{\nu\beta}(\xi_f). \tag{4.16}$$

We may chain together eqs. 4.11 and 4.13 in order to construct comparators between the metric at ξ_0 and ξ_f. For the covariant metric, this is

$$\begin{aligned}\overline{g}_{\mu_1\nu_1}(\xi_0) &= \prod_{i=2}^{N} \left(\delta^{\mu_i}_{\mu_{i-1}}\delta^{\nu_i}_{\nu_{i-1}} + \frac{1}{4}\overline{\alpha}^{\mu_i\nu_i}_{\mu_{i-1}\nu_{i-1}}(\zeta_{i-1}, \zeta_i)\right) \overline{g}_{\mu_N\nu_N}(\xi_f) \\ &= \overline{\Delta}^{\mu_N\nu_N}_{\mu_1\nu_1}(\xi_0, \xi_f)\overline{g}_{\mu_N\nu_N}(\xi_f)\end{aligned} \tag{4.17}$$

where $\{\zeta_1, \ldots \zeta_N\} = \{\xi_0, \ldots, \upsilon_0, \xi_f\}$ are the centers of the N patches. The comparator for the contravariant metric may be defined in a similar way.

4.3.2. Comparators of Other Fields

We construct the comparators for other fields (such as the metric perturbation $h_{\mu\nu}$, the electromagnetic four potential A_μ, and the scalar boson ϕ) in a way that is different in form from, but equivalent to, our comparator for $\overline{g}_{\mu\nu}$. As with the metric, it is necessary that fields be separated into high- and low-frequency components according to a lengthscale $\mathcal{L}$. For both high- and low-frequency fields, the comparator is constructed as, e.g. for scalars:

$$\begin{aligned}\phi(\xi_0) &= \phi(\xi_f) + \sum_{i=2}^{N} \partial_{\alpha_1}\phi(\zeta_i)\left(\zeta_{i-1}^{\alpha_1} - \zeta_i^{\alpha_1}\right) \\ &\qquad + \frac{1}{2}\sum_{i=2}^{N} \partial_{\alpha_1}\partial_{\alpha_2}\phi(\zeta_i)\left(\zeta_{i-1}^{\alpha_1} - \zeta_i^{\alpha_1}\right)\left(\zeta_{i-1}^{\alpha_2} - \zeta_i^{\alpha_2}\right) + \ldots \\ &\equiv \phi(\xi_f) + \Delta\phi(\xi_0, \xi_f). \end{aligned} \tag{4.18}$$

Similarly, for a generic tensor $B_{\mu_1\ldots\mu_n}$:

$$\begin{aligned}B_{\mu_1\ldots\mu_n}(\xi_0) &= \phi(\xi_f) + \sum_{i=2}^{N} B_{\mu_1\ldots\mu_n,\alpha_1}(\zeta_i)\left(\zeta_{i-1}^{\alpha_1} - \zeta_i^{\alpha_1}\right) \\ &\qquad + \frac{1}{2}\sum_{i=2}^{N} B_{\mu_1\ldots\mu_n,\alpha_1\alpha_2}(\zeta_i)\left(\zeta_{i-1}^{\alpha_1} - \zeta_i^{\alpha_1}\right)\left(\zeta_{i-1}^{\alpha_2} - \zeta_i^{\alpha_2}\right) + \ldots \\ &\equiv B_{\mu_1\ldots\mu_n}(\xi_f) + \Delta B_{\mu_1\ldots\mu_n}(\xi_0, \xi_f). \end{aligned} \tag{4.19}$$

4.3.3. Verifying the Comparator: The Kretschmann Scalar

As a test of the validity of these comparators, we compute the Kretschmann scalar $K = R_{\mu\nu\rho\sigma}R^{\mu\nu\rho\sigma}$, in Schwarzschild geometry, using eq. 4.18. To do this, we choose two points and a geodesic connecting them; in this example, the points are located

at $r = r_0$ and $r = r_f$ (in Schwarzschild coordinates), with the same values of θ and ϕ, and the geodesic corresponds to a particle moving radially away from the black hole.

Our goal is to calculate K at the center of each locally flat patch along the geodesic, i.e. to evaluate eq. 4.18 for different values of N; we expect to show that, when one reaches the final patch, located at r_f, one gets a value for the Kretschmann scalar that matches the known value of K at r_f. This value is given by $K = \frac{12r_s^2}{r_f^6}$, where r_s is the Schwarzschild radius. Before we may do this, however, we must determine the size of each patch. Ultimately, this choice is somewhat arbitrary, provided $s_i < \mathcal{R}_i$. We choose to define each proper length s_i as the distance at which the first-order corrections are 10% of the zeroth order corrections,

$$\frac{\partial_\alpha K\big|_{s_i=0}\, s_i\, a_i^\alpha}{K\big|_{s_i=0}} \sim 10^{-1}. \tag{4.20}$$

This fixes s_i for each local spacetime patch given that we fix a_i to be a unit vector in the time direction. The comparison of the Kretschmann scalar, computed using Schwarzschild geometry, with the Kretschmann scalar is plotted in Fig. 4.2.

It must be noted, however, that Fig. 4.2 was plotted using LRNC, rather than NRNC, i.e. we ignored all the higher-order terms in eq. 4.6. This makes the results in Fig. 4.2 trivial, as in this case our comparator essentially just becomes a Taylor series,

$$K(\xi_f) = K(\xi_0) + \partial_\mu K(\xi_0) \sum_{i=1}^{N} a_i^\mu s_i + \frac{1}{2}\partial_\mu\partial_\nu K(\xi_0) \sum_{i,j=1}^{N} a_i^\mu a_j^\nu s_i s_j + \dots. \tag{4.21}$$

This demonstrates the importance of our choice of NRNC, rather than LRNC; using NRNC allows us to encode the curvature of spacetime into our coordinate definition, and, without this, our comparator has no way of actually introducing curvature corrections. Thus, in LRNC, the comparators become trivial Taylor expansions, and for

this reason the work in this section was not included in [85].

Instead, [85] contains an analogous computation, in which the higher-order terms are not discarded. The resulting computation is not as trivial as the one performed here, but it still yields a value for the Kretschmann scalar that matches with its known value, lending credence to the comparators we have defined.

Section 4.4

Naive Dimensional Analysis

As stated earlier, the work in this section does not appear in [85], because it was not completed at the time when [85] was published.

In the previous section, we defined comparators that can be used to relate quantities at ξ_0 with those at ξ_f, thereby allowing us to construct a Lagrangian at ξ_f that incorporates nonlocal corrections from ξ_0. It is useful to have an estimate of the coefficients for the resulting operators. We use naive dimensional analysis (NDA) [140] to provide such an estimate. We saw earlier that the metric must be divided into a high-frequency component $h_{\mu\nu}$ and a low-frequency component $g_{\mu\nu}$, according to a lengthscale $\mathcal{L}$. The same must be done for all fields, e.g. the electromagnetic four-potential A_μ and the scalar field ϕ. Note that the defining lengthscale for A_μ and ϕ need not be the same as the lengthscale for metric perturbations, but for the sake of simplicity we will here assume that all three have the same lengthscale $\mathcal{L}$ and the same reduced frequency $\lambda\!\!\!^{-} \ll \mathcal{L}$. Thus, in the Lagrangian, every derivative of a high-frequency field is of order $\lambda\!\!\!^{-1}$, and every derivative of a low-frequency field is of order $\mathcal{L}^{-1}$.

Consider a $4+k$ dimensional operator in our Lagrangian. Generically, this operator contains n factors of the background metric, n' factors of ϕ, A_μ, and $h_{\mu\nu}$, n_D derivatives on these three fields, a coefficient c, and k factors of Planck suppression.

(a)

(b)

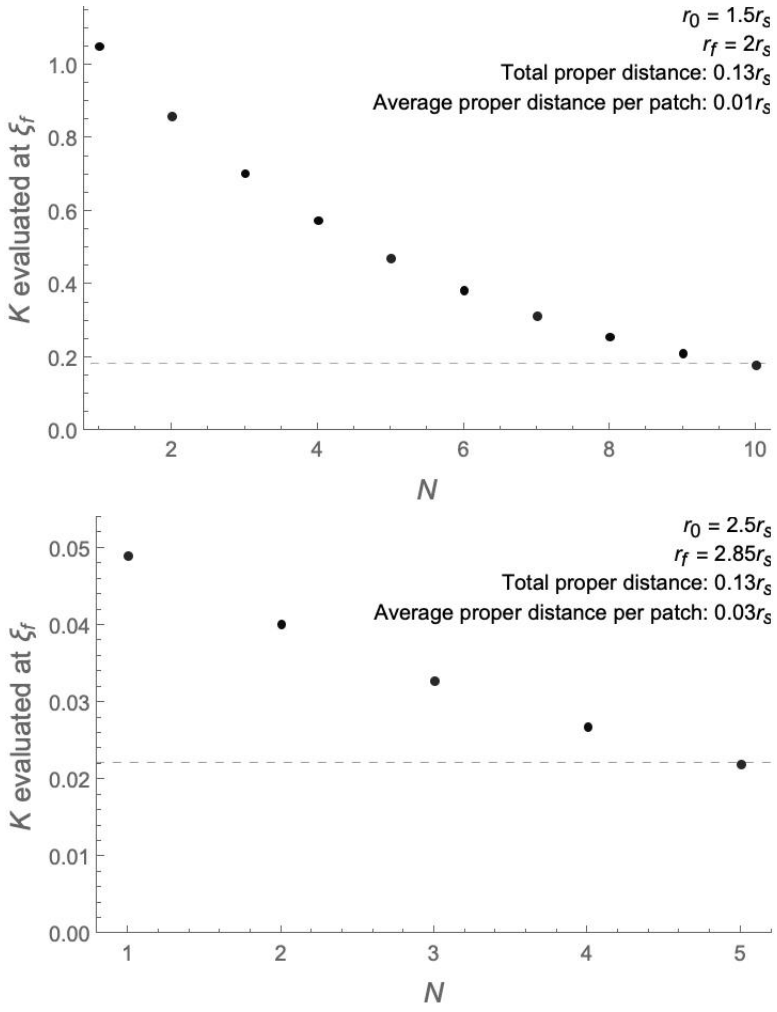

Figure 4.2: Comparing Kretschmann scalar computed in Schwarzschild coordinates with the Kretschmann scalar computed in coordinates defined according to eq. 4.6. We consider a particle moving away from a Schwarzschild black hole in the radial direction. As the particle moves away from the black hole, it passes through a number of locally flat patches, and the value of the Kretschmann scalar K at the center of each patch is shown, calculated according to eq. 4.18. The size of each patch is given by eq. 4.20. The value of K at r_f is also calculated using the formula $K = \frac{12r_s^2}{r_f^6}$; this value is indicated with a dashed line. In (a), the $N = 10$ patch is centered at $r = 2r_s$, and, in (b), $N = 5$ is centered at $r = 2.85r_s$, so we can see that the value of K we get from our comparator agrees well with reality. Ultimately, however, this result is trivial, as it was done without the inclusion of the higher-order terms in eq. 4.6 (i.e., it assumes a LRNC rather than a NRNC). A far more important and nontrivial computation would be analogous to this, but with the higher-order terms included; this is performed in [85]. The vertical axis has units of $r_s = 1$.

Schematically, this operator is

$$\mathcal{O} = \frac{c}{m_{\rm Pl}^k} \underbrace{\overline{g}^{\cdots}\cdots\overline{g}^{\cdots}}_{n \text{ factors}} \underbrace{\begin{array}{l}(\partial\cdots\partial\phi)\cdots(\partial\cdots\partial\phi) \\ \times(\partial\cdots\partial A)\cdots(\partial\cdots\partial A) \\ \times(\partial\cdots\partial h_{\cdots})\cdots(\partial\cdots\partial h_{\cdots})\end{array}}_{n' \text{ factors, } n_D \text{ derivatives}} \tag{4.22}$$

where the "..." in the superscripts of $\overline{g}$ and the subscripts of h are used to emphasize that both of those quantities have indices, which are summed over in some combination (i.e., we are not taking the trace of either $\overline{g}$ or h). We may expand the metrics using eq. 4.13, and we may expand the factors of ϕ, A_μ, and $h_{\mu\nu}$ using eqs. 4.18 and 4.19, and we may use NDA to estimate the coefficient of this term as

$$\text{coeff} = \frac{c}{m_{\rm Pl}^k}\frac{1}{\lambda^{n_D}}\left(\frac{1}{\mathcal{L}}\right)^{i_1+\ldots+i_n}\left(\frac{1}{\lambda}\right)^{j_1+\ldots+j_{n'}}\frac{(\xi_0-\xi_f)^{i_1+\cdots+i_n+j_1+\cdots+j_{n'}}}{i_1!\ldots i_n!\; j_1!\ldots j_{n'}!}\,,$$

where the i's indicate the number of factors of $\xi_0-\xi_f$ introduced by each factor of $\overline{g}$, and the j's indicate the number of factors of $\xi_0-\xi_f$ introduced by each factor of ϕ, A, and h. It is useful to define

$$t = i_1 + \ldots + i_n + j_1 + \ldots + j_{n'}, \tag{4.23}$$

which is the total order of the term we are looking at, within the Taylor expansion of $\mathcal{O}$. Thus our coefficient becomes

$$\text{coeff} = \frac{c}{m_{\rm Pl}^k}\frac{1}{\lambda^{n_D}}\left(\frac{1}{\mathcal{L}}\right)^{i_1+\ldots+i_n}\left(\frac{1}{\lambda}\right)^{j_1+\ldots+j_{n'}}\frac{(\xi_0-\xi_f)^{t}}{i_1!\ldots i_n!\; j_1!\ldots j_{n'}!}\,. \tag{4.24}$$

Each possible value of $i_1,\ldots,i_n,\ j_1,\ldots,j_{n'}$ corresponds to a different term within the Taylor expansion of $\mathcal{O}$. In practice, however, many of these terms are highly suppressed, and therefore we only care about the most enhanced terms in this Taylor

expansion. For a given value of t, eq. 4.24 is maximized when $i_1 = \ldots = i_n = 0$ and $j_1 = \ldots = j_{n'} = \frac{t}{n'}$, and thus may well approximate $\mathcal{O}$ by only considering these terms:

$$\text{coeff} \sim \frac{c}{m_{\text{Pl}}^k} \frac{1}{\lambda\!\!\!^{-}{}^{n_D}} \left(\left(\frac{t}{n'} \right)! \right)^{-n'} \left(\frac{\xi_0 - \xi_f}{\lambda\!\!\!^{-}} \right)^t . \tag{4.25}$$

As an example, consider the following, term, which comes from the stress-energy part of the Lagrangian for electromagnetism:

$$\mathcal{L} \supset \frac{\epsilon\kappa}{2} \overline{g}^{\mu\rho} \overline{g}^{\nu\sigma} \overline{g}^{\tau\lambda} h_{\mu\nu} F^{(1)}_{\rho\tau} F^{(1)}_{\sigma\lambda}, \tag{4.26}$$

where $F^{(1)}_{\mu\nu}$ is the high-frequency part of the electromagnetic tensor. (There also exist analogous terms in which one or more of the $F^{(1)}$'s are replaced with an $\overline{F}$, indicating the low-frequency part of the electromagnetic tensor.) Recall that $\epsilon \sim O\left(\frac{\lambda\!\!\!^{-}}{\mathcal{L}}\right)$ and $\kappa \sim m_{\text{Pl}}^{-1}$. So we have $k = 1$, $n = n' = 3$, and $n_D = 2$ (corresponding to the derivative internal to each $F^{(1)}_{\mu\nu}$), and we see that, when this term is expanded using the comparators established earlier, the coefficient at order t is given by

$$\text{coeff} \sim \frac{1}{m_{\text{Pl}}} \frac{1}{\lambda\!\!\!^{-}\mathcal{L}} \left(\left(\frac{t}{3} \right)! \right)^{-3} \left(\frac{\xi_0 - \xi_f}{\lambda\!\!\!^{-}} \right)^t . \tag{4.27}$$

$\xi_0 - \xi_f$ refers to the typical value of components of the curvature-corrected separation, as given by eq. 4.6. We plot this coefficient against t and $\frac{\xi_0 - \xi_f}{\lambda\!\!\!^{-}}$ in Fig. 4.3.

4.4.1. Additional Higher-Dimensional Operators

General relativity is an effective field theory, which may in general have extensions, e.g. [70, 78, 141]

$$\mathcal{L}_1 = \frac{2}{\kappa^2} R + c_1 R^2 + c_2 R_{\mu\nu} R^{\mu\nu} + \ldots . \tag{4.28}$$

There may also be operators that mix gravitational and Standard Model field content,

$$\begin{aligned}\mathcal{L}_2 = &\frac{c_3}{\Lambda^2}\, B^{\mu\nu} B^{\rho\sigma} C_{\mu\nu\rho\sigma} + \frac{c_4}{\Lambda^2}\, W^{\mu\nu} W^{\rho\sigma} C_{\mu\nu\rho\sigma} \\ &+ \frac{c_5}{\Lambda^2}\, G^{\mu\nu} G^{\rho\sigma} C_{\mu\nu\rho\sigma} + \frac{c_6}{\Lambda^2}\, H^\dagger H\, C_{\mu\nu\rho\sigma} + \dots ,\end{aligned} \tag{4.29}$$

where $C_{\mu\nu\rho\sigma}$ is the Weyl tensor,

$$C_{\mu\nu\rho\sigma} = R_{\mu\nu\rho\sigma} - \left(g_{\mu[\rho} R_{\sigma]\nu} - g_{\nu[\rho} R_{\sigma]\mu} \right) + \frac{1}{3} g_{\mu[\rho}\, g_{\sigma]\nu}\, R\,. \tag{4.30}$$

Similar to the energy-momentum tensor discussed earlier, we can expand the metric into the background metric and metric perturbation and then relate the Lagrangian at ξ_0 with the Lagrangian at ξ_f using the comparators. At energies much less the weak scale, the photon-conformal tensor operator, i.e. the operator generated by the first line of operators in equation (4.29), is now

$$\mathcal{O} = \frac{c_3 \sin^2\theta_W + c_4 \cos^2\theta_W}{m_{\text{Pl}}^2}\, F^{\mu\nu} F^{\rho\sigma} C_{\mu\nu\rho\sigma}\,, \tag{4.31}$$

where θ_W is the Weinberg angle. After expanding using the comparators, the coefficient for a term at order t, without renormalization group corrections, is

$$\text{coeff} \sim \frac{c_3 \sin^2\theta_W + c_4 \cos^2\theta_W}{m_{\text{Pl}}^2} \frac{1}{\lambda\!\!\!^{-4}} \left(\left(\frac{t}{3} \right)! \right)^{-3} \left(\frac{\xi_0 - \xi_f}{\lambda\!\!\!^{-}} \right)^t . \tag{4.32}$$

Like with eq. 4.27, we plot this coefficient against t and $\frac{\xi_0 - \xi_f}{\lambda\!\!\!^{-}}$ in Fig. 4.3. While these terms are traditionally ignored because of their additional suppression by the Planck scale, our result suggests that there are regimes of parameter space where they will become relevant for observation.

(a)

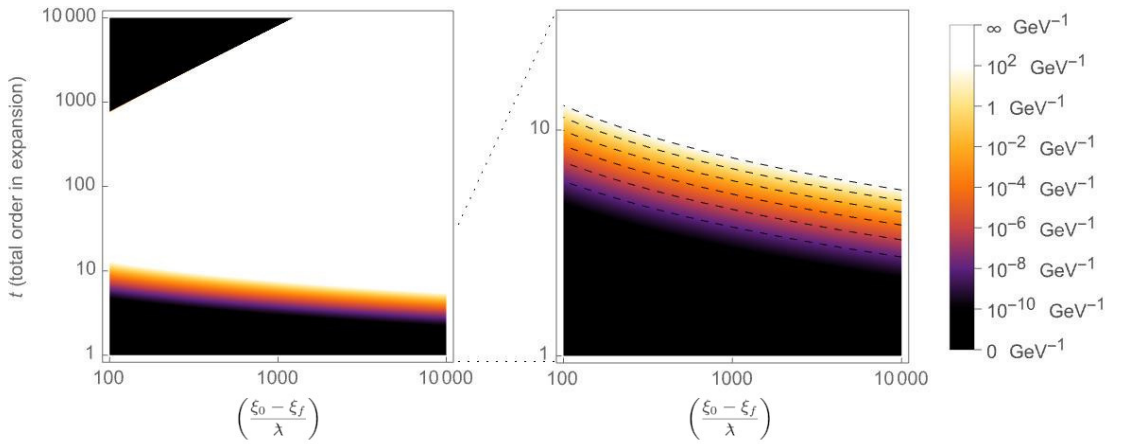

(b)

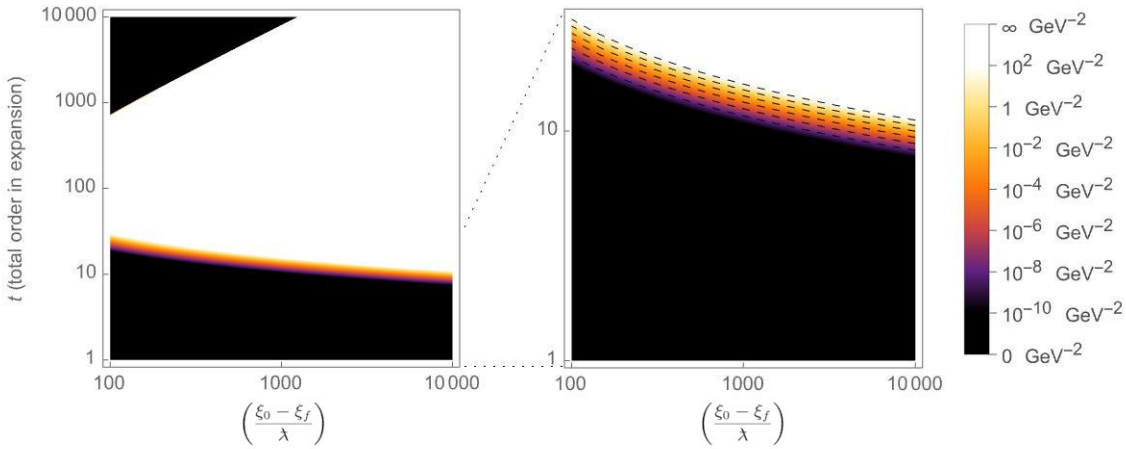

Figure 4.3: Density plots of eqs. 4.27 and 4.32, showing the enhancement of terms in the Lagrangian introduced by the comparators defined in section 4.3. Values less than 1 are all the same shade of indigo, i.e. this plot does not distinguish between different levels of suppression. We can see that, for every value of $\frac{\xi_0 - \xi_f}{\lambda}$, the enhancement increases as we examine higher-order terms, until eventually we reach a point where the enhancement drops off and becomes suppression. The value of t at which this drop-off occurs increases with the value of $\frac{\xi_0 - \xi_f}{\lambda}$.

Section 4.5

Conclusion

In this chapter, we showed how nonlocal corrections may be introduced into an EFT in curved spacetime. These nonlocal corrections emerge as a particle travels from one point in spacetime ξ_0 to a point ξ_f; one may construct comparators between the field content at ξ_0 and at ξ_f, so that the Lagrangian at ξ_0 can be expressed in terms of the field content at ξ_f. The resulting Lagrangian will contain terms introduced by these comparators, these being the nonlocal corrections. Because of the infrared (long-distance) divergence of the metric, these corrections can be quite substantial.

One consequence of this is that Planck-suppressed terms may receive enhancements. Whereas these terms are typically ignored and considered to be inconsequential, we see that, in curved spacetime, with the introduction of these nonlocal corrections, such operators may become experimentally probable.

More generally, these nonlocal corrections are important for any exploration of particle behavior in curved spacetime. For example, chapter 2 uses the rate of axion-photon decay in flat spacetime; in reality, this decay rate may receive substantial corrections, as the axions in question surround a black hole. There has been significant research interest in searching for axion dark matter by detecting the axion's interactions in astrophysical settings, e.g. [44, 45, 52–54, 57, 142–145]; any such search must account for these nonlocal corrections, and this is an important consideration in research going forward.

Chapter 5

Primakoff Mixing in a Single Riemann Normal Patch

Section 5.1

Introduction

There exists a plethora of data supporting the existence of dark matter, including the mass of galaxy clusters [146–151], galaxy rotation curves [152–156], the shape of the CMB power spectrum [157], simulations of large-scale structure formation [158, 159], and observational evidence from the bullet cluster [160] as well as other cluster mergers [161–164]. The composition of dark matter, however, remains one of the most significant open questions in modern physics. There are currently many ongoing experiments attempting to shed light on this topic [165–173].

The axion, originally proposed as solution to the strong CP problem, has emerged as a leading candidate for dark matter [86–92]. Besides these QCD axions, as they are sometimes called, there also exists a broader category of axion-like particles (ALPs) that have been proposed, including majorons [174, 175], familons [176–178], and axions emerging out of string theory [179–181]. In this chapter, we will use the term

"axion" to refer to both QCD axions and axion-like particles.

Like other dark matter candidates, conclusive evidence of the axion remains elusive, despite the efforts of many experiments, both laboratory-based [40–43] and astrophysical [44–57]. In these experimental efforts, the primary mechanism through which axions are expected to be observed is via Primakoff conversion [33–39]. This is a phenomenon where, in the presence of a strong background field, one species of boson can transition into another; in the case of axion searches, the relevant transition is an axion into a photon (or vice-versa) in the presence of a background electromagnetic field.

It has long been expected that regions of high dark matter density, known as dark matter spikes, will be found around supermassive black holes [1–6], and recent observational evidence seems to support this prediction [7, 8]. Thus, areas surrounding black holes are a prime candidate for asrophysical dark matter experiments. In order to conduct these experiments, then, it is essential that we have a working understanding of how mixing is performed in curved spacetime. The purpose of this chapter is to perform a simplified version of these calculations.

To do this, we will employ Riemann normal coordinates to construct a patch of locally flat spacetime, in which the problem of mixing becomes tractable. In order to incorporate nonlocal effects, one must use the method described in the previous chapter; for more on this, see [85]. In this chapter, we focus on the more basic question of mixing in a single Riemann normal patch, without nonlocal corrections. However, it must be stated that, do to the lack of these nonlocal corrections, the calculation presented in this chapter is incomplete and of little meaning on its own. Indeed, the curvature corrections that we find are highly suppressed, to the point where they are insignificant; in contrast, the curvature corrections would likely receive enhancements and become significant with the inclusion of nonlocal corrections. These nonlocal

corrections are accounted for in [83].

This chapter is divided as follows. In section 5.2, we review the literature on mixing in Minkowski space. In section 5.3, we detail our effective field theory approach and our use of Riemann normal coordinates, both of which are necessary to set up mixing in curved spacetime. In section 5.4 we present a derivation of the transition probabilities in curved spacetime Section 5.5 is the conclusion. Throughout this chapter, we will work in natural units of $c = \hbar = \epsilon_0 = 1$.

Section 5.2

Review of Bosonic Mixing in Minkowski Space

Many important papers [35–39] have detailed the mixing of low-mass scalar bosons with photons and gravitational waves in Minkowski space. Here we review these papers to establish notation and detail the seminal points of mixing in general. To date, in Minkowski space the mixing between axions and electromagnetic waves as well as the mixing between gravitational and electromagnetic waves has been detailed in the literature. Axion-gravitational wave Minkowski mixing has not appeared in the literature, although as we will see this can occur in Minkowski space, provided that there is a background axion field.

5.2.1. Axion-Electromagnetic Wave Mixing

Axions are pseudo-Nambu-Goldstone bosons that are hypothesized to result from the spontaneous breakdown of Peccei-Quinn symmetry (ALPs may result from the breakdown of other symmetries, depending on the specific ALP model). The axion can mix with the neutral pion to generate an effective coupling to photons,

$$\mathcal{L}_{\text{effective}} = -\frac{\tilde{\lambda}}{4}\,\phi\, F_{\mu\nu}\tilde{F}^{\mu\nu}\,, \tag{5.1}$$

where ϕ is the axion field and $F_{\mu\nu}$ ($\tilde{F}^{\mu\nu}$) is the electromagnetic field (dual) strength tensor. $\tilde{\lambda}$ is the axion-photon coupling constant with the dimensions of an inverse mass. $\tilde{\lambda}$ can very widely depending on the axion model. This coupling facilitates the conversion of axion waves to electromagnetic waves via static, background magnetic fields [35–38]. In other words, the background magnetic field provides the necessary quantum numbers needed so spin-zero bosons can oscillate into spin-one photons and vice-versa. For a system containing axions and photons in Minkowski space, the Lagrangian is

$$\begin{aligned}\mathcal{L} = &-\tfrac{1}{2}\big(\partial_\mu\phi\partial^\mu\phi + m^2\phi^2\big) - \tfrac{1}{4}F_{\mu\nu}F^{\mu\nu} - \tfrac{\tilde{\lambda}}{4}\,\phi\,F_{\mu\nu}\tilde{F}^{\mu\nu} \\ &+ \frac{1}{90\,m_e^4}\left(\frac{e^2}{4\pi}\right)^2\left((F_{\mu\nu}F^{\mu\nu})^2 + \frac{7}{4}(F_{\mu\nu}\tilde{F}^{\mu\nu})^2\right) .\end{aligned} \tag{5.2}$$

where ϕ is the axion field, m is the axion mass, and m_e is the electron mass. The second line is the weak-field limit of the Euler-Heisenberg Lagrangian, which encapsulates the one-loop QED vacuum polarization effect. The Euler-Heisenberg correction has the effect of inducing birefringence in the presence of a strong magnetic field [182, 183]:

$$n_\parallel = 1 + \frac{14}{45m_e^4}\left(\frac{e^2}{4\pi}\right)^2 B_T^2 \tag{5.3}$$

$$n_\perp = 1 + \frac{8}{45m_e^4}\left(\frac{e^2}{4\pi}\right)^2 B_T^2, \tag{5.4}$$

where B_T is the component of the magnetic field perpendicular to the propagation direction. Similar to neutrino oscillations [184–186], an effective Hamiltonian can be constructed,

$$i\frac{d}{dz}\begin{pmatrix}\phi\\ A_\parallel\end{pmatrix} = \begin{pmatrix}\omega+\Delta_a & \Delta_m\\ \Delta_m & \omega+\Delta_\parallel\end{pmatrix}\begin{pmatrix}\phi\\ A_\parallel\end{pmatrix} \tag{5.5}$$

where ω is the energy of the cohered wave. We have assumed the wave propagates in the z-direction. $A_\parallel$ is the part of the vector potential that is in the plane spanned by the z-axis and the magnetic field. The matrix elements are defined as

$$\Delta_\parallel = \omega\,(n_\parallel - 1) \tag{5.6}$$

$$\Delta_a = -\frac{m_a^2}{2\omega} \tag{5.7}$$

$$\Delta_m = \tfrac{1}{2}\,\tilde{\lambda}\,B_T. \tag{5.8}$$

Note that there is only mixing between axions and the parallel photon mode, not the perpendicular mode. Diagonalizing the Hamiltonian yields the following mixing angle,

$$\tan 2\theta_{\rm mix} = \frac{2\Delta_m}{\Delta_a - \Delta_\parallel}. \tag{5.9}$$

Similar to neutrino oscillations, the axion-photon oscillations are determined by a length scale [38],

$$\Delta_{\rm osc}^{-1} = 1/\sqrt{(\Delta_a - \Delta_\parallel)^2 + 4\Delta_m^2}\,. \tag{5.10}$$

The oscillation length parametrically depends on the dimensionful coupling, the axion mass, and the background magnetic field. The corresponding oscillation probabilities after traveling a distance z are [38]

$$P(A_\parallel \leftrightarrow \phi) = \sin^2 2\theta_{\rm mix}\ \sin^2\!\left(\tfrac{1}{2}\Delta_{\rm osc} z\right) \tag{5.11}$$

$$P(\phi \leftrightarrow \phi) = 1 - \sin^2 2\theta_{\rm mix}\ \sin^2\!\left(\tfrac{1}{2}\Delta_{\rm osc} z\right) \tag{5.12}$$

$$P(A_\parallel \leftrightarrow A_\parallel) = 1 - \sin^2 2\theta_{\rm mix}\ \sin^2\!\left(\tfrac{1}{2}\Delta_{\rm osc} z\right) \tag{5.13}$$

$$P(A_\perp \leftrightarrow A_\perp) = 1. \tag{5.14}$$

As we will show in Section 5.4, curved spacetime adds a new dimensionful parameter which alters the oscillating length and the resulting probabilities.

5.2.2. Gravity-Electromagnetic Wave Mixing

In addition to axion-photon mixing, background electromagnetic fields can also induce electromagnetic and gravitational wave mixing in Minkowski space [35, 36, 39]. This mixing is suppressed by the Planck mass and therefore requires the cohered state to travel long distances to observe an effect. Consider a gravitational wave perturbation of the Minkowski metric,

$$g_{\mu\nu} = \eta_{\mu\nu} + \kappa h_{\mu\nu}, \tag{5.15}$$

where $\kappa = 4\sqrt{\pi}/m_{\rm Pl}$, $m_{\rm Pl}$ is the Planck mass, and $\eta_{\mu\nu}$ is the Minkowski metric. Taking the metric to have $(-+++)$ signature, the resulting Lagrangian that is minimally coupled to gravity is [39]

$$\mathcal{L} = \frac{1}{\kappa^2}\sqrt{-g}\,R - \frac{1}{4}\sqrt{-g}\,F_{\mu\nu}F^{\mu\nu} + \frac{1}{90\,m_e^4}\left(\frac{e^2}{4\pi}\right)^2\left((F_{\mu\nu}F^{\mu\nu})^2 + \frac{7}{4}(\tilde{F}_{\mu\nu}F^{\mu\nu})^2\right). \tag{5.16}$$

The effective Hamiltonian [39] is

$$i\frac{d}{dz}\begin{pmatrix} A_\parallel \\ h_+ \\ A_\perp \\ h_\times \end{pmatrix} = \begin{pmatrix} \omega\, n_\parallel & B_T/m_{\rm pl} & 0 & 0 \\ B_T/m_{\rm pl} & \omega & 0 & 0 \\ 0 & 0 & \omega\, n_\perp & B_T/m_{\rm pl} \\ 0 & 0 & B_T/m_{\rm pl} & \omega \end{pmatrix}\begin{pmatrix} A_\parallel \\ h_+ \\ A_\perp \\ h_\times \end{pmatrix}. \tag{5.17}$$

where the indices of refraction are the same as in the previous section. The oscillation probabilities for a cohered state traveling a distance z are [39]

$$P(h_+ \leftrightarrow A_\perp) = \sin^2 2\theta_1 \, \sin^2(\Delta_\perp z/2) \tag{5.18}$$

$$P(h_\times \leftrightarrow A_\parallel) = \sin^2 2\theta_2 \, \sin^2(\Delta_\parallel z/2) \tag{5.19}$$

$$P(A_\perp \leftrightarrow A_\perp) = 1 - P(A_\perp \leftrightarrow h_+) \tag{5.20}$$

$$P(A_\parallel \leftrightarrow A_\parallel) = 1 - P(A_\parallel \leftrightarrow h_\times) \tag{5.21}$$

where

$$\tan 2\theta_1 = -\frac{2\kappa \, B_T}{\Delta_\perp} \qquad \text{and} \qquad \tan 2\theta_2 = -\frac{2\kappa \, B_T}{\Delta_\parallel} \,, \tag{5.22}$$

and $\Delta_{\perp,\parallel} = \omega \, (n_{\perp,\parallel} - 1)$.

It is worth noting that, in both photon-axion and photon-graviton mixing, the frequencies of the transition probabilities are solely a function of the on-diagonal components in eqs. 5.5 and 5.17, while the amplitudes of the transition probabilities are a function of both the on-diagonal and off-diagonal components. The photon-axion interaction term, $\sqrt{-g}\frac{\tilde{\lambda}}{4} F_{\mu\nu}\tilde{F}^{\mu\nu} = \frac{\tilde{\lambda}}{8}\epsilon^{\mu\nu\rho\sigma}F_{\mu\nu}F_{\rho\sigma}$ is topological (i.e., it has no dependence on the metric), so one might naively think that going from flat spacetime to curved spacetime will have no effect on photon-axion mixing. However, we will show that curved spacetime can alter the effective mass of both the photon and the graviton, changing the on-diagonal components of the mixing matrix.

Section 5.3

Effective Field Theory

To understand the evolution of electromagnetic, gravitational, and axion waves in a strong gravity environment, we use concepts from gravitational wave effective field

theory (GWEFT) in order to separate out the high-frequency degrees of freedom from the low-frequency, background physics [134, 137, 138]. In general relativity, this separation allows for linear, high-frequency gravitational waves to be separated from the low-frequency non-linear, background gravitational waves. We also apply the same concepts for the electromagnetic and axion waves.

To apply these techniques, we consider a locally flat patch of spacetime over which the external, background fields are roughly homogeneous. Importantly, this locally flat patch of spacetime can be relatively close to a compact object. This GWEFT allows for the curvature corrections to be calculated in a perturbative, systematic framework. The locally flat patch of spacetime allows for a relative inertial frame to be constructed. This, therefore, enables the orientation of the low-frequency, slowly varying background fields to be specified in relation to the high-frequency oscillating state. Thus, the mixing between the high-frequency axion, electromagnetic, and gravitational waves can be computed with the curvature corrections.

Applying these GWEFT techniques to Primakoff mixing is novel. At the length scales of interest and up to a chosen curvature correction, we mix the axion, electromagnetic, and gravitational waves in order to place the equations of motions into their mass eigenstates. The diagonalized equations of motion carry information about the probability of conversion of axion, electromagnetic and gravitational wave into each other in local Minkowski space. These results are valid across a limited patch of spacetime, but these patches may be chained together, according to the techniques in chapter 4, in order to estimate the total mixing along a longer length scale [83, 85].

As in flat spacetime, gravitational waves in curved spacetime are a perturbation of the background metric. The perturbation propagates on top of a larger-scale, (relatively) slowly changing background curvature. The background curvature is defined by two length scales, the radius of the background curvature $\mathcal{R}$ and the scale of in-

homogeneity of background curvature $\mathcal{L}$. The metric perturbation is defined by the reduced wavelength of the gravitational wave, $\lambda\!\!\!^{-} \equiv \lambda/(2\pi)$. We require $\lambda\!\!\!^{-} \ll \mathcal{L}$, which separates the lengthscales of the gravitational wave perturbation and the background. Defining a new parameter ϵ with parametric dependence $\epsilon \sim O(\lambda\!\!\!^{-}/\mathcal{L})$, we perform a perturbative expansion

$$g_{\mu\nu} = \overline{g}_{\mu\nu} + \epsilon\kappa h_{\mu\nu} + \frac{1}{2}\epsilon^2\kappa^2\overline{g}^{\rho\sigma}h_{\mu\rho}h_{\nu\sigma} + O(\epsilon^3). \tag{5.23}$$

In order for us to have $\delta^\mu_\nu = g^{\mu\rho}g_{\rho\nu}$, our expansion for the contravariant metric must be

$$g^{\mu\nu} = \overline{g}^{\mu\nu} - \epsilon\kappa h^{\mu\nu} + \frac{1}{2}\epsilon^2\kappa^2\overline{g}_{\rho\sigma}h^{\mu\rho}h^{\nu\sigma} + O(\epsilon^3), \tag{5.24}$$

where $h^{\mu\nu} = \overline{g}^{\mu\rho}\overline{g}^{\nu\sigma}h_{\rho\sigma}$. The higher-order terms in eq. 5.23 have been chosen such that the perturbation in the metric determinant g depends only on the trace of the metric perturbation, $h = h_{\mu\nu}\overline{g}^{\mu\nu}$. To see this, we define $p_{\mu\nu} = g_{\mu\nu} - \overline{g}_{\mu\nu}$, the total metric perturbation (to all orders in ϵ) and expressing g as a Taylor expansion in $p_{\mu\nu}$:

$$\begin{aligned} g &= \overline{g} + p_{\mu\nu}\left.\frac{\partial g}{\partial p_{\mu\nu}}\right|_{p_{\mu\nu}=0} + \frac{1}{2}p_{\mu\nu}p_{\rho\sigma}\left.\frac{\partial^2 g}{\partial p_{\mu\nu}\partial p_{\rho\sigma}}\right|_{p_{\mu\nu}=0} + \dots \\ &= \overline{g}\left(1 + p_{\mu\nu}\overline{g}^{\mu\nu} + \frac{1}{2}p_{\mu\nu}p_{\rho\sigma}\left(\overline{g}^{\mu\nu}\overline{g}^{\rho\sigma} - \overline{g}^{\mu\rho}\overline{g}^{\nu\sigma}\right) + \dots\right) \\ &= \overline{g}\left(1 + \epsilon\kappa h_{\mu\nu}\overline{g}^{\mu\nu} + \frac{1}{2}\epsilon^2\kappa^2 h_{\mu\nu}h_{\rho\sigma}\overline{g}^{\mu\nu}\overline{g}^{\rho\sigma} + \dots\right), \end{aligned} \tag{5.25}$$

where the derivatives were performed using Jacobi's equation, $\frac{\partial g}{\partial g_{\mu\nu}} = gg^{\mu\nu}$.

Henceforth, all quantities with a bar will be calculated using only the background metric (e.g. $\overline{\Gamma}^\rho_{\mu\nu}$ is the background Christoffel symbol, $\overline{R}_{\mu\nu}$ is the background Ricci tensor, etc.). Unlike in previous works on Primakoff-type mixing, where the background metric was set to the Minkowski metric, $\overline{g}_{\mu\nu} = \eta_{\mu\nu}$, we make no assumptions about $\overline{g}_{\mu\nu}$.

We perform a similar perturbative decomposition to the electromagnetic and scalar fields. We define $\mathcal{L}_{\text{em}}$ and $\mathcal{L}_{\text{ax}}$ as the lengthscale of inhomogeneities in the background electromagnetic and axion fields, respectively, with $\mathcal{L}_{\text{em}} \sim \mathcal{L}_{\text{ax}} \sim \mathcal{L}$. Since the electromagnetic, gravitational, and axion waves are cohered, they share the same reduced wavelength λ. Then the expansion is

$$\phi = \overline{\phi} + \alpha\phi^{(1)} \qquad\qquad A_\mu = \overline{A}_\mu + \beta A_\mu^{(1)}, \tag{5.26}$$

where

$$\alpha \sim O(\lambda/\mathcal{L}_{\text{ax}}) \qquad\qquad \beta \sim O(\lambda/\mathcal{L}_{\text{em}}). \tag{5.27}$$

ϵ, α, and β are merely bookkeeping variables, and at a later point they will be set equal to each other so as to cancel out.

Note that, while this sort of perturbative expansion has been performed on the electromagnetic and gravitational fields in previous works on mixing [35–39], previous works have not done so for the axion field, effectively treating the entire axion field as perturbative, i.e. assuming $\overline{\phi} = 0$. However, it has been demonstrated that there may exist a cosmic axion background [187], so we do away with this assumption and allow for a nonzero background axion field.

All of these scales are approximate and not precisely defined, but they will allow us to fix our gauge and specify our approximating assumptions, which we do in the coming subsections.

5.3.1. Linear Riemann Normal Coordinates

As in other types of mixing, e.g. neutrino oscillations, Primakoff-type bosonic mixing entails the existence of mass eigenstates that are linear combinations of the original

polarization eigenstates, and these mass eigenstates propagate independently of each other. The masses of these eigenstates depend on the background fields, which in turn depend on one's frame of reference; thus, mixing is a frame-dependent phenomenon, which does not lend itself easily to a covariant description. Instead, we must choose a specific frame of reference. We choose to work in linear Riemann normal coordinates (LNRC), defined as in chapter 3 by

$$\xi^\mu = \xi_0^\mu + a^\mu s, \tag{5.28}$$

where ξ_0^μ is the origin, a^μ is a vector tangent to the geodesic connecting ξ_0^μ to ξ^μ, and s is an affine parameter. This choice will offer us several advantages.

The first advantage is that, as discussed in section 3.4, it allows us to choose a gauge in which the metric perturbation has the form

$$h_{\mu\nu} = \begin{bmatrix} 0 & 0 & 0 & 0 \\ 0 & h_+ & h_\times & 0 \\ 0 & h_\times & -h_+ & 0 \\ 0 & 0 & 0 & 0 \end{bmatrix} + O\left((\xi - \xi_0)^2\right). \tag{5.29}$$

(This assumes that the gravitational wave is propagating in the 0 and 3 directions.) Thus, provided that we only proceed in our calculations up to first order in $\xi^\mu - \xi_0^\mu$, we may treat $h_{\mu\nu}$ as having the same form as in flat spacetime. This gauge choice is known as the transverse-traceless (TT) gauge, defined by $h = 0$ and $\overline{\nabla}_\alpha h^{\alpha\beta}$. Furthermore, because eq. 5.29 is traceless, the perturbed metric determinant becomes equal to the background metric determinant, $g = \overline{g}$, per eq. 5.25.

The second benefit of working in LRNC is that it gives both the metric and the

connection a convenient form, to first order in $\xi^\mu - \xi_0^\mu$:

$$\overline{g}_{\mu\nu} = \eta_{\mu\nu} + O\left((\xi - \xi_0)^2\right) \tag{5.30}$$

$$\overline{\Gamma}^\rho_{\mu\nu} = -\frac{2}{3}\,\overline{R}^\rho{}_{(\mu\nu)\alpha}\Big|_{s=0}(\xi^\alpha - \xi_0^\alpha) + O\left((\xi - \xi_0)^2\right). \tag{5.31}$$

If we know the Riemann tensor in some arbitrary coordinate system, and we have chosen a tetrad that converts between this coordinate system and LRNC (as discussed in chapter 3, this tetrad is a gauge choice), then we may contract the Riemann tensor in this coordinate system with the tetrad in order to get $\overline{R}^\rho{}_{(\mu\nu)\alpha}\Big|_{s=0}$.

Lastly, because LRNC is locally flat, we are able to split the electromagnetic field into an electric and magnetic component, which is not generally possible in curved spacetime. In astrophysical contexts, the electric field is generally negligible compared to the magnetic field, and so we assume the background electromagnetic tensor has the form

$$\overline{F}_{\mu\nu} = \begin{bmatrix} 0 & 0 & 0 & 0 \\ 0 & 0 & B_L & 0 \\ 0 & -B_L & 0 & B_T \\ 0 & 0 & B_T & 0 \end{bmatrix}, \tag{5.32}$$

where B_T is the component of the background magnetic field perpendicular to the propagation direction, and B_L is the component of the background magnetic field parallel to the propagation direction.

5.3.2. Order of Approximation

Any EFT is only valid up to a certain order of approximation. With our local inertial frame and our lengthscales defined, we must now choose that order of approximation. We will retain all terms in the Lagrangian of at least order $\frac{\lambda^2}{\mathcal{L}^4}\mathcal{A}^2 \sim \frac{\lambda^2}{\mathcal{L}^4_{\rm em}}\mathcal{A}^2 \sim \frac{\lambda^2}{\mathcal{L}^4_{\rm ax}}\mathcal{A}^2$, where $\mathcal{A}$ is the amplitude of the perturbative (high-frequency) fields. A consequence of this is that we will only keep terms with at most two combined factors of ϵ, α, and β. This corresponds to only keeping terms with at most two high-frequency fields, which

is in line with our desire to examine mixing, specifically; an interaction involving more than two high-frequency fields could result in the creation or destruction of a high-frequency particle, whereas mixing keeps the total number of (high-frequency, non-background) particles constant. That is to say, interactions involving three or more high-frequency fields are not mixing.

A consequence of this approximation is that we will keep some terms proportional to $\partial\overline{F}$. This is a departure from previous works on mixing, in which the background electromagnetic field has been treated as uniform. The standard practice in these investigations has been to divide spacetime into regions in which the variance of the background electromagnetic field could be neglected; this is known as the domain-like sharp-edges method (DLSHE; see [188] for a review of the DLSHE and for the presentation of an alternative treatment). However, in order to encapsulate the effects of curved spacetime on mixing, it is necessary that we not neglect effects of this order.

A specific caveat must be made for the Euler-Heisenberg terms. As we will see, all Euler-Heisenberg terms are, in the Lagrangian, at least of order $\frac{B^2}{m_e^4\mathcal{L}_{\text{em}}^2}\mathcal{A}^2$, where m_e is the electron mass and $B = \sqrt{B_T^2 + B_L^2}$ is the magnitude of the magnetic field. Thus it is not clear where they fit in our approximation scheme. We will keep all Euler-Heisenberg terms at the level of the Lagrangian (with an exception to be described momentarily). However, at the level of the equation of motion, some Euler-Heisenberg terms will be order $\frac{B^2}{m_e^4\mathcal{L}_{\text{em}}^3}\mathcal{A}$ and others will be order $\frac{B^2}{m_e^4\mathcal{L}_{\text{em}}^2\lambda}\mathcal{A}$; we will keep the latter but not the former.

The final approximation we will make is, at the level of the equation of motion, to keep terms with at most only one factor of κ, $\tilde{\lambda}$, $\xi^\mu - \xi_0^\mu$, and $\frac{1}{m_e^4}$. We will later diagonalize the mixing matrix using perturbation theory, treating these as the perturbative variables; therefore, any term with more than one factor of these variables will not contribute to the final transition probabilities. As a result, we will neglect

the expansion of the background metric within the Euler-Heisenberg terms, as such terms would be proportional to $\frac{\kappa}{m_e^4}$.

Another consequence of this last approximation is that we may neglect the background Ricci tensor, $\overline{R}_{\mu\nu} \sim 0$. This is a direct consequence of the trace-reversed Einstein field equation, $\overline{R}_{\mu\nu} = \frac{\kappa^2}{2}\left(\overline{T}_{\mu\nu} - \frac{1}{2}\overline{T}\,\overline{g}_{\mu\nu}\right)$, where $\overline{T}_{\mu\nu}$ is the stress-energy tensor calculated using only background quantities, and $\overline{T}$ is its trace.

Section 5.4

Mixing in Curved Spacetime

We have now established the necessary principles to calculate Primakoff-type bosonic mixing in curved spacetime. Let us consider a system consisting only of photons, gravitons, and axions. The action for such a system is

$$\begin{aligned} S = \int \mathrm{d}^4x\sqrt{-g}\Bigg(&\frac{1}{\kappa^2}R - \frac{1}{4}g^{\alpha\beta}g^{\gamma\delta}F_{\alpha\gamma}F_{\beta\delta} - \frac{1}{2}\left(g^{\alpha\beta}\partial_a\phi\partial_b\phi + m^2\phi^2\right) \\ &+ \frac{1}{90m_e^4}\left(\frac{e^2}{4\pi}\right)^2\left(\left(g^{\alpha\beta}g^{\gamma\delta}F_{\alpha\gamma}F_{\beta\delta}\right)^2 + \frac{7}{4}\left(\frac{1}{2\sqrt{-g}}\epsilon^{\alpha\beta\gamma\delta}F_{\alpha\beta}F_{\gamma\delta}\right)^2\right) \\ &+ \frac{\tilde{\lambda}}{8\sqrt{-g}}\epsilon^{\alpha\beta\gamma\delta}\phi F_{\alpha\beta}F_{\gamma\delta}\Bigg). \end{aligned} \tag{5.33}$$

We assume from this point onward that we are in LRNC.

5.4.1. Equations of Motion

We perform the perturbative expansions described in section 5.3, with the metric perturbation subject to the TT gauge conditions, $h = \overline{\nabla}_\alpha h^{\alpha\beta} = 0$. As described in section 5.3.2, we keep the terms in the Lagrangian with at most two (combined) factors of ϵ, α, and β. Thus our action, in terms of the perturbative variables $h_{\alpha\beta}$,

$F^{(1)}_{\alpha\beta}$ and $\phi^{(1)}$, becomes

$$
\begin{aligned}
S = \int \mathrm{d}^4x\sqrt{-\overline{g}}\Bigg(&\frac{1}{\kappa^2}\overline{R} - \frac{\epsilon}{\kappa}\overline{R}_{\beta\delta}h^{\beta\delta} + \frac{\epsilon^2}{4}h^{\beta\delta}\overline{\Box}h_{\beta\delta} - \epsilon^2 g^{\alpha\gamma}\overline{R}_{\alpha\beta}h^{\beta\delta}h_{\gamma\delta} + \frac{3\epsilon^2}{2}h^{\beta\delta}h^{\alpha\gamma}\overline{R}_{\alpha\beta\gamma\delta} \\
&- \frac{1}{4}\overline{g}^{\alpha\beta}\overline{g}^{\gamma\delta}\Big(\overline{F}_{\alpha\gamma}\overline{F}_{\beta\delta} + 2\beta\overline{F}_{\alpha\gamma}F^{(1)}_{\beta\delta} + \beta^2F^{(1)}_{\alpha\gamma}F^{(1)}_{\beta\delta}\Big) \\
&+ \frac{\epsilon\kappa}{2}g^{\alpha\beta}h_{\gamma\delta}\Big(\overline{F}_{\alpha\gamma}\overline{F}_{\beta\delta} + 2\beta\overline{F}_{\alpha\gamma}F^{(1)}_{\beta\delta}\Big) - \frac{\epsilon^2\kappa^2}{4}h^{\alpha\beta}h^{\gamma\delta}\overline{F}_{\alpha\gamma}\overline{F}_{\beta\delta} \\
&- \frac{\epsilon^2\kappa^2}{4}g^{\alpha\beta}\overline{g}_{\mu\nu}h^{ce}h^{df}\overline{F}_{\alpha\gamma}\overline{F}_{\beta\delta} - \tfrac{1}{2}\overline{g}_{\alpha\beta}\Big(\partial_a\overline{\phi}\partial_b\overline{\phi} + 2\alpha\partial_a\overline{\phi}\partial_b\phi^{(1)} + \alpha^2\partial_a\phi^{(1)}\partial_b\phi^{(1)}\Big) \\
&+ \frac{\epsilon\kappa}{2}h^{\alpha\beta}\Big(\partial_a\overline{\phi}\partial_b\overline{\phi} + 2\alpha\partial_a\overline{\phi}\partial_b\phi^{(1)}\Big) - \frac{\epsilon^2\kappa^2}{4}\overline{g}_{\gamma\delta}h^{\alpha\gamma}h^{\beta\delta}\partial_a\overline{\phi}\partial_b\overline{\phi} \\
&- \tfrac{1}{2}m^2\overline{\phi}^2 - \alpha m^2\overline{\phi}\phi^{(1)} - \frac{\alpha^2}{2}m^2\big(\phi^{(1)}\big)^2 \\
&+ \frac{\tilde{\lambda}}{8\sqrt{-\overline{g}}}\epsilon^{\alpha\beta\gamma\delta}\overline{\phi}\Big(\overline{F}_{\alpha\beta}\overline{F}_{\gamma\delta} + 2\beta\overline{F}_{\alpha\beta}F^{(1)}_{\gamma\delta} + \beta^2F^{(1)}_{\alpha\beta}F^{(1)}_{\gamma\delta}\Big) \\
&+ \frac{\alpha\tilde{\lambda}}{8\sqrt{-\overline{g}}}\phi^{(1)}\Big(\overline{F}_{\alpha\beta}\overline{F}_{\gamma\delta} + 2\beta\overline{F}_{\alpha\beta}F^{(1)}_{\gamma\delta}\Big) \\
&+ \frac{1}{90m_e^4}\Big(\frac{e^2}{4\pi}\Big)^2\Big(\big(\overline{g}^{\alpha\beta}\overline{g}^{\gamma\delta}\overline{F}_{\alpha\gamma}\overline{F}_{\beta\delta}\big)^2 + \frac{7}{4}\Big(\frac{1}{2\sqrt{-\overline{g}}}\epsilon^{\alpha\beta\gamma\delta}\overline{F}_{\alpha\beta}\overline{F}_{\gamma\delta}\Big)^2\Big) \\
&+ \frac{2\beta}{45m_e^4}\Big(\frac{e^2}{4\pi}\Big)^2\Bigg(\big(\overline{g}^{\alpha\beta}\overline{g}^{\gamma\delta}\overline{F}_{\alpha\gamma}\overline{F}_{\beta\delta}\big)\big(\overline{g}^{\mu\nu}\overline{g}^{\rho\sigma}\overline{F}_{\mu\rho}F^{(1)}_{\nu\sigma}\big) \\
&\qquad + \frac{7}{4}\left(\frac{1}{2\sqrt{-\overline{g}}}\epsilon^{\alpha\beta\gamma\delta}\overline{F}_{\alpha\beta}\overline{F}_{\gamma\delta}\right)\left(\frac{1}{2\sqrt{-\overline{g}}}\epsilon^{\mu\nu\rho\sigma}\overline{F}_{\mu\nu}F^{(1)}_{\rho\sigma}\right)\Bigg) \\
&+ \frac{\beta^2}{45m_e^4}\Big(\frac{e^2}{4\pi}\Big)^2\Bigg(\big(\overline{g}^{\alpha\beta}\overline{g}^{\gamma\delta}\overline{F}_{\alpha\gamma}\overline{F}_{\beta\delta}\big)\big(\overline{g}^{\mu\nu}\overline{g}^{\rho\sigma}F^{(1)}_{\mu\rho}F^{(1)}_{\nu\sigma}\big) \\
&\qquad + \frac{7}{4}\left(\frac{1}{2\sqrt{-\overline{g}}}\epsilon^{\alpha\beta\gamma\delta}\overline{F}_{\alpha\beta}\overline{F}_{\gamma\delta}\right)\left(\frac{1}{2\sqrt{-\overline{g}}}\epsilon^{\mu\nu\rho\sigma}F^{(1)}_{\mu\nu}F^{(1)}_{\rho\sigma}\right)\Bigg) \\
&+ \frac{2\beta^2}{45m_e^4}\Big(\frac{e^2}{4\pi}\Big)^2\left(\big(\overline{g}^{\alpha\beta}\overline{g}^{\gamma\delta}\overline{F}_{\alpha\gamma}F^{(1)}_{\beta\delta}\big)^2 + \frac{7}{4}\left(\frac{1}{2\sqrt{-\overline{g}}}\epsilon^{\alpha\beta\gamma\delta}\overline{F}_{\alpha\beta}F^{(1)}_{\gamma\delta}\right)^2\right)\Bigg).
\end{aligned}
\tag{5.34}
$$

From this, we get the equations of motion for $h_{\beta\delta}$, $A^{(1)}_\delta$, and $\phi^{(1)}$. We make further use of the approximations from section 5.3.2 in order to simplify. We additionally set $\epsilon = \alpha = \beta$, which we may freely do, as they are simply bookkeeping variables. We

get

$$\overline{\Box} h_{\beta\delta} + 6h^{\alpha\gamma}\overline{R}_{\alpha\beta\gamma\delta} - 2\kappa\overline{g}^{\alpha\gamma}\overline{\nabla}_{(\beta}\overline{F}_{\delta)\alpha}A^{(1)}_{\gamma} + 2\kappa\overline{F}_{\alpha(\beta}\overline{\nabla}^{\alpha}A^{(1)}_{\delta)} - 2\kappa\phi^{(1)}\overline{\nabla}_{\beta}\overline{\nabla}_{\delta}\overline{\phi} = \overline{J}^{(h)}_{\beta\delta} \tag{5.35}$$

$$(\overline{g}^{\beta\gamma}\overline{g}^{\alpha\delta} - \overline{g}^{\alpha\gamma}\overline{g}^{\beta\delta})\,\overline{\nabla}_{\beta}\overline{\nabla}_{\gamma}A^{(1)}_{\delta} - \overline{M}^{\alpha\beta\gamma\delta}\overline{\nabla}_{\beta}\overline{\nabla}_{\gamma}A^{(1)}_{\delta} + \tilde{\lambda}\epsilon^{\alpha\beta\gamma\delta}\overline{\nabla}_{\beta}\overline{\nabla}_{\gamma}A^{(1)}_{\delta} - \frac{\tilde{\lambda}}{2}\epsilon^{\alpha\beta\gamma\delta}\overline{F}_{\beta\delta}\overline{\nabla}_{\gamma}\phi^{(1)} + \kappa\overline{g}^{\beta\alpha}h^{\gamma\delta}\overline{\nabla}_{\gamma}\overline{F}_{\beta\delta} + \kappa\overline{g}^{\gamma\delta}\overline{F}_{\beta\delta}\overline{\nabla}_{\gamma}h^{\alpha\beta} = \overline{J}^{(A)^{\alpha}} \tag{5.36}$$

$$\overline{\Box}\phi^{(1)} - m^2\phi^{(1)} - \kappa h^{\alpha\beta}\overline{\nabla}_{\alpha}\overline{\nabla}_{\beta}\overline{\phi} + \frac{\tilde{\lambda}}{2}\epsilon^{abcd}\overline{F}_{\alpha\beta}\overline{\nabla}_{\gamma}A^{(1)}_{\delta} = \overline{J}^{(\phi)}, \tag{5.37}$$

where

$$\overline{M}^{\alpha\beta\gamma\delta} = \frac{4}{45m_e^4}\Big(\frac{e^2}{4\pi}\Big)^2\bigg(\big(\overline{g}^{\beta\gamma}\overline{g}^{\alpha\delta} - \overline{g}^{\alpha\gamma}\overline{g}^{\beta\delta}\big)\overline{F}^2 - 4\overline{g}^{\alpha\nu}\overline{g}^{\beta\sigma}\overline{g}^{\gamma\mu}\overline{g}^{\delta\rho}\overline{F}_{\mu\rho}\overline{F}_{\nu\sigma} - \frac{7}{4}\frac{\epsilon^{\alpha\beta\rho\sigma}\epsilon^{\gamma\delta\mu\nu}}{-\overline{g}}\overline{F}_{\mu\nu}\overline{F}_{\rho\sigma}\bigg) \tag{5.38}$$

$$\overline{J}^{(h)}_{\beta\delta} = \frac{\kappa}{\epsilon}\big(\overline{g}^{\alpha\gamma}\overline{F}_{\alpha(\beta}\overline{F}_{\delta)\gamma} - \overline{\nabla}_{\beta}\overline{\phi}\,\overline{\nabla}_{\delta}\overline{\phi}\big) \tag{5.39}$$

$$\overline{J}^{(A)^a} = \frac{1}{\beta}\,\frac{\tilde{\lambda}}{2}\,\epsilon^{\alpha\beta\gamma\delta}\overline{F}_{\beta\delta}\,\overline{\nabla}_{\gamma}\overline{\phi} \tag{5.40}$$

$$\overline{J}^{(\phi)} = \frac{1}{\alpha}\Big(m^2\overline{\phi} - \overline{\nabla}^{\alpha}\overline{\nabla}_{\alpha}\overline{\phi} - \frac{\tilde{\lambda}}{8}\epsilon^{\alpha\beta\gamma\delta}\overline{F}_{\alpha\beta}\overline{F}_{\gamma\delta}\Big). \tag{5.41}$$

We may expand the background metric and the covariant derivatives using eqs. 5.30 and 5.31, out to first order in $\xi^{\mu} - \xi^{\mu}_0$. Similarly, because we are only going to first order in $\xi^{\mu} - \xi^{\mu}_0$, we may write the metric perturbation in terms of its polarization modes,

$$h_{\mu\nu} = \big(\delta^1_{\mu}\delta^1_{\nu} - \delta^2_{\mu}\delta^2_{\nu}\big)\,h_{+} + \big(\delta^1_{\mu}\delta^2_{\nu} + \delta^2_{\mu}\delta^1_{\nu}\big)\,h_{\times}. \tag{5.42}$$

Similarly, we gauge fix the electromagnetic four-potential to the Coulomb gauge, in

which

$$0 = \partial^1 A_1^{(1)} + \partial^2 A_2^{(1)} + \partial^3 A_3^{(1)} = \partial^3 A_3^{(1)}, \tag{5.43}$$

where in the last step we have assumed that the system only varies along the 0 and 3 directions. Because $A_\mu^{(1)}$ contains the perturbative (i.e. nonconstant) component of the electromagnetic four-potential, we conclude $A_3^{(1)} = 0$. Furthermore, in the Coulomb gauge, A_0 is given by an integral of the electric charge density over all space; since we are in free space with no electric charges, we get $A_0 = 0$. We may therefore write

$$A_\mu^{(1)} = \delta_\mu^1 A_1^{(1)} + \delta_\mu^2 A_2^{(1)}. \tag{5.44}$$

After performing these substitutions, we may contract the gravitational equation of motion with $\frac{1}{2}\left(\delta_1^\beta \delta_1^\delta - \delta_2^\beta \delta_2^\delta\right)$ to get the equation of motion for h_+, and we may contract it with $\frac{1}{2}\left(\delta_1^\beta \delta_2^\delta + \delta_2^\beta \delta_1^\delta\right)$ to get the equation of motion for $h_\times$. Similarly, we may contract the equation of motion for electromagnetism with δ_1^α and δ_2^α to get the equation of motion for $A_1^{(1)}$ and $A_2^{(1)}$, respectively. Thus we arrive at the equations of motion for our five degrees of freedom:

$$\begin{aligned}
&\partial^\alpha \partial_\alpha h_+ + \tfrac{2}{3}\eta^{\alpha\gamma}\Big(\overline{R}_{1\gamma1\rho}\big|_{s=0} + \overline{R}_{2\gamma2\rho}\big|_{s=0}\Big)(\xi^\rho - \xi_0^\rho)\partial_\alpha h_+ - 6\overline{R}_{1212} h_+ \\
&\qquad - 2\eta^{\alpha\gamma}\overline{R}_{12\gamma\rho}\big|_{s=0}(\xi^\rho - \xi_0^\rho)\partial_\alpha h_\times - \kappa\big(\partial_1\partial_1\overline{\phi} - \partial_2\partial_2\overline{\phi}\big)\,\phi^{(1)} \\
&\qquad - \kappa\partial_2 B_L A_1^{(1)} - \kappa\partial_1 B_L A_2^{(1)} + \kappa B_T \partial_3 A_2^{(1)} = \tfrac{1}{2}\big(\overline{J}_{11}^{(h)} - \overline{J}_{22}^{(h)}\big),
\end{aligned} \tag{5.45}$$

$$\begin{aligned}
&\partial^\alpha \partial_\alpha h_\times + \tfrac{2}{3}\eta^{\alpha\gamma}\Big(\overline{R}_{1\gamma1\rho}\big|_{s=0} + \overline{R}_{2\gamma2\rho}\big|_{s=0}\Big)(\xi^\rho - \xi_0^\rho)\partial_\alpha h_\times - 6\overline{R}_{1212} h_\times \\
&\qquad - 2\eta^{\alpha\gamma}\overline{R}_{21\gamma\rho}\big|_{s=0}(\xi^\rho - \xi_0^\rho)\partial_\alpha h_+ - 2\kappa(\partial_1\partial_2\overline{\phi})\,\phi^{(1)} \\
&\qquad + \kappa\partial_1 B_L A_1^{(1)} - \kappa\partial_2 B_L A_2^{(1)} - \kappa B_T \partial_3 A_1^{(1)} = \tfrac{1}{2}\big(\overline{J}_{12}^{(h)} + \overline{J}_{21}^{(h)}\big),
\end{aligned} \tag{5.46}$$

$$\partial^\alpha\partial_\alpha A_1^{(1)} - \overline{M}_1^{\beta\gamma}\,\partial_\beta\partial_\gamma A_1^{(1)} + \eta^{\alpha\gamma}\overline{R}_{1\gamma1\rho}\big|_{s=0}(\xi^\rho - \xi_0^\rho)\partial_\alpha A_1^{(1)} - \eta^{\alpha\gamma}\overline{R}_{\gamma21\rho}\big|_{s=0}(\xi^\rho - \xi_0^\rho)\partial_\alpha A_2^{(1)} + \tilde{\lambda}\,\epsilon^{1\beta\gamma2}\partial_\beta\overline{\phi}\,\partial_\gamma A_2^{(1)} - \tilde{\lambda}B_T\partial_0\phi^{(1)} - \kappa\partial_2 B_L h_+ + \kappa\partial_1 B_L h_\times + \kappa B_T\partial_3 h_\times = \overline{J}^{(A)1}, \tag{5.47}$$

$$\partial^\alpha\partial_\alpha A_2^{(1)} - \overline{M}_2^{\beta\gamma}\,\partial_\beta\partial_\gamma A_2^{(1)} + \eta^{\alpha\gamma}\overline{R}_{2\gamma2\rho}\big|_{s=0}(\xi^\rho - \xi_0^\rho)\partial_\alpha A_2^{(1)} - \eta^{\alpha\gamma}\overline{R}_{\gamma12\rho}\big|_{s=0}(\xi^\rho - \xi_0^\rho)\partial_\alpha A_1^{(1)} + \tilde{\lambda}\,\epsilon^{2\beta\gamma1}\partial_\beta\overline{\phi}\,\partial_\gamma A_1^{(1)} - \kappa\partial_1 B_L h_+ - \kappa\partial_2 B_L h_\times - \kappa B_T\partial_3 h_+ = \overline{J}^{(A)2}, \tag{5.48}$$

$$\partial^\alpha\partial_\alpha\phi^{(1)} - m^2\phi^{(1)} - \kappa\big(\partial_1\partial_1\overline{\phi} - \partial_2\partial_2\overline{\phi}\big)h_+ - 2\kappa\partial_1\partial_2\overline{\phi}\,h_\times + \tilde{\lambda}B_T\partial_0 A_1^{(1)} = \overline{J}^{(\phi)}, \tag{5.49}$$

where

$$\overline{M}_1^{\beta\gamma} = \frac{4}{45m_e^4}\left(\frac{e^2}{4\pi}\right)^2\begin{bmatrix} -2B_L^2+5B_T^2 & 0 & 0 & 0\\ 0 & 0 & 0 & 0\\ 0 & 0 & 6B_L^2+2B_T^2 & 0\\ 0 & 0 & 0 & 2B_L^2+2B_T^2\end{bmatrix} \tag{5.50}$$

$$\overline{M}_2^{\beta\gamma} = \frac{4}{45m_e^4}\left(\frac{e^2}{4\pi}\right)^2\begin{bmatrix} -2B_L^2-2B_T^2 & 0 & 0 & 0\\ 0 & 6B_L^2+2B_T^2 & 0 & -4B_LB_T\\ 0 & 0 & 0 & 0\\ 0 & -4B_LB_T & 0 & 2B_L^2+6B_T^2\end{bmatrix}. \tag{5.51}$$

5.4.2. Ansatz in Curved Spacetime

In flat spacetime, the high-frequency fields are assumed to have the form

$$\psi \propto e^{ik_\alpha(\xi^\alpha - \xi_0^\alpha)}, \tag{5.52}$$

where ψ is one of h_+, $h_\times$, $A_1^{(1)}$, $A_2^{(1)}$, $\phi^{(1)}$; and $k_\alpha k^\alpha = -m_\psi^2$, where m_ψ is the effective mass of ψ. a solution to the wave equation without interactions. However, in curved spacetime, the wave equation without interaction takes a different form, as can be seen from eqs. 5.45 through 5.49. In all of the above equations of motion, the kinetic

and mass terms take the form

$$N^{\alpha\beta}\partial_\alpha\partial_\beta\psi + \eta^{\alpha\beta}P_{\beta\gamma}(\xi^\gamma - \xi_0^\gamma)\partial_\alpha\psi - m_\psi^2\psi. \tag{5.53}$$

Due to the dependence of the middle term on $\xi^\gamma - \xi_0^\gamma$, the solution to this will not be a plane wave. The middle term is a correction caused by the background curvature, so it makes sense that it would prevent ψ from being a plane wave, as the solution to the wave equation in curved spacetime is not a plane wave. Background curvature causes corrections to both the phase and amplitude of the solution to the wave equation [189, 190]. We may calculate those corrections by setting eq. 5.53 equal to 0 and finding a solution.

Before we do so, it is useful to reduce our indices. Because we are assuming that the system propagates only in the 0 and 3 directions, we assume that $\xi^\rho - \xi_0^\rho = 0$ if $\rho = 1, 2$, and the derivative of any high-frequency field in either the 1 or 2 direction is 0. We may therefore constrain all Greek indices in eqs. 5.45 through 5.49 to be either 0 or 3. To make this clear, we will use capital Latin letters to indicate indices that can only be 0 or 3. In particular,

$$\eta^{AB} = \begin{bmatrix} -1 & 0 \\ 0 & 1 \end{bmatrix} \tag{5.54}$$

$$\overline{M}_1^{AB} = \frac{4}{45m_e^4}\left(\frac{e^2}{4\pi}\right)^2 \begin{bmatrix} -2B_L^2 + 5B_T^2 & 0 \\ 0 & 2B_L^2 + 2B_T^2 \end{bmatrix} \tag{5.55}$$

$$\overline{M}_2^{AB} = \frac{4}{45m_e^4}\left(\frac{e^2}{4\pi}\right)^2 \begin{bmatrix} -2B_L^2 - 2B_T^2 & 0 \\ 0 & 2B_L^2 + 6B_T^2 \end{bmatrix}, \tag{5.56}$$

and the wave equation we wish to solve becomes

$$N^{AB}\partial_A\partial_B\psi + \eta^{AB}P_{BC}(\xi^C - \xi_0^C)\partial_A\psi - m_\psi^2\psi = 0. \tag{5.57}$$

The solution to eq. 5.57 is given by the ansatz

$$\psi = \Psi e^{ik_A(\xi^A - \xi_0^A) + K_{AB}(\xi^A - \xi_0^A)(\xi^B - \xi_0^B)}, \tag{5.58}$$

where Ψ is the amplitude (which is assumed to vary slowly), and K is a (species-dependent) symmetric tensor, such that

$$4N^{AB}K_{BC} + \eta^{AB}P_{BC} = 0. \tag{5.59}$$

Note that this is an order $(\xi - \xi_0)^2$ correction to the amplitude of the wave. If we substitute this ansatz into eq. 5.57, the terms that are first-order in $\xi - \xi_0$ cancel out, so we get

$$\left(2N^{AB}K_{AB} - N^{AB}k_Ak_B - m_\psi^2\right)\psi + O\left((\xi - \xi_0)^2\right) = 0. \tag{5.60}$$

The K's are given by

$$K^+_{AB} = K^\times_{AB} = -\tfrac{1}{6}\begin{bmatrix} \overline{R}_{1010}\big|_{s=0} + \overline{R}_{2020}\big|_{s=0} & \overline{R}_{1013}\big|_{s=0} + \overline{R}_{2023}\big|_{s=0} \\ \overline{R}_{1013}\big|_{s=0} + \overline{R}_{2023}\big|_{s=0} & \overline{R}_{1313}\big|_{s=0} + \overline{R}_{2323}\big|_{s=0} \end{bmatrix} \tag{5.61}$$

$$K^\parallel_{AB} = -\tfrac{1}{4}\begin{bmatrix} \overline{R}_{1010}\big|_{s=0} & \overline{R}_{1013}\big|_{s=0} \\ \overline{R}_{1013}\big|_{s=0} & \overline{R}_{1313}\big|_{s=0} \end{bmatrix} \tag{5.62}$$

$$K^\perp_{AB} = -\tfrac{1}{4}\begin{bmatrix} \overline{R}_{2020}\big|_{s=0} & \overline{R}_{2023}\big|_{s=0} \\ \overline{R}_{2023}\big|_{s=0} & \overline{R}_{2323}\big|_{s=0} \end{bmatrix} \tag{5.63}$$

$$K^\phi_{AB} = 0. \tag{5.64}$$

Strictly speaking, $K^\parallel$ and $K^\perp$ should also contain Euler-Heisenberg corrections, but we neglect this. For brevity, we write out species-dependent ansatz as

$$E^n = e^{ik_A(\xi^A - \xi_0^A) + K^n_{AB}(\xi^A - \xi_0^A)(\xi^B - \xi_0^B)}. \tag{5.65}$$

We then define our amplitudes as

$$h_+ = G_+E^+ \qquad h_\times = G_\times E^\times \qquad \phi^{(1)} = aE^\phi$$
$$A_1^{(1)} = i\sqrt{\mu_\parallel}A_\parallel E^\parallel \qquad A_2^{(1)} = -i\sqrt{\mu_\perp}A_\perp E^\perp \tag{5.66}$$

where

$$\mu_\parallel^{-1} = 1 - \overline{M}_1^{33} = 1 - \frac{4}{45m_e^4}\left(\frac{e^2}{4\pi}\right)^2\left(2B_L^2 + 2B_T^2\right) \tag{5.67}$$
$$\mu_\perp^{-1} = 1 - \overline{M}_2^{33} = 1 - \frac{4}{45m_e^4}\left(\frac{e^2}{4\pi}\right)^2\left(2B_L^2 + 6B_T^2\right). \tag{5.68}$$

Defining the elements of k as $k_\alpha = (-\omega, 0, 0, k)$, the equations of motion become

$$\begin{aligned}
&\Big(\omega^2 - k^2 - \tfrac{16}{3}\,\overline{R}_{1212}\big|_{\xi_0} + 6\,\overline{R}_{1212,\rho}\big|_{\xi_0}(\xi^\rho - \xi_0^\rho)\Big)G_+E^+ \\
&\qquad - 2i(\xi^\rho - \xi_0^\rho)\big(\omega\,\overline{R}_{120\rho}\big|_{\xi_0} + k\,\overline{R}_{123\rho}\big|_{\xi_0}\big)G_\times E^\times \\
&\qquad + \kappa\sqrt{\mu_\perp}\big(kB_T + i\partial_1 B_L\big)A_\perp E^\perp - i\kappa\sqrt{\mu_\parallel}\partial_2 B_L A_\parallel E^\parallel \\
&\qquad - \kappa\big(\partial_1\partial_1\overline{\phi} - \partial_2\partial_2\overline{\phi}\big)aE^\phi = \tfrac{1}{2}\big(\overline{J}_{11}^{(h)} - \overline{J}_{22}^{(h)}\big)
\end{aligned} \tag{5.69}$$

$$\begin{aligned}
&\Big(\omega^2 - k^2 - \tfrac{16}{3}\,\overline{R}_{1212}\big|_{\xi_0} + 6\,\overline{R}_{1212,\rho}\big|_{\xi_0}(\xi^\rho - \xi_0^\rho)\Big)G_\times E^\times \\
&\qquad + 2i(\xi^\rho - \xi_0^\rho)\big(\omega\,\overline{R}_{120\rho}\big|_{\xi_0} + k\,\overline{R}_{123\rho}\big|_{\xi_0}\big)G_+E^+ \\
&\qquad + \kappa\sqrt{\mu_\parallel}\big(kB_T + i\partial_1 B_L\big)A_\parallel E^\parallel + i\kappa\sqrt{\mu_\perp}\partial_2 B_L A_\perp E^\perp \\
&\qquad - 2\kappa(\partial_1\partial_2\overline{\phi})\,aE^\phi = \tfrac{1}{2}\big(\overline{J}_{12}^{(h)} + \overline{J}_{21}^{(h)}\big)
\end{aligned} \tag{5.70}$$

$$\Big(\mu_\parallel\epsilon_\parallel\omega^2 - k^2 + \tfrac{1}{2}\mu_\parallel\,\overline{R}_{1212}\big|_{\xi_0}\Big)A_\parallel E^\parallel + i\sqrt{\mu_\parallel\mu_\perp}(\xi^\rho-\xi_0^\rho)\big(\omega\,\overline{R}_{021\rho}\big|_{\xi_0} + k\,\overline{R}_{321\rho}\big|_{\xi_0}\big)A_\perp E^\perp + i\kappa\sqrt{\mu_\parallel}\partial_2 B_L G_+ E^+ + \kappa\sqrt{\mu_\parallel}\big(kB_T - i\partial_1 B_L\big)G_\times E^\times - i\tilde\lambda\sqrt{\mu_\parallel\mu_\perp}\big(\omega\partial_3\overline{\phi} + k\partial_0\overline{\phi}\big)A_\perp E^\perp + \tilde\lambda\sqrt{\mu_\parallel}\omega B_T a E^\phi = -i\sqrt{\mu_\parallel}\,\overline{J}^{(A)1} \tag{5.71}$$

$$\Big(\mu_\perp\epsilon_\perp\omega^2 - k^2 + \tfrac{1}{2}\mu_\perp\,\overline{R}_{1212}\big|_{\xi_0}\Big)A_\perp E^\perp + i\sqrt{\mu_\parallel\mu_\perp}(\xi^\rho-\xi_0^\rho)\big(\omega\,\overline{R}_{012\rho}\big|_{\xi_0} + k\,\overline{R}_{312\rho}\big|_{\xi_0}\big)A_\parallel E^\parallel - i\kappa\sqrt{\mu_\perp}\partial_2 B_L G_\times E^\times + \kappa\sqrt{\mu_\perp}\big(kB_T - i\partial_1 B_L\big)G_+ E^+ + i\tilde\lambda\sqrt{\mu_\parallel|\mu_\perp|}\,\big(\omega\partial_3\overline{\phi} + k\partial_0\overline{\phi}\big)\,A_\parallel E^\parallel = i\sqrt{\mu_\perp}\,\overline{J}^{(A)2} \tag{5.72}$$

$$\big(\omega^2 - k^2 - m^2\big)aE^\phi + \tilde\lambda\omega B_T A_\parallel E^\parallel - \kappa(\partial_1\partial_1\overline{\phi} - \partial_2\partial_2\overline{\phi})G_+E^+ - 2\kappa\partial_1\partial_2\overline{\phi}\,G_\times E^\times = \overline{J}^{(\phi)}, \tag{5.73}$$

where

$$\epsilon_\parallel = 1 - \overline{M}_1^{00} = 1 - \frac{4}{45m_e^4}\left(\frac{e^2}{4\pi}\right)^2\big(2B_L^2 - 5B_T^2\big) \tag{5.74}$$

$$\epsilon_\perp = 1 - \overline{M}_2^{00} = 1 - \frac{4}{45m_e^4}\left(\frac{e^2}{4\pi}\right)^2\big(2B_L^2 + 2B_T^2\big)\,. \tag{5.75}$$

Note that, at our order of approximation, $\sqrt{\mu_\perp}$ and $\sqrt{\mu_\parallel}$ may be treated as 1 when multiplied by $\xi^\rho - \xi_0^\rho$, κ, and $\tilde\lambda$. Note also that

$$\frac{E^n}{E^m} = e^{(K^n_{AB}-K^m_{AB})(\xi^A-\xi_0^A)(\xi^B-\xi_0^B)} = 1 + O\left((\xi-\xi_0)^2\right). \tag{5.76}$$

Therefore, our equation of motion can be written in matrix form, eq. 5.78, as presented on the next page, where $n_\perp = \sqrt{\epsilon_\perp\mu_\perp^{-1}}$ and $n_\parallel = \sqrt{\epsilon_\parallel\mu_\parallel^{-1}}$ are the indices of refraction,

and

$$\vec{W} = \begin{bmatrix} \frac{1}{2E^+}\left(\overline{J}^{(h)}_{11} - \overline{J}^{(h)}_{22}\right) \\ \frac{i\sqrt{\mu_\perp}}{E^\perp}\overline{J}^{(A)^2} \\ \frac{1}{2E^\times}\left(\overline{J}^{(h)}_{12} + \overline{J}^{(h)}_{21}\right) \\ \frac{-i\sqrt{\mu_\parallel}}{E^\parallel}\overline{J}^{(A)^1} \\ \frac{1}{E^\phi}\overline{J}^{(\phi)} \end{bmatrix} \tag{5.77}$$

represents the purely low-frequency source terms. In the limit where the Riemann tensor, the background axion field, and the derivative of the magnetic field are set to zero, eq. 5.78 recovers the results of [36], as we would expect.

One important note should be made about eq. 5.78: the mixing matrix is not Hermitian, specifically because of the $A_\parallel A_\perp$ off-diagonal components. As we will see momentarily, it is physically necessary for the mixing matrix to be Hermitian, and so this surely represents a calculational mistake. The fact that this mistake is only found in the $A_\parallel A_\perp$ component suggests that this mistake relates to our ansatz for electromagnetic waves, but the author has been unable to specifically locate and correct this error. We proceed ignoring this error, assuming for our purposes that the mixing matrix is indeed Hermitian.

5.4.3. Transition Probabilities

We are interested in the homogeneous solutions to eq. 5.78, so we may set $\vec{W} = 0$. We now linearize according to the prescription of [36]: k and ω are related by $k = n\omega$, and, since $|n-1| \ll 1$, we approximate $\omega + k \approx 2\omega$. Therefore, we approximate

$$\omega^2 - k^2 = (\omega + k)(\omega - k) \approx 2\omega(\omega + i\partial_z), \tag{5.79}$$

$$
\left(\omega^2 - k^2 + \begin{bmatrix}
-\frac{16}{3}\,\bar{R}_{1212}|_{\xi_0} + 6\,\bar{R}_{1212,\rho}|_{\xi_0}\,(\xi^\rho - \xi_0^\rho) & \kappa\,(kB_T + i\partial_1 B_L) & -2i\,(\xi^\rho - \xi_0^\rho)\left(\omega\,\bar{R}_{120\rho}|_{\xi_0} + k\,\bar{R}_{123\rho}|_{\xi_0}\right) & -ik\kappa\partial_2 B_L \\
\kappa\,(kB_T - i\partial_1 B_L) & 2\omega^2\,(n_\perp - 1) + \frac{1}{2}\mu_\perp\,\bar{R}_{1212}|_{\xi_0} & -ik\kappa\partial_2 B_L & i\,(\xi^\rho - \xi_0^\rho)\left(\omega\,\bar{R}_{012\rho}|_{\xi_0} + k\,\bar{R}_{312\rho}|_{\xi_0}\right) + i\bar{\lambda}\left(\omega\bar{\partial}_3\bar{\phi} + k\bar{\partial}_0\bar{\phi}\right) \\
2i\,(\xi^\rho - \xi_0^\rho)\left(\omega\,\bar{R}_{120\rho}|_{\xi_0} + k\,\bar{R}_{123\rho}|_{\xi_0}\right) & ik\kappa\partial_2 B_L & -\frac{16}{3}\,\bar{R}_{1212}|_{\xi_0} + 6\,\bar{R}_{1212,\rho}|_{\xi_0}\,(\xi^\rho - \xi_0^\rho) & \kappa\,(kB_T + i\partial_1 B_L) \\
ik\kappa\partial_2 B_L & i\,(\xi^\rho - \xi_0^\rho)\left(\omega\,\bar{R}_{021\rho}|_{\xi_0} + k\,\bar{R}_{321\rho}|_{\xi_0}\right) - i\bar{\lambda}\left(\omega\bar{\partial}_3\bar{\phi} + k\bar{\partial}_0\bar{\phi}\right) & \kappa\,(kB_T - i\partial_1 B_L) & 2\omega^2\,(n_\parallel - 1) + \frac{1}{2}\mu_\parallel\,\bar{R}_{1212}|_{\xi_0} \\
-\kappa\left(\partial_1\partial_1\bar{\phi} - \partial_2\partial_2\bar{\phi}\right) & 0 & -2k\kappa\partial_1\partial_2\bar{\phi} & \bar{\lambda}\omega B_T
\end{bmatrix}\right)
\begin{bmatrix} G_+ \\ A_\perp \\ G_\times \\ A_\parallel \end{bmatrix}
\begin{bmatrix} \\ \\ \\ \\ \end{bmatrix}
\begin{bmatrix}
0 \\
-2k\partial_1\partial_2\bar{\phi} \\
\bar{\lambda}\omega B_T \\
-m^2
\end{bmatrix}
= \vec{W}
$$

Mixing equation in curved spacetime (5.78)

and the mixing equation assumes a Schrödinger-like form:

$$(\omega + i\partial_3 + H) \begin{bmatrix} G_+ \\ A_\perp \\ G_\times \\ A_\parallel \\ a \end{bmatrix} = 0, \tag{5.80}$$

where

$$H = H_0 + (\xi^\rho - \xi_0^\rho)\, V_{1,\rho} + \kappa V_2 + \tilde{\lambda} V_3 \tag{5.81}$$

and

$$H_0 = \begin{bmatrix} -\frac{8}{3\omega}\, \overline{R}_{1212}\Big|_{s=0} & 0 & 0 & 0 & 0 \\ 0 & \omega(n_\perp - 1) + \frac{\mu_\perp}{4\omega}\, \overline{R}_{1212}\Big|_{s=0} & 0 & 0 & 0 \\ 0 & 0 & -\frac{8}{3\omega}\, \overline{R}_{1212}\Big|_{s=0} & 0 & 0 \\ 0 & 0 & 0 & \omega(n_\parallel - 1) + \frac{\mu_\parallel}{4\omega}\, \overline{R}_{1212}\Big|_{s=0} & 0 \\ 0 & 0 & 0 & 0 & \frac{-m^2}{2\omega} \end{bmatrix} \tag{5.82}$$

$$V_{1,\rho} = \begin{bmatrix} \frac{3}{\omega}\, \overline{R}_{1212,\rho}\Big|_{s=0} & 0 & -i\left(\overline{R}_{120\rho}\Big|_{s=0} + \overline{R}_{123\rho}\right) & 0 & 0 \\ 0 & 0 & 0 & \frac{i}{2}\left(\overline{R}_{012\rho}\Big|_{s=0} + \overline{R}_{312\rho}\Big|_{s=0}\right) & 0 \\ i\left(\overline{R}_{120\rho}\Big|_{s=0} + \overline{R}_{123\rho}\right) & 0 & \frac{3}{\omega}\, \overline{R}_{1212,\rho}\Big|_{s=0} & 0 & 0 \\ 0 & \frac{i}{2}\left(\overline{R}_{021\rho}\Big|_{s=0} + \overline{R}_{321\rho}\Big|_{s=0}\right) & 0 & 0 & 0 \\ 0 & 0 & 0 & 0 & 0 \end{bmatrix} \tag{5.83}$$

$$V_2 = \begin{bmatrix} 0 & \frac{1}{2}B_T + \frac{i}{2\omega}\partial_1 B_L & 0 & \frac{-i}{2\omega}\partial_2 B_L & \frac{-1}{2\omega}\left(\partial_1\partial_1\overline{\phi} - \partial_2\partial_2\overline{\phi}\right) \\ \frac{1}{2}B_T - \frac{i}{2\omega}\partial_1 B_L & 0 & \frac{-i}{2\omega}\partial_2 B_L & 0 & 0 \\ 0 & \frac{i}{2\omega}\partial_2 B_L & 0 & \frac{1}{2}B_T + \frac{i}{2\omega}\partial_1 B_L & \frac{-1}{\omega}\partial_1\partial_2\overline{\phi} \\ \frac{i}{2\omega}\partial_2 B_L & 0 & \frac{1}{2}B_T - \frac{i}{2\omega}\partial_1 B_L & 0 & 0 \\ \frac{-1}{2\omega}\left(\partial_1\partial_1\overline{\phi} - \partial_2\partial_2\overline{\phi}\right) & 0 & \frac{-1}{\omega}\partial_1\partial_2\overline{\phi} & 0 & 0 \end{bmatrix} \tag{5.84}$$

$$V_3 = \begin{bmatrix} 0 & 0 & 0 & 0 & 0 \\ 0 & 0 & 0 & \frac{i}{2}\left(\partial_3\overline{\phi} + \partial_0\overline{\phi}\right) & 0 \\ 0 & 0 & 0 & 0 & 0 \\ 0 & \frac{-i}{2}\left(\partial_3\overline{\phi} + \partial_0\overline{\phi}\right) & 0 & 0 & \frac{1}{2}B_T \\ 0 & 0 & 0 & \frac{1}{2}B_T & 0 \end{bmatrix}. \tag{5.85}$$

Here, H_0 is related to the masses of the polarization modes in the absence of mixing. We note that all polarization modes, except for axion, acquire an effective mass as a result of being in curved spacetime. As we will see momentarily, and similar to what we saw in section 5.2, these effective masses will alter both the amplitude and

frequency of all transition probabilities. $V_{1,\rho}$ represents mixing that arises due to curvature corrections; we see that, at our order of approximation, curvature corrections are responsible for mixing the two photon modes together and for mixing the two graviton modes together. However, curvature corrections do not result in photons mixing with non-photons or with gravitons mixing with non- gravitons. V_2 represents mixing caused by gravity (not to be confused with mixing caused by curvature corrections; the mixing in V_2 occurs regardless of the curvature of the background metric). We can see that, by accounting for the derivative of the background magnetic field and the background axion field, we can predict mixing between + gravitons and $\parallel$ photons, between $\times$ gravitons and $\perp$ photons, and between both graviton modes and axions, none of which was predicted by previous research. Lastly, V_3 represents mixing caused by photon-axion coupling; it is responsible not only for photon-axion mixing, as was already known, but also for mixing between $\parallel$ and $\perp$ photons. Thus, we can see that going to curved spacetime both introduces new mixing modes and changes the rate at which all other mixing occurs.

To calculate the evolution of the polarization modes, as with other forms of mixing, we proceed by transforming into the mass eigenstate basis. Provided that H is Hermitian, there exists a unitary matrix U that diagonalizes it,

$$U^{-1}HU = \mathcal{H} \equiv \begin{bmatrix} e_+ & 0 & 0 & 0 & 0 \\ 0 & e_\perp & 0 & 0 & 0 \\ 0 & 0 & e_\times & 0 & 0 \\ 0 & 0 & 0 & e_\parallel & 0 \\ 0 & 0 & 0 & 0 & e_a \end{bmatrix}, \tag{5.86}$$

where e_i are the (real) eigenvalues. The amplitudes of the polarization modes are

given by

$$\begin{bmatrix} \mathcal{G}_+ \\ \mathcal{A}_\perp \\ \mathcal{G}_\times \\ \mathcal{A}_\parallel \\ \Phi \end{bmatrix} = U^{-1} \begin{bmatrix} G_+ \\ A_\perp \\ G_\times \\ A_\parallel \\ a \end{bmatrix}, \tag{5.87}$$

and thus eq. 5.80 becomes, in the mass eigenstate basis,

$$(\omega + i\partial_3 + \mathcal{H}) \begin{bmatrix} \mathcal{G}_+ \\ \mathcal{A}_\perp \\ \mathcal{G}_\times \\ \mathcal{A}_\parallel \\ \Phi \end{bmatrix} = 0. \tag{5.88}$$

This has as its solution

$$\begin{bmatrix} \mathcal{G}_+(z) \\ \mathcal{A}_\perp(z) \\ \mathcal{G}_\times(z) \\ \mathcal{A}_\parallel(z) \\ \Phi(z) \end{bmatrix} = \begin{bmatrix} e^{i(\omega+e_+)z} & 0 & 0 & 0 & 0 \\ 0 & e^{i(\omega+e_\perp)z} & 0 & 0 & 0 \\ 0 & 0 & e^{i(\omega+e_\times)z} & 0 & 0 \\ 0 & 0 & 0 & e^{i(\omega+e_\parallel)z} & 0 \\ 0 & 0 & 0 & 0 & e^{i(\omega+e_a)z} \end{bmatrix} \begin{bmatrix} \mathcal{G}_+(0) \\ \mathcal{A}_\perp(0) \\ \mathcal{G}_\times(0) \\ \mathcal{A}_\parallel(0) \\ \Phi(0) \end{bmatrix}, \tag{5.89}$$

where $z = \xi^3 - \xi_0^3$, and therefore the evolution of the polarization modes is given by

$$\begin{aligned} \begin{bmatrix} G_+(z) \\ A_\perp(z) \\ G_\times(z) \\ A_\parallel(z) \\ a(z) \end{bmatrix} &= U \begin{bmatrix} e^{i(\omega+e_+)z} & 0 & 0 & 0 & 0 \\ 0 & e^{i(\omega+e_\perp)z} & 0 & 0 & 0 \\ 0 & 0 & e^{i(\omega+e_\times)z} & 0 & 0 \\ 0 & 0 & 0 & e^{i(\omega+e_\parallel)z} & 0 \\ 0 & 0 & 0 & 0 & e^{i(\omega+e_a)z} \end{bmatrix} U^{-1} \begin{bmatrix} G_+(0) \\ A_\perp(0) \\ G_\times(0) \\ A_\parallel(0) \\ a(0) \end{bmatrix} \\ &\equiv \mathcal{M}(z) \begin{bmatrix} G_+(0) \\ A_\perp(0) \\ G_\times(0) \\ A_\parallel(0) \\ a(0) \end{bmatrix}. \end{aligned} \tag{5.90}$$

The transition probability is defined as $P(i \to j) = |\mathcal{M}_{ij}|^2$, and this represents the probability that a particle of polarization mode i will have transitioned into a particle of polarization mode j after traveling distance z. For example, $P_{+\to\perp}$ represents the probability of a + graviton transitioning into a $\perp$ photon. A few properties of the

transition probability should be noted. First, it is clear that $P(i \to j) \in \mathbb{R}$, by construction. Second, by writing $P(i \to j)$ in terms of U,

$$P(i \to j) = \sum_{k\ell} e^{i(e_k - e_\ell)} U_{ik} U^*_{jk} U^*_{i\ell} U_{j\ell}, \tag{5.91}$$

we may easily see that $P(i \to j) = P(j \to i)^*$, and therefore $P(i \to j) = P(j \to i)$; in other words, each transition is as likely to happen in one direction as it is to happen in the other directoin. To make this symmetry clear, we will henceforth write $P(i \leftrightarrow j)$. The final property is that

$$\begin{aligned} \sum_j P(i \leftrightarrow j) &= \sum_{ik\ell} e^{i(e_k - e_\ell)} U_{ik} U^*_{jk} U^*_{i\ell} U_{j\ell} = \sum_{k\ell} e^{i(e_k - e_\ell)} \delta_{k\ell} U^*_{jk} U_{j\ell} \\ &= \sum_k U^*_{jk} U_{jk} = \delta_{jj} = 1. \end{aligned} \tag{5.92}$$

This is an important sanity check: a particle i must transition into something (including the possibility of remaining in its original polarization mode, represented by $P(i \leftrightarrow i)$), and thus the sum of probabilities of all states i could transition to should be unity. Importantly, these properties have been proven using the unitarity of U and the realness of the eigenvalues; thus we see that, if the mixing matrix H is not Hermitian, then unphysical behavior will occur.

The above provides us with a scheme for finding the transition probabilities, but it depends on finding an expression for U. To do this, we treat $\xi^\rho - \xi^\rho_0$, κ, and $\tilde{\lambda}$ as small, so that we may calculate U using perturbation theory. To first order, it is given by

$$U_{ij} = \delta_{ij} - (\xi^\rho - \xi^\rho_0) \frac{V_{1,\rho,ij}}{H_{0,ii} - H_{0,jj}} - \kappa \frac{V_{2,ij}}{H_{0,ii} - H_{0,jj}} - \tilde{\lambda} \frac{V_{3,ij}}{H_{0,ii} - H_{0,jj}}. \tag{5.93}$$

We will combine all perturbative components of U into a single variable $U^{(1)}$:

$$U = 1 + U^{(1)}, \tag{5.94}$$

and we may perform a similar perturbative decomposition on the mass eigenvalues and $\mathcal{M}(z)$:

$$e_i = H_{0,ii} + e_i^{(1)} \tag{5.95}$$

$$\mathcal{M}(z) = \begin{bmatrix} e^{i(\omega+H_{0,++})z} & 0 & 0 & 0 & 0 \\ 0 & e^{i(\omega+H_{0,\perp\perp})z} & 0 & 0 & 0 \\ 0 & 0 & e^{i(\omega+H_{0,\times\times})z} & 0 & 0 \\ 0 & 0 & 0 & e^{i(\omega+H_{0,\parallel\parallel})z} & 0 \\ 0 & 0 & 0 & 0 & e^{i(\omega+H_{0,aa})z} \end{bmatrix} + \mathcal{M}^{(1)}(z). \tag{5.96}$$

There are higher-order terms as well, and, in calculating the transition probabilities, there is insight to be gained by considering up to second order:

$$\begin{aligned} P(i \leftrightarrow j) = &\left|\mathcal{M}_{ij}^{(0)}\right|^2 + 2\mathrm{Re}\left(\mathcal{M}_{ij}^{(0)}\mathcal{M}_{ij}^{(1)*}\right) \\ &+ \left|\mathcal{M}_{ij}^{(1)}\right|^2 + 2\mathrm{Re}\left(\mathcal{M}_{ij}^{(0)}\mathcal{M}_{ij}^{(2)*}\right) + O(3), \end{aligned} \tag{5.97}$$

where $O(3)$ indicates terms whose combined order in $\xi^\rho - \xi_0^\rho$, κ, and $\tilde{\lambda}$ is at least 3. For $i \neq j$, $\mathcal{M}_{ij}^{(0)} = 0$, and therefore the off-diagonal transition probabilities become

$$P(i \leftrightarrow j) = \left|\mathcal{M}_{ij}^{(0)}\right|^2 + \left|\mathcal{M}_{ij}^{(1)}\right|^2 + O(3). \tag{5.98}$$

In other words, we may calculate the off-diagonal transition probabilities to second order while calculating $\mathcal{M}(z)$ to only first order. We may then calculate the on-diagonal transition probabilities via

$$P(i \leftrightarrow i) = 1 - \sum_{j \neq i} P(i \leftrightarrow j). \tag{5.99}$$

The probability transitions, found via this prescription, are given in Appendix C.

Section 5.5

Conclusion

Primakoff mixing is an important phenomenon to understand, both in the search for scalar boson dark matter and in the study of gravitational waves. There has been substantial interest in detecting dark matter by looking for mixing in the vicinity of a compact object (black holes, neutron stars, and white dwarfs) [44–57]. In any such experiment efforts, it will be crucial to incorporate the effects of curved spacetime into calculations of the rate of mixing.

Mixing behaves significantly differently in curved spacetime than it does in flat spacetime; going to curved spacetime introduces new mixing modes, and it alters the amplitude and frequency of all transition probabilities. One important quality of Primakoff mixing is that it is generic to all scalar boson dark matter models, i.e. not necessarily the axion. While V_3, which results from the axion-photon coupling, is obviously specific to an axion model, $V_{1,\rho}$ and V_2 remains unchanged regardless of the type of scalar boson dark matter under consideration. (Essentially, the non-axion case is found by setting $\tilde{\lambda} = 0$.) In other words, the majority of our results are model-independent for scalar dark matter. However, it must be stressed that the results presented here are incomplete, as they do not include nonlocal corrections, and as a consequence the curvature corrections that we find are highly suppressed. A complete version of these calculations are performed in [83].

Chapter 6

Conclusion

The topic of particle interactions in curved spacetime is relevant, at least to some extent, to every subject of astrophysics. In this thesis, we have examined two specific situations in which these interactions are acutely relevant, namely superradiant axion lasers and Primakoff-type bosonic mixing, and we have discussed a general treatment of particle interactions that incorporates nonlocal corrections. To conclude, we offer some brief comments on future research directions in which these three areas might progress.

Superradiant axion lasers are a relatively new research subject. While the idea of an axion laser dates back to 1995 [58], the idea that an axion cloud of the necessary density could be formed by superradiance was not considered in the literature until 2018 [61, 62]. As such, there is much work that remains in this field. Research up to this point has primarily focused on the affects of plasmas on the laser [62, 63, 65], as black holes are expected to be surrounded by plasmas drawn in via accretion. The work of chapter 2 fits well within this context, showing that a certain amount of the plasma around a superradiant axion laser will come from the laser itself, via the Schwinger effect. [65] simulated in significant detail the interaction between plasmas and an axion laser; the inclusion of the Schwinger effect into simulations of this kind

would be an interesting direction for future research.

While chapter 2, as well as the work that inspired it [61], approach the topic of axion lasers from a particle perspective, the field has since then tended to take a classical field theoretic approach [62–65]. One advantage to this approach is that the equation of motion for a classical field in curved spacetime may be solved (numerically or in some cases analytically) *without* working within a locally flat patch of spacetime. Thus there is no need to introduce nonlocal corrections, per chapter 4. However, this has not been done in all research [62, 65], and the results of chapter 4 suggests that ignoring the effects of curved spacetime may result in missing important effects.

Much of the research that remains to be done on axion lasers lies in identifying phenomena that may be relevant, and then incorporating them into an analysis of axion lasers. Proverbially, we must find all of the pieces of the puzzle before we can put them together. Chapter 2 represents an example of this, as we have identified the Schwinger effect as relevant and shown how it may be incorporated into research on axion lasers. Another phenomenon that may be relevant is the self-interaction of axions, which, at certain densities, triggers the axion cloud to collapse in what has been dubbed a bosenova [94, 191, 192]. Given that plasmas (both Schwinger plasmas and accreted plasmas) can allow for unbounded axion growth, it is easy to see how a bosenova collapse could be an important consideration. To date, however, this specific question has not yet been researched.

Aside from the intricacies of axion lasers, there are also ways in which this research may be extended to similar situations. One example would be to examine the question of lasing in a multi-axion model. A recent paper [193] examined the question of laser-like parametric resonance in one particular multi-axion model, but not in the specific context superradiance. Another extension of this research would be to consider not the laser-like production of photons from axion decay, but the laser-like photons of

gravitational waves from axion decay, via a Chern-Simons coupling (see [194] for a review). The Chern-Simons coupling constant is at present highly unconstrained, with the best current constraints coming from frame-dragging effects around the earth [195], and the laser-like production of gravitational waves may offer a more sensitive means of constraining this parameter. Additionally, plasma effects are likely to be much less significant to the laser-like production of gravitational waves, as plasmas will only be relevant insofar as their energy will curve spacetime, i.e. they do not kinematically prevent axion-graviton decay in the same way that they do with axion-photon decay.

In contrast to superradiant axion lasers, Primakoff mixing is a much more well-established field, having been researched continuously since its proposal in the 1980s [35, 36], with its astrophysical application having been immediately recognized. As such, while there is certainly more research to be done, the open questions are less fundamental and less obvious than in superradiant axion lasers. As such, it suffices for the purpose of this thesis to say that, in most if not all astrophysical contexts, the curvature of spacetime appears highly relevant to the behavior of Primakoff mixing. This topic is explored in greater detail in [83], and it is advisable that any proposal to observe Primakoff mixing occurring around a compact object should incorporate these considerations.

Lastly there is the topic of nonlocal corrections, established in chapter 4 and discussed in greater detail in [85]. This is an entirely novel effective field theory tool, and so there is much work to be done here. The most obvious statement here is that all research in which one makes use of a locally flat approximation to curved spacetime would benefit from incorporating nonlocal corrections. Additionally, as noted in chapter 4, these nonlocal corrections can cause Planck-suppressed operators to be enhanced, potentially enabling them to be observable. This would be a valuable

way of probing otherwise inaccessible physics, which ought to be explored.

Another observation is that the determination of nonlocal corrections is, at present, highly computationally expensive. The development of faster ways to compute, or at least estimate, these corrections would be highly valuable in expediting additional research.

Appendix A

Calculation of the Rate of Pair Production

In this appendix we perform the integral in eq. 2.24 in order to attain an expression for $\Gamma_{\rm Schw}$. We begin by rewriting our integral in terms only of $E_\parallel$, $B_\parallel$, and θ:

$$\Gamma_{\rm Schw} = \frac{e^2 V}{4\pi^3 \sigma_{\rm EM}^6} \int_0^\pi \int_0^\infty \int_0^\infty \mathrm{d}\theta \mathrm{d}E_\parallel \mathrm{d}B_\parallel E_\parallel^3 B_\parallel^3 \left(E_\parallel^2 + B_\parallel^2\right) \frac{\sin\theta |\sec^3\theta| e^{-\frac{\sqrt{\left(E_\parallel^2 - B_\parallel^2\right)^2 + 4E_\parallel^2 B_\parallel^2 \sec^2\theta}}{2\sigma_{\rm EM}^2}}}{\sqrt{\left(E_\parallel^2 - B_\parallel^2\right)^2 + 4E_\parallel^2 B_\parallel^2 \sec^2\theta}} \sum_{n=1}^\infty \frac{1}{n} \coth\frac{n\pi B_\parallel}{E_\parallel} e^{-n\pi\frac{E_c}{E_\parallel}}. \quad \text{(A.1)}$$

The integral over θ may be performed through the substitution $u = \sqrt{\left(E_\parallel^2 - B_\parallel^2\right)^2 + 4E_\parallel^2 B_\parallel^2 \sec^2\theta}$, yielding

$$\Gamma_{\rm Schw} = \frac{e^2 V}{4\pi^3 \sigma_{\rm EM}^4} \int_0^\infty \int_0^\infty \mathrm{d}E_\parallel \mathrm{d}B_\parallel E_\parallel B_\parallel \left(E_\parallel^2 + B_\parallel^2\right) e^{-\frac{E_\parallel^2 + B_\parallel^2}{2\sigma_{\rm EM}^2}} \sum_{n=1}^\infty \frac{1}{n} \coth\frac{n\pi B_\parallel}{E_\parallel} e^{-n\pi\frac{E_c}{E_\parallel}}. \quad \text{(A.2)}$$

We may expand coth as a series of exponentials, allowing us to rewrite this as

$$\Gamma_{\text{Schw}} = \frac{e^2 V}{4\pi^3 \sigma_{\text{EM}}^4} \sum_{n=1}^{\infty} \frac{1}{n} \int_0^{\infty} \mathrm{d}E_{\parallel} E_{\parallel} e^{-\frac{E_{\parallel}^2}{2\sigma_{\text{EM}}^2}} e^{-n\pi \frac{E_c}{E_{\parallel}}} \sum_{k=0}^{\infty} (2-\delta_{k0}) \int_0^{\infty} \mathrm{d}B_{\parallel} B_{\parallel} \left(E_{\parallel}^2 + B_{\parallel}^2\right) e^{-\frac{B_{\parallel}^2}{2\sigma_{\text{EM}}^2}} e^{-2nk\pi \frac{B_{\parallel}}{E_{\parallel}}}. \quad \text{(A.3)}$$

To perform the inner integral, we may rewrite the $B_{\parallel}^2$ exponential as a Meijer G-function, $\exp\left(-\frac{B_{\parallel}^2}{2\sigma_{\text{EM}}^2}\right) = G_{0,1}^{1,0}\left(\frac{B_{\parallel}^2}{2\sigma_{\text{EM}}^2} \middle| \begin{matrix} - \\ 0 \end{matrix}\right)$, and then make use of the identity [196]

$$\int_0^{\infty} \mathrm{d}x x^{\alpha-1} e^{-\sigma x} G_{pq}^{mn}\left(\omega x^{\ell} \middle| \begin{matrix} (a_p) \\ (b_q) \end{matrix}\right) = \frac{\ell^{\alpha-\frac{1}{2}} \sigma^{-\alpha}}{(2\pi)^{\frac{1}{2}(\ell-1)}} G_{p+\ell,q}^{m,n+\ell}\left(\frac{\omega}{(\sigma/\ell)^{\ell}} \middle| \begin{matrix} \frac{1-\alpha}{\ell}, \frac{2-\alpha}{\ell}, \ldots, \frac{\ell-\alpha}{\ell}, (a_p) \\ (b_q) \end{matrix}\right). \quad \text{(A.4)}$$

This identity requires a number of conditions for its validity, but the only ones relevant to this discussion are that σ and ω must both be nonzero; consequently, we must separate the $k = 0$ term from the $k \neq 0$ terms, applying the above identity only to the latter. This yields

$$\Gamma_{\text{Schw}} = \frac{e^2 V}{4\pi^3 \sigma_{\text{EM}}^4} \sum_{n=1}^{\infty} \frac{1}{n} \int_0^{\infty} \mathrm{d}E_{\parallel} E_{\parallel} e^{-\frac{E_{\parallel}^2}{2\sigma_{\text{EM}}^2}} e^{-n\pi \frac{E_c}{E_{\parallel}}} \left(2\sigma_{\text{EM}}^4 + \sigma_{\text{EM}}^2 E_{\parallel}^2 + \sum_{k=1}^{\infty} \frac{E_{\parallel}^4}{n^4 k^4 \pi^{4.5}} \left(n^2 k^2 \pi^2 G_{2,1}^{1,2}\left(\frac{E_{\parallel}^2}{2n^2 k^2 \pi^2 \sigma_{\text{EM}}^2} \middle| \begin{matrix} 0, -\frac{1}{2} \\ 0 \end{matrix}\right) + G_{2,1}^{1,2}\left(\frac{E_{\parallel}^2}{2n^2 k^2 \pi^2 \sigma_{\text{EM}}^2} \middle| \begin{matrix} -1, -\frac{3}{2} \\ 0 \end{matrix}\right)\right)\right). \quad \text{(A.5)}$$

Defining $v = E_\parallel^2$:

$$\Gamma_{\text{Schw}} = \frac{e^2 V}{8\pi^{3.5}\sigma_{\text{EM}}^4}\sum_{n=1}^{\infty}\frac{1}{n}\int_0^\infty \mathrm{d}v e^{-\frac{v}{2\sigma_{\text{EM}}^2}} G_{2,0}^{0,2}\left(\frac{4v}{n^2\pi^2 E_c^2}\,\middle|\, \begin{matrix} 1, \frac{1}{2} \\ - \end{matrix}\right)\left(2\sigma_{\text{EM}}^4 + \sigma_{\text{EM}}^2 v \right.$$
$$+\sum_{k=1}^{\infty}\frac{v^2}{n^4 k^4 \pi^{4.5}}\left(n^2k^2\pi^2 G_{2,1}^{1,2}\left(\frac{v}{2n^2k^2\pi^2\sigma_{\text{EM}}^2}\,\middle|\, \begin{matrix} 0, -\frac{1}{2} \\ 0 \end{matrix}\right)\right.$$
$$\left.\left.+G_{2,1}^{1,2}\left(\frac{v}{2n^2k^2\pi^2\sigma_{\text{EM}}^2}\,\middle|\, \begin{matrix} -1, -\frac{3}{2} \\ 0 \end{matrix}\right)\right)\right). \quad \text{(A.6)}$$

The first two terms may be integrated using eq. A.4. Integrating the higher-order terms requires the use of the bivariate Meijer G-function [197–199], defined as

$$G_{p_1, q_1 : p_2, q_2 ; p_3, q_3}^{m_1, n_1 : m_2, n_2 ; m_3, n_3}\left(x, y \,\middle|\, \begin{matrix} \left(\alpha_{p_1}^{(1)}\right) & : & \left(\alpha_{p_2}^{(2)}\right) & ; & \left(\alpha_{p_3}^{(3)}\right) \\ \left(\beta_{q_1}^{(1)}\right) & : & \left(\beta_{q_2}^{(2)}\right) & ; & \left(\beta_{q_3}^{(3)}\right) \end{matrix}\right)$$
$$= \frac{-1}{4\pi^2}\int_{L_1}\int_{L_2}\Psi_1(s+t)\Psi_2(s)\Psi_3(t)x^s y^t \mathrm{d}s\mathrm{d}t, \quad \text{(A.7)}$$

where L_1 and L_2 are suitable contours and

$$\Psi_i(u) = \frac{\prod_{j=1}^{m_i}\Gamma\left(\beta_j^{(i)} - u\right)\prod_{j=1}^{n_i}\Gamma\left(1 - \alpha_j^{(i)} + u\right)}{\prod_{j=m_i+1}^{q_i}\Gamma\left(1 - \beta_j^{(i)} + u\right)\prod_{j=n_i+1}^{p_i}\Gamma\left(\alpha_j^{(i)} - u\right)}. \quad \text{(A.8)}$$

When $p_1 = q_1 = 0$, the bivariate Meijer G-function becomes a product of two univariate Meijer G-functions. The integral may then be performed using the identity

[200]

$$\int_0^\infty \mathrm{d}x x^{\lambda-1} e^{-\mu x} G^{m_1,n_1:m_2,n_2;m_3,n_3}_{p_1,q_1:p_2,q_2;p_3,q_3}\left(\rho x, \sigma x \left| \begin{matrix} \left(\alpha^{(1)}_{p_1}\right) & : & \left(\alpha^{(2)}_{p_2}\right) & ; & \left(\alpha^{(3)}_{p_3}\right) \\ \left(\beta^{(1)}_{q_1}\right) & : & \left(\beta^{(2)}_{q_2}\right) & ; & \left(\beta^{(3)}_{q_3}\right) \end{matrix} \right.\right)$$
$$= \mu^{-\lambda} G^{m_1,n_1+1:m_2,n_2;m_3,n_3}_{p_1,\ q_1\ :p_2,q_2;p_3,q_3}\left(\frac{\rho}{\mu}, \frac{\sigma}{\mu} \left| \begin{matrix} 1-\lambda, \left(\alpha^{(1)}_{p_1}\right) & : & \left(\alpha^{(2)}_{p_2}\right) & ; & \left(\alpha^{(3)}_{p_3}\right) \\ \left(\beta^{(1)}_{q_1}\right) & : & \left(\beta^{(2)}_{q_2}\right) & ; & \left(\beta^{(3)}_{q_3}\right) \end{matrix} \right.\right), \tag{A.9}$$

yielding

$$\begin{aligned}\Gamma_{\mathrm{Schw}} = &\sum_{n=1}^{\infty} \frac{e^2 V \sigma_{\mathrm{EM}}^2}{2\pi^{3.5} n}\left(G^{0,3}_{3,0}\left(\frac{8\sigma^2_{\mathrm{EM}}}{n^2\pi^2 E_c^2}\left| \begin{matrix} 1, \frac{1}{2}, 0 \\ - \end{matrix}\right.\right) + G^{0,3}_{3,0}\left(\frac{8\sigma^2_{\mathrm{EM}}}{n^2\pi^2 E_c^2}\left| \begin{matrix} 1, \frac{1}{2}, -1 \\ - \end{matrix}\right.\right)\right) \\ &+ \sum_{n=1}^{\infty}\sum_{k=1}^{\infty} \frac{e^2 V \sigma_{\mathrm{EM}}^2}{n^5 k^4 \pi^8}\left(n^2k^2\pi^2 G^{0,1:0,2;1,2}_{1,0:2,0;2,1}\left(\frac{8\sigma^2_{\mathrm{EM}}}{n^2\pi^2E_c^2}, \frac{1}{n^2k^2\pi^2}\left| \begin{matrix} -2 & : & 1, \frac{1}{2} & ; & 0, -\frac{1}{2} \\ - & : & - & ; & 0 \end{matrix}\right.\right)\right. \\ &\left. + G^{0,1:0,2;1,2}_{1,0:2,0;2,1}\left(\frac{8\sigma^2_{\mathrm{EM}}}{n^2\pi^2E_c^2}, \frac{1}{n^2k^2\pi^2}\left| \begin{matrix} -2 & : & 1, \frac{1}{2} & ; & -1, -\frac{3}{2} \\ - & : & - & ; & 0 \end{matrix}\right.\right)\right).\end{aligned} \tag{A.10}$$

With some manipulation, we may rewrite this as

$$\begin{aligned}\Gamma_{\mathrm{Schw}} = &\frac{e^2 V \sigma_{\mathrm{EM}}^2}{2\pi^{3.5}} \sum_{n=1}^{\infty} \frac{1}{n}\left(G^{0,4}_{4,1}\left(\frac{8\sigma^2_{\mathrm{EM}}}{n^2\pi^2E_c^2}\left| \begin{matrix} 1, \frac{1}{2}, 0, -2 \\ -1 \end{matrix}\right.\right)\right. \\ &\left. + \frac{2}{\sqrt{\pi}} \sum_{k=1}^{\infty} G^{0,1:0,3;1,2}_{1,0:3,1;2,1}\left(\frac{8\sigma^2_{\mathrm{EM}}}{n^2\pi^2E_c^2}, \frac{1}{n^2k^2\pi^2}\left| \begin{matrix} 0 & : & 1, \frac{1}{2}, -2 & ; & 1, \frac{1}{2} \\ - & : & -1 & ; & 1 \end{matrix}\right.\right)\right).\end{aligned} \tag{A.11}$$

We now wish to evaluate this in the limit $\sigma_{\mathrm{EM}} \ll E_c$. To do this, we first rewrite

the bivariate Meijer G-function as

$$G^{0,1:0,3;1,2}_{1,0:3,1;2,1}\left(\frac{8\sigma_{\mathrm{EM}}^2}{n^2\pi^2E_c^2},\frac{1}{n^2k^2\pi^2}\,\middle|\,\begin{array}{ccccccc}0 & : & 1,\frac{1}{2},-2 & ; & 1,\frac{1}{2}\\ - & : & -1 & ; & 1\end{array}\right)$$
$$=\frac{1}{2\pi i}\int_L\Gamma(t)\Gamma\left(\frac{1}{2}+t\right)\Gamma(1-t)G^{0,4}_{4,1}\left(\frac{8\sigma_{\mathrm{EM}}^2}{n^2\pi^2E_c^2}\,\middle|\,\begin{array}{c}1,\frac{1}{2},-2,-t\\ -1\end{array}\right)\left(\frac{1}{n^2k^2\pi^2}\right)^t\mathrm{d}t. \tag{A.12}$$

In the aforementioned limit,

$$G^{0,4}_{4,1}\left(\frac{8\sigma_{\mathrm{EM}}^2}{n^2\pi^2E_c^2}\,\middle|\,\begin{array}{c}1,\frac{1}{2},-2,-t\\ -1\end{array}\right)\approx\frac{2\pi}{\sqrt{3}}e^{-3\left(\frac{8\sigma_{\mathrm{EM}}^2}{n^2\pi^2E_c^2}\right)^{\frac{-1}{3}}}\left(\frac{8\sigma_{\mathrm{EM}}^2}{n^2\pi^2E_c^2}\right)^{-\frac{1}{2}-\frac{t}{3}}, \tag{A.13}$$

and thus we get

$$G^{0,1:0,3;1,2}_{1,0:3,1;2,1}\left(\frac{8\sigma_{\mathrm{EM}}^2}{n^2\pi^2E_c^2},\frac{1}{n^2k^2\pi^2}\,\middle|\,\begin{array}{ccccccc}0 & : & 1,\frac{1}{2},-2 & ; & 1,\frac{1}{2}\\ - & : & -1 & ; & 1\end{array}\right)$$
$$\approx\frac{n\pi^2E_c}{\sqrt{6}\sigma_{\mathrm{EM}}}e^{-3\left(\frac{8\sigma_{\mathrm{EM}}^2}{n^2\pi^2E_c^2}\right)^{\frac{-1}{3}}}\frac{1}{2\pi i}\int_L\Gamma(t)\Gamma\left(\frac{1}{2}+t\right)\Gamma(1-t)\left(\frac{1}{k^2}\left(\frac{E_c^2}{8n^4\pi^4\sigma_{\mathrm{EM}}^2}\right)^{\frac{1}{3}}\right)^t\mathrm{d}t. \tag{A.14}$$

The sum over k becomes a Riemann zeta function:

$$\sum_{k=1}^{\infty}G^{0,1:0,3;1,2}_{1,0:3,1;2,1}\left(\frac{8\sigma_{\mathrm{EM}}^2}{n^2\pi^2E_c^2},\frac{1}{n^2k^2\pi^2}\,\middle|\,\begin{array}{ccccccc}0 & : & 1,\frac{1}{2},-2 & ; & 1,\frac{1}{2}\\ - & : & -1 & ; & 1\end{array}\right)$$
$$=\frac{n\pi^2E_c}{\sqrt{6}\sigma_{\mathrm{EM}}}e^{-3\left(\frac{8\sigma_{\mathrm{EM}}^2}{n^2\pi^2E_c^2}\right)^{\frac{-1}{3}}}\frac{1}{2\pi i}\int_L\Gamma(t)\Gamma\left(\frac{1}{2}+t\right)\Gamma(1-t)\left(\left(\frac{E_c^2}{8n^4\pi^4\sigma_{\mathrm{EM}}^2}\right)^{\frac{1}{3}}\right)^t\zeta(2t)\mathrm{d}t$$
$$=\frac{n\pi^2E_c}{\sqrt{6}\sigma_{\mathrm{EM}}}e^{-3\left(\frac{8\sigma_{\mathrm{EM}}^2}{n^2\pi^2E_c^2}\right)^{\frac{-1}{3}}}\frac{1}{2\pi i}\int_0^\infty\frac{x^{-1}\mathrm{d}x}{e^x-1}$$
$$\int_L\frac{\Gamma(t)\Gamma\left(\frac{1}{2}+t\right)}{\Gamma(2t)}\Gamma(1-t)\left(x^2\left(\frac{E_c^2}{8n^4\pi^4\sigma_{\mathrm{EM}}^2}\right)^{\frac{1}{3}}\right)^t\mathrm{d}t, \tag{A.15}$$

where we have used the zeta function's integral representation,

$$\zeta(t) = \sum_{k=1}^{\infty} \frac{1}{k^t} = \frac{1}{\Gamma(t)} \int_0^{\infty} \frac{x^{t-1}}{e^x - 1} \mathrm{d}x. \tag{A.16}$$

With some manipulation, the inner integral may be rewritten as a Meijer G-function with a known form, yielding

$$\begin{aligned} &\sum_{k=1}^{\infty} G^{0,1:0,3;1,2}_{1,0:3,1;2,1}\left(\frac{8\sigma_{\mathrm{EM}}^2}{n^2\pi^2 E_c^2}, \frac{1}{n^2k^2\pi^2} \,\middle|\, \begin{array}{ccccc} 0 & : & 1, \frac{1}{2}, -2 & ; & 1, \frac{1}{2} \\ - & : & -1 & ; & 1 \end{array}\right) \\ &\qquad = \frac{n\pi^2 E_c}{\sqrt{6}\sigma_{\mathrm{EM}}} e^{-3\left(\frac{8\sigma_{\mathrm{EM}}^2}{n^2\pi^2E_c^2}\right)^{\frac{-1}{3}}} \left(\frac{E_c^2}{8n^4\pi^4\sigma_{\mathrm{EM}}^2}\right)^{\frac{1}{3}} \frac{\sqrt{\pi}}{2} \int_0^{\infty} \frac{x\mathrm{d}x}{e^x - 1} e^{-\frac{x^2}{4}\left(\frac{E_c^2}{8n^4\pi^4\sigma_{\mathrm{EM}}^2}\right)^{\frac{1}{3}}}. \end{aligned} \tag{A.17}$$

Our expression for the total rate of pair production then becomes

$$\begin{aligned} \Gamma_{\mathrm{Schw}} = \frac{e^2 E_c V \sigma_{\mathrm{EM}}}{2\sqrt{6}\pi^{1.5}} \sum_{n=1}^{\infty} &e^{-3\left(\frac{8\sigma_{\mathrm{EM}}^2}{n^2\pi^2E_c^2}\right)^{\frac{-1}{3}}} \\ &\left(1 + \left(\frac{E_c^2}{8n^4\pi^4\sigma_{\mathrm{EM}}^2}\right)^{\frac{1}{3}} \int_0^{\infty} \frac{x\mathrm{d}x}{e^x - 1} e^{-\frac{x^2}{4}\left(\frac{E_c^2}{8n^4\pi^4\sigma_{\mathrm{EM}}^2}\right)^{\frac{1}{3}}}\right). \end{aligned} \tag{A.18}$$

Terms in this summation vanish as n increases, so that we may assume n is small, and therefore $\frac{E_c^2}{8n^4\pi^4\sigma_{\mathrm{EM}}^2} \gg 1$. In this limit,

$$\left(\frac{E_c^2}{8n^4\pi^4\sigma_{\mathrm{EM}}^2}\right)^{\frac{1}{3}} \int_0^{\infty} \frac{x\mathrm{d}x}{e^x - 1} e^{-\frac{x^2}{4}\left(\frac{E_c^2}{8n^4\pi^4\sigma_{\mathrm{EM}}^2}\right)^{\frac{1}{3}}} \approx \sqrt{\pi}\left(\frac{E_c^2}{8n^4\pi^4\sigma_{\mathrm{EM}}^2}\right)^{\frac{1}{6}} - 1, \tag{A.19}$$

and so we get

$$\Gamma_{\mathrm{Schw}} \approx \frac{e^2 E_c^2 V}{8\sqrt{3}\pi} \sum_{n=1}^{\infty} e^{-3\left(\frac{8\sigma_{\mathrm{EM}}^2}{n^2\pi^2E_c^2}\right)^{\frac{-1}{3}}} \left(\frac{8\sigma_{\mathrm{EM}}^2}{n^2\pi^2E_c^2}\right)^{\frac{1}{3}}. \tag{A.20}$$

Substituting the expression for $\sigma_{\rm EM}$ found from eq. 2.27, and using the definition for $N_\gamma^{\rm Schw}$, yields eq. 2.28. Numerical calculations show that eq. 2.28 approximates eq. A.2 well for $N_\gamma \lesssim .1 N_\gamma^{\rm Schw}$, and continues to be accurate to within an order of magnitude for all $N_\gamma < N_\gamma^{\rm Schw}$.

Appendix B

Behavior of Functions of χ

The dimensionless parameter χ represents the rate at which electrons and positrons are accelerated to relativistic velocities by radiation pressure. A number of quantities may be expressed solely as a function of χ, and in this appendix we establish the mathematical tools to analyze these functions.

It is helpful to rescale quantities of length by a factor of $\frac{\chi}{\Delta r}$; we label quantities that have been rescaled in this way with a hat, e.g. $\hat{\rho}_0 = \chi\frac{\rho_0}{\Delta r}$. With this notation, the relation between the location of an electron or positron's creation and the time it takes for that electron or positron to exit the $2p$-cloud may be written as

$$\chi - \hat{\rho}_0 = \sqrt{\hat{T}_{e^\pm}\left(2+\hat{T}_{e^\pm}\right)} + \frac{\pi}{3} - 2\tan^{-1}\frac{\sqrt{3}\left(1+\hat{T}_{e^\pm}\right) + 2\sqrt{\hat{T}_{e^\pm}\left(2+\hat{T}_{e^\pm}\right)}}{3+\hat{T}_{e^\pm}}, \quad \text{(B.1)}$$

and the escape rate is

$$\Gamma_{e^\pm} = \frac{\chi^3}{6\int_0^\chi \hat{T}_{e^\pm}\hat{\rho}_0 \mathrm{d}\hat{\rho}_0}\Gamma_\gamma. \quad \text{(B.2)}$$

This makes it clear that $\frac{\Gamma_{e^\pm}}{\Gamma_\gamma}$ is a function only of χ. Its asymptotic behavior may be derived by noting that, in the limit $\chi \to \infty$, the arctangent term in eq. B.1 becomes insignificant, and therefore

$$\Gamma_{e^\pm} \xrightarrow[\chi\to\infty]{} \frac{\chi^3}{6\int_0^\chi \left(\sqrt{(\chi-\hat{\rho}_0)^2+1}-1\right)\hat{\rho}_0 \mathrm{d}\hat{\rho}_0}\Gamma_\gamma. \tag{B.3}$$

This may be evaluated to find that

$$\lim_{\chi\to\infty}\Gamma_{e^\pm} = \Gamma_\gamma, \tag{B.4}$$

which is what one would expect physically.

An integral which appears in pair annihilation, when written using hat notation, is

$$\Gamma_{\mathrm{ann}}V = \frac{8}{\chi^2}\int_0^\chi \mathrm{d}\hat{\rho}\int_0^{\hat{\rho}}\mathrm{d}\hat{\rho}_{0e^+}\int_0^{\hat{\rho}}\mathrm{d}\hat{\rho}_{0e^-}\frac{\hat{\rho}_{0e^+}\hat{\rho}_{0e^-}}{\hat{\rho}^3}|v_{e^+}-v_{e^-}|\sigma(v_{\mathrm{com}}), \tag{B.5}$$

where

$$\hat{\rho}-\hat{\rho}_{0e^\pm} = \frac{v_{e^\pm}}{\sqrt{1-v_{e^\pm}^2}} - \tan^{-1}\frac{v_{e^\pm}}{\sqrt{1-v_{e^\pm}^2}}. \tag{B.6}$$

The asymptotic behavior of $\Gamma_{\mathrm{ann}}V$ may be examined in a similar manner to $\Gamma_{e^\pm}$, although in this case it is convenient to examine $\frac{\mathrm{d}\left(\chi^2\Gamma_{\mathrm{ann}}V\right)}{\mathrm{d}\chi}$:

$$\begin{aligned}\frac{\mathrm{d}\left(\chi^2\Gamma_{\mathrm{ann}}V\right)}{\mathrm{d}\chi} \xrightarrow[\chi\to\infty]{} \frac{8}{\chi^3}\int_0^{\frac{\chi}{\sqrt{\chi^2+1}}}\int_0^{\frac{\chi}{\sqrt{\chi^2+1}}}\mathrm{d}v_{e^+}\mathrm{d}v_{e^-}\gamma_{e^+}^3\gamma_{e^-}^3 \\ \times\left(\chi-\frac{v_{e^+}}{\sqrt{1-v_{e^+}^2}}\right)\left(\chi-\frac{v_{e^-}}{\sqrt{1-v_{e^-}^2}}\right)|v_{e^+}-v_{e^-}|\sigma(v_{\mathrm{com}}).\end{aligned} \tag{B.7}$$

We may convert the double integral into a single integral by differentiating three

times:

$$\frac{\mathrm{d}^3}{\mathrm{d}\chi^3}\chi^3\frac{\mathrm{d}\left(\chi^2\Gamma_{\mathrm{ann}}V\right)}{\mathrm{d}\chi} \xrightarrow[\chi\to\infty]{} 16\int_0^{\frac{\chi}{\sqrt{\chi^2+1}}}\mathrm{d}v_{e^-}\gamma_{e^-}^3\left(3+\left(\chi-\frac{v_{e^-}}{\sqrt{1-v_{e^-}^2}}\right)\frac{\mathrm{d}}{\mathrm{d}\chi}\right) \left(|v_{e^+}-v_{e^-}|\sigma(v_{\mathrm{com}})\Big|_{v_{e^+}=\frac{\chi}{\sqrt{\chi^2+1}}}\right) \tag{B.8}$$

In the limit $\chi\to\infty$, the integrand becomes

$$\gamma_{e^-}^3\left(3+\left(\chi-\frac{v_{e^-}}{\sqrt{1-v_{e^-}^2}}\right)\frac{\mathrm{d}}{\mathrm{d}\chi}\right)\left(|v_{e^+}-v_{e^-}|\sigma(v_{\mathrm{com}})\Big|_{v_{e^+}=\frac{\chi}{\sqrt{\chi^2+1}}}\right) \xrightarrow[\chi\to\infty]{} \frac{3(1+v_{e^-})\ln\left(2\chi\sqrt{\frac{1-v_{e^-}}{1+v_{e^-}}}\right)}{8\chi^2\left(1-v_{e^-}^2\right)^{\frac{3}{2}}}\sigma_T. \tag{B.9}$$

When this is integrated, we arrive at our asymptotic form for $\Gamma_{\mathrm{ann}}V$:

$$\Gamma_{\mathrm{ann}}V \xrightarrow[\chi\to\infty]{} \frac{3(\ln\chi)^2}{2\chi^2}\sigma_T. \tag{B.10}$$

eq. 2.59 follows straightforwardly.

Appendix C

Transition Probabilities in Curved Spacetime

The following are the transition probabilities $P(i \leftrightarrow j) = |\mathcal{M}_{ij}(z)|^2$, calculated per section 5.4.3.

$$P(+ \leftrightarrow \perp) = \kappa^2 \frac{B_T^2 + \left(\frac{\partial_1 B_L}{\omega}\right)^2}{\left(\omega(n_\perp - 1) + \frac{32+3\mu_\perp}{12\omega}\,\overline{R}_{1212}\big|_{s=0}\right)^2} \times \sin^2\Big(\big(\tfrac{\omega}{2}(n_\perp - 1) + \tfrac{32+3\mu_\perp}{24\omega}\,\overline{R}_{1212}\big|_{s=0}\big) z\Big), \tag{C.1}$$

$$P(+ \leftrightarrow \parallel) = \kappa^2 \frac{(\partial_2 B_L)^2}{\left(\omega^2(n_\parallel - 1) + \frac{32+3\mu_\parallel}{12}\,\overline{R}_{1212}\big|_{s=0}\right)^2} \times \sin^2\Big(\big(\tfrac{\omega}{2}(n_\parallel - 1) + \tfrac{32+3\mu_\parallel}{24\omega}\,\overline{R}_{1212}\big|_{s=0}\big) z\Big), \tag{C.2}$$

$$P(+ \leftrightarrow \phi) = \kappa^2 \frac{4\big(\partial_2\partial_2\overline{\phi} - \partial_1\partial_1\overline{\phi}\big)^2}{\left(m^2 - \frac{20}{3}\,\overline{R}_{1212}\big|_{s=0}\right)^2} \times \sin^2\Big(\big(\tfrac{m^2}{4\omega} - \tfrac{5}{3\omega}\,\overline{R}_{1212}\big|_{s=0}\big) z\Big), \tag{C.3}$$

$$P(+ \leftrightarrow \times) = \Big((\xi^\rho - \xi_0^\rho)(\overline{R}_{120\rho}\big|_{s=0} + \overline{R}_{123\rho}\big|_{s=0})\, z\Big)^2, \tag{C.4}$$

$$P(\times \leftrightarrow \perp) = \kappa^2 \frac{(\partial_2 B_L)^2}{\left(\omega^2(n_\perp - 1) + \frac{32+3\mu_\perp}{12}\overline{R}_{1212}\big|_{s=0}\right)^2} \times \sin^2\Big(\big(\tfrac{\omega}{2}(n_\perp - 1) + \tfrac{32+3\mu_\perp}{24\omega}\overline{R}_{1212}\big|_{s=0}\big)z\Big), \tag{C.5}$$

$$P(\times \leftrightarrow \parallel) = \kappa^2 \frac{B_T^2 + (\partial_1 B_L/\omega)^2}{\left(\omega(n_\parallel - 1) + \frac{32+3\mu_\parallel}{12\omega}\overline{R}_{1212}\big|_{s=0}\right)^2} \times \sin^2\Big(\big(\tfrac{\omega}{2}(n_\parallel - 1) + \tfrac{32+3\mu_\parallel}{24\omega}\overline{R}_{1212}\big|_{s=0}\big)z\Big), \tag{C.6}$$

$$P(\times \leftrightarrow \phi) = \kappa^2 \frac{16(\partial_1\partial_2\overline{\phi})^2}{\left(m^2 - \frac{20}{3}\overline{R}_{1212}\big|_{s=0}\right)^2} \times \sin^2\Big(\big(\tfrac{m^2}{4\omega} - \tfrac{5}{3\omega}\overline{R}_{1212}\big|_{s=0}\big)z\Big), \tag{C.7}$$

$$P(\parallel \leftrightarrow \perp) = \frac{\left(\tilde{\lambda}(\partial_3\overline{\phi} + \partial_0\overline{\phi}) + (\xi^\rho - \xi_0^\rho)(\overline{R}_{021\rho}\big|_{s=0} + \overline{R}_{321\rho}\big|_{s=0})\right)^2}{\left(\omega(n_\parallel - n_\perp) + \frac{\mu_\parallel - \mu_\perp}{4\omega}\overline{R}_{1212}\big|_{s=0}\right)^2} \times \sin^2\Big(\big(\tfrac{\omega}{2}(n_\parallel - n_\perp) + \tfrac{\mu_\parallel - \mu_\perp}{8\omega}\overline{R}_{1212}\big|_{s=0}\big)z\Big), \tag{C.8}$$

$$P(\parallel \leftrightarrow \phi) = \tilde{\lambda}^2 \frac{B_T^2\omega^2}{\left(\frac{m^2}{2} + \omega^2(n_\parallel - 1) + \frac{\mu_\parallel}{4}\overline{R}_{1212}\big|_{s=0}\right)^2} \times \sin^2\Big(\tfrac{m^2 + 2(n_\parallel - 1)\omega^2}{4\omega}z\Big), \tag{C.9}$$

$$P(\perp \leftrightarrow \phi) = 0. \tag{C.10}$$

The probability that a given species remains the same can be found by using the fact that total probability must sum to 1. Note that, in the limit where $\overline{R}_{\alpha\beta\gamma\delta}\Big|_{s=0}$, $\partial\overline{\phi}$, and ∂B_L go to 0, these match with the flat-spacetime probabilities [35–39]

Bibliography

[1] Paolo Gondolo and Joseph Silk. Dark matter annihilation at the galactic center. *Physical Review Letters*, 83(9):1719–1722, August 1999. ISSN 1079-7114. doi: 10.1103/physrevlett.83.1719. URL http://dx.doi.org/10.1103/PhysRevLett.83.1719.

[2] Piero Ullio, HongSheng Zhao, and Marc Kamionkowski. Dark-matter spike at the galactic center? *Physical Review D*, 64(4), July 2001. ISSN 1089-4918. doi: 10.1103/physrevd.64.043504. URL http://dx.doi.org/10.1103/PhysRevD.64.043504.

[3] David Merritt. Evolution of the dark matter distribution at the galactic center. *Physical Review Letters*, 92(20), May 2004. ISSN 1079-7114. doi: 10.1103/physrevlett.92.201304. URL http://dx.doi.org/10.1103/PhysRevLett.92.201304.

[4] Oleg Y. Gnedin and Joel R. Primack. Dark matter profile in the galactic center. *Physical Review Letters*, 93(6), August 2004. ISSN 1079-7114. doi: 10.1103/physrevlett.93.061302. URL http://dx.doi.org/10.1103/PhysRevLett.93.061302.

[5] Laleh Sadeghian, Francesc Ferrer, and Clifford M. Will. Dark-matter distributions around massive black holes: A general relativistic analysis. *Physical*

Review D, 88(6), September 2013. ISSN 1550-2368. doi: 10.1103/physrevd.88.063522. URL http://dx.doi.org/10.1103/PhysRevD.88.063522.

[6] Sourabh Nampalliwar, Saurabh Kumar, Kimet Jusufi, Qiang Wu, Mubasher Jamil, and Paolo Salucci. Modeling the sgr a* black hole immersed in a dark matter spike. *The Astrophysical Journal*, 916(2):116, August 2021. ISSN 1538-4357. doi: 10.3847/1538-4357/ac05cc. URL http://dx.doi.org/10.3847/1538-4357/ac05cc.

[7] Man Ho Chan and Chak Man Lee. Indirect evidence for dark matter density spikes around stellar-mass black holes. *The Astrophysical Journal Letters*, 943 (2):L11, January 2023. ISSN 2041-8213. doi: 10.3847/2041-8213/acaafa. URL http://dx.doi.org/10.3847/2041-8213/acaafa.

[8] Man Ho Chan and Chak Man Lee. The first robust evidence showing a dark matter density spike around the supermassive black hole in oj 287, 2024. URL https://arxiv.org/abs/2402.03751.

[9] HongSheng Zhao and Joseph Silk. Dark minihalos with intermediate mass black holes. *Physical Review Letters*, 95(1), June 2005. ISSN 1079-7114. doi: 10.1103/physrevlett.95.011301. URL http://dx.doi.org/10.1103/PhysRevLett.95.011301.

[10] Gianfranco Bertone, Andrew R. Zentner, and Joseph Silk. New signature of dark matter annihilations: Gamma rays from intermediate-mass black holes. *Physical Review D*, 72(10), November 2005. ISSN 1550-2368. doi: 10.1103/physrevd.72.103517. URL http://dx.doi.org/10.1103/PhysRevD.72.103517.

[11] Gianfranco Bertone. Prospects for detecting dark matter with neutrino telescopes in intermediate mass black hole scenarios. *Physical Review D*, 73(10),

May 2006. ISSN 1550-2368. doi: 10.1103/physrevd.73.103519. URL http://dx.doi.org/10.1103/PhysRevD.73.103519.

[12] J. Aschersleben, G. Bertone, D. Horns, E. Moulin, R.F. Peletier, and M. Vecchi. Gamma rays from dark matter spikes in eagle simulations. *Journal of Cosmology and Astroparticle Physics*, 2024(09):005, September 2024. ISSN 1475-7516. doi: 10.1088/1475-7516/2024/09/005. URL http://dx.doi.org/10.1088/1475-7516/2024/09/005.

[13] Katherine J. Mack, Jeremiah P. Ostriker, and Massimo Ricotti. Growth of structure seeded by primordial black holes. *The Astrophysical Journal*, 665 (2):1277–1287, August 2007. ISSN 1538-4357. doi: 10.1086/518998. URL http://dx.doi.org/10.1086/518998.

[14] Massimo Ricotti. Bondi accretion in the early universe. *The Astrophysical Journal*, 662(1):53–61, June 2007. ISSN 1538-4357. doi: 10.1086/516562. URL http://dx.doi.org/10.1086/516562.

[15] Massimo Ricotti and Andrew Gould. A new probe of dark matter and high-energy universe using microlensing. *The Astrophysical Journal*, 707(2):979–987, December 2009. ISSN 1538-4357. doi: 10.1088/0004-637x/707/2/979. URL http://dx.doi.org/10.1088/0004-637X/707/2/979.

[16] Yu. N. Eroshenko. Dark matter density spikes around primordial black holes. *Astronomy Letters*, 42(6):347–356, June 2016. ISSN 1562-6873. doi: 10.1134/s1063773716060013. URL http://dx.doi.org/10.1134/S1063773716060013.

[17] Mathieu Boudaud, Thomas Lacroix, Martin Stref, Julien Lavalle, and Pierre Salati. In-depth analysis of the clustering of dark matter particles around primordial black holes. part i. density profiles. *Journal of Cosmology and*

Astroparticle Physics, 2021(08):053, August 2021. ISSN 1475-7516. doi: 10.1088/1475-7516/2021/08/053. URL http://dx.doi.org/10.1088/1475-7516/2021/08/053.

[18] Gianfranco Bertone and Malcolm Fairbairn. Compact stars as dark matter probes. *Physical Review D*, 77(4), February 2008. ISSN 1550-2368. doi: 10.1103/physrevd.77.043515. URL http://dx.doi.org/10.1103/PhysRevD.77.043515.

[19] Arnaud de Lavallaz and Malcolm Fairbairn. Neutron stars as dark matter probes. *Physical Review D*, 81(12), June 2010. ISSN 1550-2368. doi: 10.1103/physrevd.81.123521. URL http://dx.doi.org/10.1103/PhysRevD.81.123521.

[20] Chris Kouvaris and Peter Tinyakov. Can neutron stars constrain dark matter? *Physical Review D*, 82(6), September 2010. ISSN 1550-2368. doi: 10.1103/physrevd.82.063531. URL http://dx.doi.org/10.1103/PhysRevD.82.063531.

[21] Paolo Ciarcelluti and Fredrik Sandin. Have neutron stars a dark matter core? *Physics Letters B*, 695(1–4):19–21, January 2011. ISSN 0370-2693. doi: 10.1016/j.physletb.2010.11.021. URL http://dx.doi.org/10.1016/j.physletb.2010.11.021.

[22] Antonino Del Popolo, Morgan Le Delliou, and Maksym Deliyergiyev. Neutron stars and dark matter. *Universe*, 6(12):222, November 2020. ISSN 2218-1997. doi: 10.3390/universe6120222. URL http://dx.doi.org/10.3390/universe6120222.

[23] Matthew McCullough and Malcolm Fairbairn. Capture of inelastic dark matter in white dwarves. *Physical Review D*, 81(8), April 2010. ISSN 1550-2368. doi:

10.1103/physrevd.81.083520. URL http://dx.doi.org/10.1103/PhysRevD.81.083520.

[24] Dan Hooper, Douglas Spolyar, Alberto Vallinotto, and Nickolay Y. Gnedin. Inelastic dark matter as an efficient fuel for compact stars. *Physical Review D*, 81(10), May 2010. ISSN 1550-2368. doi: 10.1103/physrevd.81.103531. URL http://dx.doi.org/10.1103/PhysRevD.81.103531.

[25] Basudeb Dasgupta, Aritra Gupta, and Anupam Ray. Dark matter capture in celestial objects: improved treatment of multiple scattering and updated constraints from white dwarfs. *Journal of Cosmology and Astroparticle Physics*, 2019(08):018–018, August 2019. ISSN 1475-7516. doi: 10.1088/1475-7516/2019/08/018. URL http://dx.doi.org/10.1088/1475-7516/2019/08/018.

[26] Nicole F. Bell, Giorgio Busoni, Maura E. Ramirez-Quezada, Sandra Robles, and Michael Virgato. Improved treatment of dark matter capture in white dwarfs. *Journal of Cosmology and Astroparticle Physics*, 2021(10):083, October 2021. ISSN 1475-7516. doi: 10.1088/1475-7516/2021/10/083. URL http://dx.doi.org/10.1088/1475-7516/2021/10/083.

[27] Masha Baryakhtar, Regina Caputo, Djuna Croon, Kerstin Perez, Emanuele Berti, Joseph Bramante, Malte Buschmann, Richard Brito, Thomas Y. Chen, Philippa S. Cole, Adam Coogan, William E. East, Joshua W. Foster, Marios Galanis, Maurizio Giannotti, Bradley J. Kavanagh, Ranjan Laha, Rebecca K. Leane, Benjamin V. Lehmann, Gustavo Marques-Tavares, Jamie McDonald, Ken K. Y. Ng, Nirmal Raj, Laura Sagunski, Jeremy Sakstein, B. S. Sathyaprakash, Sarah Shandera, Nils Siemonsen, Olivier Simon, Kuver Sinha, Divya Singh, Rajeev Singh, Chen Sun, Ling Sun, Volodymyr Takhistov, Yu-Dai Tsai, Edoardo Vitagliano, Salvatore Vitale, Huan Yang, and Jun

Zhang. Dark matter in extreme astrophysical environments, 2022. URL https://arxiv.org/abs/2203.07984.

[28] Enrico Cannizzaro, Andrea Caputo, Laura Sberna, and Paolo Pani. Plasma-photon interaction in curved spacetime: Formalism and quasibound states around nonspinning black holes. *Physical Review D*, 103(12), June 2021. ISSN 2470-0029. doi: 10.1103/physrevd.103.124018. URL http://dx.doi.org/10.1103/PhysRevD.103.124018.

[29] Enrico Cannizzaro, Andrea Caputo, Laura Sberna, and Paolo Pani. Plasma-photon interaction in curved spacetime. ii. collisions, thermal corrections, and superradiant instabilities. *Physical Review D*, 104(10), November 2021. ISSN 2470-0029. doi: 10.1103/physrevd.104.104048. URL http://dx.doi.org/10.1103/PhysRevD.104.104048.

[30] Leonard Parker. Quantized fields and particle creation in expanding universes. i. *Phys. Rev.*, 183:1057–1068, Jul 1969. doi: 10.1103/PhysRev.183.1057. URL https:/dx.doi.org/10.1103/PhysRev.183.1057.

[31] Leonard Parker. Quantized fields and particle creation in expanding universes. ii. *Phys. Rev. D*, 3:346–356, Jan 1971. doi: 10.1103/PhysRevD.3.346. URL https://dx.doi.org/10.1103/PhysRevD.3.346.

[32] Edward W. Kolb and Andrew J. Long. Cosmological gravitational particle production and its implications for cosmological relics, 2025. URL https://arxiv.org/abs/2312.09042.

[33] H. Primakoff. Photoproduction of neutral mesons in nuclear electric fields and the mean life of the neutral meson. *Phys. Rev.*, 81:899, 1951. doi: 10.1103/PhysRev.81.899.

[34] Duane A. Dicus, Edward W. Kolb, Vigdor L. Teplitz, and Robert V. Wagoner. Astrophysical Bounds on the Masses of Axions and Higgs Particles. *Phys. Rev. D*, 18:1829, 1978. doi: 10.1103/PhysRevD.18.1829.

[35] L. Maiani, R. Petronzio, and E. Zavattini. Effects of Nearly Massless, Spin Zero Particles on Light Propagation in a Magnetic Field. *Phys. Lett. B*, 175:359–363, 1986. doi: 10.1016/0370-2693(86)90869-5.

[36] Georg Raffelt and Leo Stodolsky. Mixing of the Photon with Low Mass Particles. *Phys. Rev. D*, 37:1237, 1988. doi: 10.1103/PhysRevD.37.1237.

[37] G. G. Raffelt. *Stars as laboratories for fundamental physics*. 1996. ISBN 9780226702728. URL `http://wwwth.mpp.mpg.de/members/raffelt/mypapers/199613.pdf`.

[38] Emi Masaki, Arata Aoki, and Jiro Soda. Photon-Axion Conversion, Magnetic Field Configuration, and Polarization of Photons. *Phys. Rev. D*, 96(4):043519, 2017. doi: 10.1103/PhysRevD.96.043519.

[39] Alexander D Dolgov and Damian Ejlli. Conversion of relic gravitational waves into photons in cosmological magnetic fields. *Journal of Cosmology and Astroparticle Physics*, 2012(12):003–003, December 2012. ISSN 1475-7516. doi: 10.1088/1475-7516/2012/12/003. URL `http://dx.doi.org/10.1088/1475-7516/2012/12/003`.

[40] K. M. Backes et al. A quantum-enhanced search for dark matter axions. *Nature*, 590(7845):238–242, 2021. doi: 10.1038/s41586-021-03226-7.

[41] T. Braine et al. Extended Search for the Invisible Axion with the Axion Dark Matter Experiment. *Phys. Rev. Lett.*, 124(10):101303, 2020. doi: 10.1103/PhysRevLett.124.101303.

[42] Jonathan L. Ouellet et al. First Results from ABRACADABRA-10 cm: A Search for Sub-μeV Axion Dark Matter. *Phys. Rev. Lett.*, 122(12):121802, 2019. doi: 10.1103/PhysRevLett.122.121802.

[43] A. Álvarez Melcón et al. First results of the CAST-RADES haloscope search for axions at 34.67 μeV. *Journal of High Energy Physics*, 2021(10):1–16, 4 2021.

[44] Malte Buschmann, Raymond T. Co, Christopher Dessert, and Benjamin R. Safdi. Axion Emission Can Explain a New Hard X-Ray Excess from Nearby Isolated Neutron Stars. *Phys. Rev. Lett.*, 126(2):021102, 2021. doi: 10.1103/PhysRevLett.126.021102.

[45] Christopher Dessert, Andrew J. Long, and Benjamin R. Safdi. X-ray Signatures of Axion Conversion in Magnetic White Dwarf Stars. *Phys. Rev. Lett.*, 123(6): 061104, 2019. doi: 10.1103/PhysRevLett.123.061104.

[46] Igor G. Irastorza and Javier Redondo. New experimental approaches in the search for axion-like particles. *Prog. Part. Nucl. Phys.*, 102:89–159, 2018. doi: 10.1016/j.ppnp.2018.05.003.

[47] Joshua W. Foster, Yonatan Kahn, Oscar Macias, Zhiquan Sun, Ralph P. Eatough, Vladislav I. Kondratiev, Wendy M. Peters, Christoph Weniger, and Benjamin R. Safdi. Green Bank and Effelsberg Radio Telescope Searches for Axion Dark Matter Conversion in Neutron Star Magnetospheres. *Phys. Rev. Lett.*, 125(17):171301, 2020. doi: 10.1103/PhysRevLett.125.171301.

[48] R. A. Battye, B. Garbrecht, J. I. Mcdonald, and S. Srinivasan. Radio Line Properties of Axion Dark Matter Conversion in Neutron Stars. *Journal of High Energy Physics*, 2021(105), 4 2021.

[49] Thomas D. P. Edwards, Bradley J. Kavanagh, Luca Visinelli, and Christoph Weniger. Transient Radio Signatures from Neutron Star Encounters with QCD Axion Miniclusters. *Physical Review Letters*, 127(13):131103, 11 2021.

[50] David B. Kaplan. Opening the Axion Window. *Nucl. Phys. B*, 260:215–226, 1985. doi: 10.1016/0550-3213(85)90319-0.

[51] MS Pshirkov and SB Popov. Conversion of dark matter axions to photons in magnetospheres of neutron stars. *Journal of Experimental and Theoretical Physics*, 108(3):384–388, 2009.

[52] Fa Peng Huang, Kenji Kadota, Toyokazu Sekiguchi, and Hiroyuki Tashiro. Radio telescope search for the resonant conversion of cold dark matter axions from the magnetized astrophysical sources. *Phys. Rev. D*, 97(12):123001, 2018. doi: 10.1103/PhysRevD.97.123001.

[53] Anson Hook, Yonatan Kahn, Benjamin R. Safdi, and Zhiquan Sun. Radio signals from axion dark matter conversion in neutron star magnetospheres. *Phys. Rev. Lett.*, 121:241102, Dec 2018. doi: 10.1103/PhysRevLett.121.241102. URL `https://link.aps.org/doi/10.1103/PhysRevLett.121.241102`.

[54] Benjamin R. Safdi, Zhiquan Sun, and Alexander Y. Chen. Detecting Axion Dark Matter with Radio Lines from Neutron Star Populations. *Phys. Rev. D*, 99(12):123021, 2019. doi: 10.1103/PhysRevD.99.123021.

[55] Richard A Battye, Bjoern Garbrecht, Jamie I McDonald, Francesco Pace, and Sankarshana Srinivasan. Dark matter axion detection in the radio/mm waveband. *Physical Review D*, 102(2):023504, 2020.

[56] Mikaël Leroy, Marco Chianese, Thomas DP Edwards, and Christoph Weniger.

Radio signal of axion-photon conversion in neutron stars: A ray tracing analysis. *Physical Review D*, 101(12):123003, 2020.

[57] Thomas D. P. Edwards, Marco Chianese, Bradley J. Kavanagh, Samaya M. Nissanke, and Christoph Weniger. Unique Multimessenger Signal of QCD Axion Dark Matter. *Phys. Rev. Lett.*, 124(16):161101, 2020. doi: 10.1103/PhysRevLett.124.161101.

[58] Thomas W. Kephart and Thomas J. Weiler. Stimulated radiation from axion cluster evolution. *Phys. Rev. D*, 52:3226–3238, 1995. doi: 10.1103/PhysRevD.52.3226.

[59] Thomas W. Kephart and Thomas J. Weiler. A model of lasing axion clusters. *Nuclear Physics B Proceedings Supplements*, 72(1-3):54–57, March 1999. doi: 10.1016/S0920-5632(98)00502-7.

[60] Liang Chen and Thomas W. Kephart. A Review of Axion Lasing in Astrophysics. *Universe*, 10(1):24, 2024. doi: 10.3390/universe10010024.

[61] João G. Rosa and Thomas W. Kephart. Stimulated axion decay in superradiant clouds around primordial black holes. *Physical Review Letters*, 120(23), June 2018. ISSN 1079-7114. doi: 10.1103/physrevlett.120.231102. URL `http://dx.doi.org/10.1103/PhysRevLett.120.231102`.

[62] Srimoyee Sen. Plasma effects on lasing of a uniform ultralight axion condensate. *Physical Review D*, 98(10), November 2018. ISSN 2470-0029. doi: 10.1103/physrevd.98.103012. URL `http://dx.doi.org/10.1103/PhysRevD.98.103012`.

[63] Mateja Bošković, Richard Brito, Vitor Cardoso, Taishi Ikeda, and Helvi Witek. Axionic instabilities and new black hole solutions. *Physical Review D*, 99(3),

February 2019. ISSN 2470-0029. doi: 10.1103/physrevd.99.035006. URL http://dx.doi.org/10.1103/PhysRevD.99.035006.

[64] Taishi Ikeda, Richard Brito, and Vitor Cardoso. Blasts of light from axions. *Physical Review Letters*, 122(8), February 2019. ISSN 1079-7114. doi: 10.1103/physrevlett.122.081101. URL http://dx.doi.org/10.1103/PhysRevLett.122.081101.

[65] Thomas F. M. Spieksma, Enrico Cannizzaro, Taishi Ikeda, Vitor Cardoso, and Yifan Chen. Superradiance: Axionic couplings and plasma effects, 2023. URL https://arxiv.org/abs/2306.16447.

[66] N. D. Birrell and P. C. W. Davies. *Quantum Fields in Curved Space*. Cambridge Monographs on Mathematical Physics. Cambridge University Press, 1982.

[67] Leonard Parker and David Toms. *Quantum Field Theory in Curved Spacetime: Quantized Fields and Gravity*. Cambridge Monographs on Mathematical Physics. Cambridge University Press, 2009.

[68] Bei-Lok B. Hu and Enric Verdaguer. *Semiclassical and Stochastic Gravity: Quantum Field Effects on Curved Spacetime*. Cambridge Monographs on Mathematical Physics. Cambridge University Press, 2020.

[69] J. B. Hartle and G. T. Horowitz. Ground State Expectation Value of the Metric in the $1/N$ or Semiclassical Approximation to Quantum Gravity. *Phys. Rev. D*, 24:257–274, 1981. doi: 10.1103/PhysRevD.24.257.

[70] John F. Donoghue. General relativity as an effective field theory: The leading quantum corrections. *Physical Review D*, 50(6):3874–3888, September 1994. ISSN 0556-2821. doi: 10.1103/physrevd.50.3874. URL http://dx.doi.org/10.1103/PhysRevD.50.3874.

[71] Cliff P. Burgess. Quantum gravity in everyday life: General relativity as an effective field theory. *Living Reviews in Relativity*, 7(1), April 2004. ISSN 1433-8351. doi: 10.12942/lrr-2004-5. URL http://dx.doi.org/10.12942/lrr-2004-5.

[72] B. L. Hu, Albert Roura, and Enric Verdaguer. Induced quantum metric fluctuations and the validity of semiclassical gravity. *Physical Review D*, 70(4), August 2004. ISSN 1550-2368. doi: 10.1103/physrevd.70.044002. URL http://dx.doi.org/10.1103/PhysRevD.70.044002.

[73] C.P. Burgess. An introduction to effective field theory. *Annual Review of Nuclear and Particle Science*, 57(1):329–362, November 2007. ISSN 1545-4134. doi: 10.1146/annurev.nucl.56.080805.140508. URL http://dx.doi.org/10.1146/annurev.nucl.56.080805.140508.

[74] Aneesh V. Manohar. Introduction to effective field theories, 2018. URL https://arxiv.org/abs/1804.05863.

[75] Boris Kayser. Neutrino mass, mixing, and oscillation. In *Theoretical Advanced Study Institute in Elementary Particle Physics (TASI 2000): Flavor Physics for the Millennium*, pages 625–650, 4 2001. doi: 10.1142/9789812811509_0017.

[76] Yuval Grossman. TASI 2002 lectures on neutrinos. In *Theoretical Advanced Study Institute in Elementary Particle Physics (TASI 2002): Particle Physics and Cosmology: The Quest for Physics Beyond the Standard Model(s)*, pages 5–48, 5 2003.

[77] Andre de Gouvea. TASI lectures on neutrino physics. In *Theoretical Advanced Study Institute in Elementary Particle Physics: Physics in D 4*, pages 197–258, 11 2004.

[78] John F. Donoghue. Quantum general relativity and effective field theory, 2023. URL https://arxiv.org/abs/2211.09902.

[79] Leo Brewin. Riemann normal coordinate expansions using cadabra. *Classical and Quantum Gravity*, 26(17):175017, August 2009. ISSN 1361-6382. doi: 10.1088/0264-9381/26/17/175017. URL http://dx.doi.org/10.1088/0264-9381/26/17/175017.

[80] Steven L. Detweiler. KLEIN-GORDON EQUATION AND ROTATING BLACK HOLES. *Phys. Rev. D*, 22:2323–2326, 1980. doi: 10.1103/PhysRevD.22.2323.

[81] Sam R. Dolan. Instability of the massive klein-gordon field on the kerr spacetime. *Physical Review D*, 76(8), October 2007. ISSN 1550-2368. doi: 10.1103/physrevd.76.084001. URL http://dx.doi.org/10.1103/PhysRevD.76.084001.

[82] Richard Brito, Vitor Cardoso, and Paolo Pani. *Superradiance: New Frontiers in Black Hole Physics*. Springer International Publishing, 2020. ISBN 9783030466220. doi: 10.1007/978-3-030-46622-0. URL http://dx.doi.org/10.1007/978-3-030-46622-0.

[83] Devin G. E. Walker, Bradley Shapiro, Paola Karapataki, Charles Wade, Nizar Ezroura, Shadi Ali Ahmad, and Morgane König. Bosonic mixing in curved spacetime. Submitted for publication but not released as preprint, .

[84] Bradley Shapiro. The role of the schwinger effect in superradiant axion lasers, 2025. URL https://arxiv.org/abs/2503.01039.

[85] Devin G. E. Walker, Bradley Shapiro, Shadi Ali Ahmad, Nizar Ezroura, Paola Karapataki, and Charles Wade. Gravitational wave effective theory with curvature corrections. Accepted for publication but not yet available, .

[86] R. D. Peccei and Helen R. Quinn. CP conservation in the presence of pseudoparticles. *Phys. Rev. Lett.*, 38:1440–1443, Jun 1977. doi: 10.1103/PhysRevLett.38.1440. URL https://link.aps.org/doi/10.1103/PhysRevLett.38.1440.

[87] Steven Weinberg. A new light boson? *Phys. Rev. Lett.*, 40:223–226, Jan 1978. doi: 10.1103/PhysRevLett.40.223. URL https://link.aps.org/doi/10.1103/PhysRevLett.40.223.

[88] F. Wilczek. Problem of strong p and t invariance in the presence of instantons. *Phys. Rev. Lett.*, 40:279–282, Jan 1978. doi: 10.1103/PhysRevLett.40.279. URL https://link.aps.org/doi/10.1103/PhysRevLett.40.279.

[89] John Preskill, Mark B. Wise, and Frank Wilczek. Cosmology of the Invisible Axion. *Phys. Lett. B*, 120:127–132, 1983. doi: 10.1016/0370-2693(83)90637-8.

[90] L. F. Abbott and P. Sikivie. A Cosmological Bound on the Invisible Axion. *Phys. Lett. B*, 120:133–136, 1983. doi: 10.1016/0370-2693(83)90638-X.

[91] Michael Dine and Willy Fischler. The Not So Harmless Axion. *Phys. Lett. B*, 120:137–141, 1983. doi: 10.1016/0370-2693(83)90639-1.

[92] C. B. Adams, N. Aggarwal, A. Agrawal, R. Balafendiev, C. Bartram, M. Baryakhtar, H. Bekker, P. Belov, K. K. Berggren, A. Berlin, C. Boutan, D. Bowring, D. Budker, A. Caldwell, P. Carenza, G. Carosi, R. Cervantes, S. S. Chakrabarty, S. Chaudhuri, T. Y. Chen, S. Cheong, A. Chou, R. T. Co, J. Conrad, D. Croon, R. T. D'Agnolo, M. Demarteau, N. DePorzio, M. Descalle, K. Desch, L. Di Luzio, A. Diaz-Morcillo, K. Dona, I. S. Drachnev, A. Droster, N. Du, K. Dunne, B. Döbrich, S. A. R. Ellis, R. Essig, J. Fan, J. W. Foster, J. T. Fry, A. Gallo Rosso, J. M. García Barceló, I. G. Irastorza, S. Gardner, A. A. Geraci, S. Ghosh, B. Giaccone, M. Giannotti, B. Gimeno, D. Grin,

H. Grote, M. Guzzetti, M. H. Awida, R. Henning, S. Hoof, G. Hoshino, V. Irsic, K. D. Irwin, H. Jackson, D. F. Jackson Kimball, J. Jaeckel, K. Jakovcic, M. J. Jewell, M. Kagan, Y. Kahn, R. Khatiwada, S. Knirck, T. Kovachy, P. Krueger, S. E. Kuenstner, N. A. Kurinsky, R. K. Leane, A. F. Leder, C. Lee, K. W. Lehnert, E. W. Lentz, S. M. Lewis, J. Liu, M. Lynn, B. Majorovits, D. J. E. Marsh, R. H. Maruyama, B. T. McAllister, A. J. Millar, D. W. Miller, J. Mitchell, S. Morampudi, G. Mueller, S. Nagaitsev, E. Nardi, O. Noroozian, C. A. J. O'Hare, N. S. Oblath, J. L. Ouellet, K. M. W. Pappas, H. V. Peiris, K. Perez, A. Phipps, M. J. Pivovaroff, P. Quílez, N. M. Rapidis, V. H. Robles, K. K. Rogers, J. Rudolph, J. Ruz, G. Rybka, M. Safdari, B. R. Safdi, M. S. Safronova, C. P. Salemi, P. Schuster, A. Schwartzman, J. Shu, M. Simanovskaia, J. Singh, S. Singh, K. Sinha, J. T. Sinnis, M. Siodlaczek, M. S. Smith, W. M. Snow, A. V. Sokolov, A. Sonnenschein, D. H. Speller, Y. V. Stadnik, C. Sun, A. O. Sushkov, T. M. P. Tait, V. Takhistov, D. B. Tanner, F. Tavecchio, D. J. Temples, J. H. Thomas, M. E. Tobar, N. Toro, Y. D. Tsai, E. C. van Assendelft, K. van Bibber, M. Vandegar, L. Visinelli, E. Vitagliano, J. K. Vogel, Z. Wang, A. Wickenbrock, L. Winslow, S. Withington, M. Wooten, J. Yang, B. A. Young, F. Yu, K. Zhou, and T. Zhou. Axion dark matter, 2023. URL `https://arxiv.org/abs/2203.14923`.

[93] Asimina Arvanitaki, Savas Dimopoulos, Sergei Dubovsky, Nemanja Kaloper, and John March-Russell. String axiverse. *Physical Review D*, 81(12), June 2010. ISSN 1550-2368. doi: 10.1103/physrevd.81.123530. URL `http://dx.doi.org/10.1103/PhysRevD.81.123530`.

[94] Asimina Arvanitaki and Sergei Dubovsky. Exploring the string axiverse with precision black hole physics. *Physical Review D*, 83(4), February 2011. ISSN

1550-2368. doi: 10.1103/physrevd.83.044026. URL http://dx.doi.org/10.1103/PhysRevD.83.044026.

[95] Richard Brito, Vitor Cardoso, and Paolo Pani. Black holes as particle detectors: evolution of superradiant instabilities. *Classical and Quantum Gravity*, 32(13): 134001, June 2015. ISSN 1361-6382. doi: 10.1088/0264-9381/32/13/134001. URL http://dx.doi.org/10.1088/0264-9381/32/13/134001.

[96] Asimina Arvanitaki, Masha Baryakhtar, Savas Dimopoulos, Sergei Dubovsky, and Robert Lasenby. Black hole mergers and the qcd axion at advanced ligo. *Physical Review D*, 95(4), February 2017. ISSN 2470-0029. doi: 10.1103/physrevd.95.043001. URL http://dx.doi.org/10.1103/PhysRevD.95.043001.

[97] Hooman Davoudiasl and Peter B. Denton. Ultralight boson dark matter and event horizon telescope observations of M87*. *Phys. Rev. Lett.*, 123:021102, Jul 2019. doi: 10.1103/PhysRevLett.123.021102. URL https://link.aps.org/doi/10.1103/PhysRevLett.123.021102.

[98] Asimina Arvanitaki, Masha Baryakhtar, and Xinlu Huang. Discovering the qcd axion with black holes and gravitational waves. *Physical Review D*, 91 (8), April 2015. ISSN 1550-2368. doi: 10.1103/physrevd.91.084011. URL http://dx.doi.org/10.1103/PhysRevD.91.084011.

[99] Daniel Baumann, Horng Sheng Chia, John Stout, and Lotte ter Haar. The spectra of gravitational atoms. *Journal of Cosmology and Astroparticle Physics*, 2019(12):006–006, December 2019. ISSN 1475-7516. doi: 10.1088/1475-7516/2019/12/006. URL http://dx.doi.org/10.1088/1475-7516/2019/12/006.

[100] J. D. Bekenstein and M. Schiffer. The many faces of superradiance. *Physical*

Review D, 58(6), August 1998. ISSN 1089-4918. doi: 10.1103/physrevd.58.064014. URL http://dx.doi.org/10.1103/PhysRevD.58.064014.

[101] R. Penrose. Gravitational collapse: The role of general relativity. *Riv. Nuovo Cim.*, 1:252–276, 1969. doi: 10.1023/A:1016578408204.

[102] R. Penrose and R. M. Floyd. Extraction of rotational energy from a black hole. *Nature*, 229:177–179, 1971. doi: 10.1038/physci229177a0.

[103] R. Alicki and A. Jenkins. Interaction of a quantum field with a rotating heat bath. *Annals of Physics*, 395:69–83, August 2018. ISSN 0003-4916. doi: 10.1016/j.aop.2018.05.001. URL http://dx.doi.org/10.1016/j.aop.2018.05.001.

[104] Visakan Balakumar, Elizabeth Winstanley, Rafael P. Bernar, and Luís C.B. Crispino. Quantum superradiance on static black hole space-times. *Physics Letters B*, 811:135904, December 2020. ISSN 0370-2693. doi: 10.1016/j.physletb.2020.135904. URL http://dx.doi.org/10.1016/j.physletb.2020.135904.

[105] Takeshi Chiba and Shuichiro Yokoyama. Spin distribution of primordial black holes. *Progress of Theoretical and Experimental Physics*, 2017(8), August 2017. ISSN 2050-3911. doi: 10.1093/ptep/ptx087. URL http://dx.doi.org/10.1093/ptep/ptx087.

[106] Tomohiro Harada, Chul-Moon Yoo, Kazunori Kohri, and Ken-Ichi Nakao. Spins of primordial black holes formed in the matter-dominated phase of the universe. *Physical Review D*, 96(8), October 2017. ISSN 2470-0029. doi: 10.1103/physrevd.96.083517. URL http://dx.doi.org/10.1103/PhysRevD.96.083517.

[107] V. De Luca, V. Desjacques, G. Franciolini, A. Malhotra, and A. Riotto. The initial spin probability distribution of primordial black holes. *Journal of Cosmology and Astroparticle Physics*, 2019(05):018–018, May 2019. ISSN 1475-7516. doi:

10.1088/1475-7516/2019/05/018. URL http://dx.doi.org/10.1088/1475-7516/2019/05/018.

[108] Minxi He and Teruaki Suyama. Formation threshold of rotating primordial black holes. *Physical Review D*, 100(6), September 2019. ISSN 2470-0029. doi: 10.1103/physrevd.100.063520. URL http://dx.doi.org/10.1103/PhysRevD.100.063520.

[109] Mehrdad Mirbabayi, Andrei Gruzinov, and Jorge Noreña. Spin of primordial black holes. *Journal of Cosmology and Astroparticle Physics*, 2020(03):017–017, March 2020. ISSN 1475-7516. doi: 10.1088/1475-7516/2020/03/017. URL http://dx.doi.org/10.1088/1475-7516/2020/03/017.

[110] Tomohiro Harada, Chul-Moon Yoo, Kazunori Kohri, Yasutaka Koga, and Takeru Monobe. Spins of primordial black holes formed in the radiation-dominated phase of the universe: First-order effect. *The Astrophysical Journal*, 908(2):140, February 2021. ISSN 1538-4357. doi: 10.3847/1538-4357/abd9b9. URL http://dx.doi.org/10.3847/1538-4357/abd9b9.

[111] Fabian Hofmann, Enrico Barausse, and Luciano Rezzolla. The final spin from binary black holes in quasi-circular orbits. *The Astrophysical Journal*, 825(2): L19, July 2016. ISSN 2041-8213. doi: 10.3847/2041-8205/825/2/l19. URL http://dx.doi.org/10.3847/2041-8205/825/2/L19.

[112] V. De Luca, G. Franciolini, P. Pani, and A. Riotto. The evolution of primordial black holes and their final observable spins. *Journal of Cosmology and Astroparticle Physics*, 2020(04):052–052, April 2020. ISSN 1475-7516. doi: 10.1088/1475-7516/2020/04/052. URL http://dx.doi.org/10.1088/1475-7516/2020/04/052.

[113] Santiago Jaraba and Juan García-Bellido. Black hole induced spins from hyperbolic encounters in dense clusters. *Physics of the Dark Universe*, 34:100882, December 2021. ISSN 2212-6864. doi: 10.1016/j.dark.2021.100882. URL http://dx.doi.org/10.1016/j.dark.2021.100882.

[114] Quinn Taylor, Glenn D. Starkman, Michael Hinczewski, Deyan P. Mihaylov, Joseph Silk, and Jose de Freitas Pacheco. Extremal Kerr Black Hole Dark Matter from Hawking Evaporation. 3 2024.

[115] Julian Schwinger. On gauge invariance and vacuum polarization. *Phys. Rev.*, 82:664–679, Jun 1951. doi: 10.1103/PhysRev.82.664. URL https://link.aps.org/doi/10.1103/PhysRev.82.664.

[116] François Gelis and Naoto Tanji. Schwinger mechanism revisited. *Progress in Particle and Nuclear Physics*, 87:1–49, March 2016. ISSN 0146-6410. doi: 10.1016/j.ppnp.2015.11.001. URL http://dx.doi.org/10.1016/j.ppnp.2015.11.001.

[117] A. Ringwald. Pair production from vacuum at the focus of an x-ray free electron laser. *Physics Letters B*, 510(1–4):107–116, June 2001. ISSN 0370-2693. doi: 10.1016/s0370-2693(01)00496-8. URL http://dx.doi.org/10.1016/S0370-2693(01)00496-8.

[118] R. Alkofer, M. B. Hecht, C. D. Roberts, S. M. Schmidt, and D. V. Vinnik. Pair creation and an x-ray free electron laser. *Physical Review Letters*, 87(19), October 2001. ISSN 1079-7114. doi: 10.1103/physrevlett.87.193902. URL http://dx.doi.org/10.1103/PhysRevLett.87.193902.

[119] Bai Song Xie, Zi Liang Li, and Suo Tang. Electron-positron pair production in ultrastrong laser fields. *Matter and Radiation at Extremes*, 2(5):225–242,

07 2017. ISSN 2468-2047. doi: 10.1016/j.mre.2017.07.002. URL https://doi.org/10.1016/j.mre.2017.07.002.

[120] Valerie Domcke, Yohei Ema, and Kyohei Mukaida. Axion assisted schwinger effect. *Journal of High Energy Physics*, 2021(5), May 2021. ISSN 1029-8479. doi: 10.1007/jhep05(2021)001. URL http://dx.doi.org/10.1007/JHEP05(2021)001.

[121] Valerie Domcke, Yohei Ema, and Kyohei Mukaida. Transient phenomena in the axion assisted schwinger effect. *Journal of High Energy Physics*, 2022(11), November 2022. ISSN 1029-8479. doi: 10.1007/jhep11(2022)033. URL http://dx.doi.org/10.1007/JHEP11(2022)033.

[122] Florian Hebenstreit. Schwinger effect in inhomogeneous electric fields, 2011. URL https://arxiv.org/abs/1106.5965.

[123] Louise C. Martin, Christian Schubert, and Victor M. Villanueva Sandoval. On the low-energy limit of the qed n-photon amplitudes. *Nuclear Physics B*, 668 (1–2):335–344, September 2003. ISSN 0550-3213. doi: 10.1016/s0550-3213(03)00578-9. URL http://dx.doi.org/10.1016/S0550-3213(03)00578-9.

[124] R. Svensson. The pair annihilation process in relativistic plasmas. *Astrophysical Journal*, 258:321–334, July 1982. doi: 10.1086/160081.

[125] P. S. Coppi and R. D. Blandford. Reaction rates and energy distributions for elementary processes in relativistic pair plasmas. *Monthly Notices of the Royal Astronomical Society*, 245(3):453–453, August 1990. doi: 10.1093/mnras/245.3.453.

[126] Paolo Pani and Abraham Loeb. Constraining primordial black-hole bombs through spectral distortions of the cosmic microwave background. *Physical*

Review D, 88(4), August 2013. ISSN 1550-2368. doi: 10.1103/physrevd.88.041301. URL http://dx.doi.org/10.1103/PhysRevD.88.041301.

[127] Joseph P. Conlon and Carlos A.R. Herdeiro. Can black hole superradiance be induced by galactic plasmas? *Physics Letters B*, 780:169–173, May 2018. ISSN 0370-2693. doi: 10.1016/j.physletb.2018.02.073. URL http://dx.doi.org/10.1016/j.physletb.2018.02.073.

[128] Enrico Cannizzaro, Fabrizio Corelli, and Paolo Pani. Nonlinear photon-plasma interaction and the black hole superradiant instability, 2023. URL https://arxiv.org/abs/2306.12490.

[129] Stefan Hollands and Robert M. Wald. Quantum fields in curved spacetime. *Physics Reports*, 574:1–35, April 2015. ISSN 0370-1573. doi: 10.1016/j.physrep.2015.02.001. URL http://dx.doi.org/10.1016/j.physrep.2015.02.001.

[130] Bernard S. Kay. *Quantum Field Theory in Curved Spacetime*, page 357–381. Elsevier, 2025. ISBN 9780323957069. doi: 10.1016/b978-0-323-95703-8.00085-9. URL http://dx.doi.org/10.1016/B978-0-323-95703-8.00085-9.

[131] B. Pontecorvo. Mesonium and Antimesonium. *Sov. Phys. JETP*, 6:429–431, 1958.

[132] Ziro Maki, Masami Nakagawa, and Shoichi Sakata. Remarks on the unified model of elementary particles. *Prog. Theor. Phys.*, 28:870–880, 1962. doi: 10.1143/PTP.28.870.

[133] B. Pontecorvo. Neutrino Experiments and the Problem of Conservation of Leptonic Charge. *Zh. Eksp. Teor. Fiz.*, 53:1717–1725, 1967.

[134] Charles W. Misner, K. S. Thorne, and J. A. Wheeler. *Gravitation*. W. H. Freeman, San Francisco, 1973. ISBN 978-0-7167-0344-0, 978-0-691-17779-3.

[135] Bruno Hoegl, Stefan Hofmann, and Maximilian Koegler. Physics in precision-dependent normal neighborhoods. *Physical Review D*, 102(8), October 2020. ISSN 2470-0029. doi: 10.1103/physrevd.102.084065. URL http://dx.doi.org/10.1103/PhysRevD.102.084065.

[136] T J Willmore. *Riemannian Geometry*. Oxford University Press, 10 1993. ISBN 9780198532538. doi: 10.1093/oso/9780198532538.001.0001. URL https://doi.org/10.1093/oso/9780198532538.001.0001.

[137] Eanna E. Flanagan and Scott A. Hughes. The Basics of gravitational wave theory. *New J. Phys.*, 7:204, 2005. doi: 10.1088/1367-2630/7/1/204.

[138] Michele Maggiore. *Gravitational Waves. Vol. 1: Theory and Experiments*. Oxford University Press, 2007. ISBN 978-0-19-171766-6, 978-0-19-852074-0. doi: 10.1093/acprof:oso/9780198570745.001.0001.

[139] Claus Lämmerzahl and Volker Perlick. Gravitational Waves. https://www.zarm.uni-bremen.de/fileadmin/user_upload/space_science/gravitational_theory/gravwave.pdf, 2014. [Online; accessed 17-May-2022].

[140] Aneesh Manohar and Howard Georgi. Chiral Quarks and the Nonrelativistic Quark Model. *Nucl. Phys. B*, 234:189–212, 1984. doi: 10.1016/0550-3213(84)90231-1.

[141] Maximilian Ruhdorfer, Javi Serra, and Andreas Weiler. Effective Field Theory of Gravity to All Orders. *JHEP*, 05:083, 2020. doi: 10.1007/JHEP05(2020)083.

[142] Malte Buschmann, Christopher Dessert, Joshua W. Foster, Andrew J. Long, and Benjamin R. Safdi. Upper limit on the qcd axion mass from isolated neutron star cooling. *Phys. Rev. Lett.*, 128:091102, Mar 2022. doi: 10.1103/PhysRevL

ett.128.091102. URL https://link.aps.org/doi/10.1103/PhysRevLett.128.091102.

[143] Smadar Naoz, Joseph Silk, and Jeremy D. Schnittman. Dark Matter Signatures of Supermassive Black Hole Binaries. *Astrophys. J. Lett.*, 885(2):L35, 2019. doi: 10.3847/2041-8213/ab4fed.

[144] Yossef Zenati, C. Albertus, M. Ángeles Pérez-García, and Joseph Silk. Neutrino signals from Neutron Star implosions to Black Holes. 4 2023.

[145] Anson Hook and Junwu Huang. Probing axions with neutron star inspirals and other stellar processes. *Journal of High Energy Physics*, 2018(6):1–22, 2018.

[146] F. Zwicky. Die Rotverschiebung von extragalaktischen Nebeln. *Helv. Phys. Acta*, 6:110–127, 1933. doi: 10.1007/s10714-008-0707-4.

[147] F. Zwicky. On the Masses of Nebulae and of Clusters of Nebulae. *Astrophys. J.*, 86:217–246, 1937. doi: 10.1086/143864.

[148] R. Narayan, R. Blandford, and R. Nityananda. Multiple imaging of quasars by galaxies and clusters. *Nature*, 310(5973):112–115, July 1984. doi: 10.1038/310112a0.

[149] Roger Lynds and Vahe Petrosian. Luminous Arcs in Clusters of Galaxies. *The Astrophysical Journal*, 336:1, January 1989. doi: 10.1086/166989.

[150] C. J. Eyles, M. P. Watt, D. Bertram, M. J. Church, T. J. Ponman, G. K. Skinner, and A. P. Willmore. The Distribution of Dark Matter in the Perseus Cluster. *The Astrophysical Journal*, 376:23, July 1991. doi: 10.1086/170251.

[151] I. Chiu et al. Baryon Content in a Sample of 91 Galaxy Clusters Selected by

the South Pole Telescope at $0.2 < z < 1.25$. *Mon. Not. Roy. Astron. Soc.*, 478 (3):3072–3099, 2018. doi: 10.1093/mnras/sty1284.

[152] Vera C. Rubin, W. Kent Ford, Jr., and Norbert Thonnard. Extended rotation curves of high-luminosity spiral galaxies. IV. Systematic dynamical properties, Sa through Sc. *Astrophys. J. Lett.*, 225:L107–L111, 1978. doi: 10.1086/182804.

[153] V. C. Rubin, W. K. Ford, Jr., and N. Thonnard. Rotational properties of 21 SC galaxies with a large range of luminosities and radii, from NGC 4605 (R=4kpc) to UGC 2885 (R=122kpc). *The Astrophysical Journal*, 238:471–487, June 1980. doi: 10.1086/158003.

[154] A. Bosma. 21-cm line studies of spiral galaxies. I. Observations of the galaxies NGC 5033, 3198, 5055, 2841, and 7331. *Astron. J.*, 86:1791–1824, December 1981. doi: 10.1086/113062.

[155] A. Bosma. 21-cm line studies of spiral galaxies. II. The distribution and kinematics of neutral hydrogen in spiral galaxies of various morphological types. *Astron. J.*, 86:1825–1846, December 1981. doi: 10.1086/113063.

[156] Yoshiaki Sofue and Vera Rubin. Rotation curves of spiral galaxies. *Annual Review of Astronomy and Astrophysics*, 39(1):137–174, September 2001. ISSN 1545-4282. doi: 10.1146/annurev.astro.39.1.137. URL `http://dx.doi.org/10.1146/annurev.astro.39.1.137`.

[157] N. Aghanim et al. Planck 2018 results. VI. Cosmological parameters. *Astron. Astrophys.*, 641:A6, 2020. doi: 10.1051/0004-6361/201833910. [Erratum: Astron.Astrophys. 652, C4 (2021)].

[158] M. Davis, G. Efstathiou, C. S. Frenk, and S. D. M. White. The evolution

of large-scale structure in a universe dominated by cold dark matter. *The Astrophysical Journal*, 292:371–394, May 1985. doi: 10.1086/163168.

[159] C.S. Frenk and S.D.M. White. Dark matter and cosmic structure. *Annalen der Physik*, 524(9–10):507–534, September 2012. ISSN 1521-3889. doi: 10.1002/andp.201200212. URL http://dx.doi.org/10.1002/andp.201200212.

[160] Douglas Clowe, Maruša Bradač, Anthony H. Gonzalez, Maxim Markevitch, Scott W. Randall, Christine Jones, and Dennis Zaritsky. A direct empirical proof of the existence of dark matter. *The Astrophysical Journal*, 648 (2):L109–L113, August 2006. ISSN 1538-4357. doi: 10.1086/508162. URL http://dx.doi.org/10.1086/508162.

[161] Andisheh Mahdavi, Henk Hoekstra, Arif Babul, David D. Balam, and Peter L. Capak. A dark core in abell 520. *The Astrophysical Journal*, 668(2):806–814, October 2007. ISSN 1538-4357. doi: 10.1086/521383. URL http://dx.doi.org/10.1086/521383.

[162] Maruša Bradač, Steven W. Allen, Tommaso Treu, Harald Ebeling, Richard Massey, R. Glenn Morris, Anja von der Linden, and Douglas Applegate. Revealing the properties of dark matter in the merging cluster macs j0025.4-1222. *The Astrophysical Journal*, 687(2):959–967, November 2008. ISSN 1538-4357. doi: 10.1086/591246. URL http://dx.doi.org/10.1086/591246.

[163] Rodrigo Stancioli, David Wittman, Kyle Finner, and Faik Bouhrik. A new dissociative galaxy cluster merger: Rm j150822.0+575515.2, 2023. URL https://arxiv.org/abs/2307.10174.

[164] David Wittman, Rodrigo Stancioli, Kyle Finner, Faik Bouhrik, Reinout van

Weeren, and Andrea Botteon. A new galaxy cluster merger capable of probing dark matter: Abell 56, 2023. URL https://arxiv.org/abs/2306.01715.

[165] Benjamin Zitzer and VERITAS Collaboration. The veritas dark matter program, 2017. URL https://arxiv.org/abs/1708.07447.

[166] K. Abe et al. Search for Cosmic-Ray Boosted Sub-GeV Dark Matter Using Recoil Protons at Super-Kamiokande. *Phys. Rev. Lett.*, 130(3):031802, 2023. doi: 10.1103/PhysRevLett.130.031802. [Erratum: Phys.Rev.Lett. 131, 159903 (2023)].

[167] V. A. Acciari et al. Combined searches for dark matter in dwarf spheroidal galaxies observed with the MAGIC telescopes, including new data from Coma Berenices and Draco. *Phys. Dark Univ.*, 35:100912, 2022. doi: 10.1016/j.dark.2021.100912.

[168] The IceCube Collaboration. Search for dark matter from the center of the earth with ten years of icecube data, 2024. URL https://arxiv.org/abs/2412.12972.

[169] H. Abdalla et al. Search for Dark Matter Annihilation Signals in the H.E.S.S. Inner Galaxy Survey. *Phys. Rev. Lett.*, 129(11):111101, 2022. doi: 10.1103/PhysRevLett.129.111101.

[170] Nathan Baltzell et al. The Heavy Photon Search Experiment. 3 2022.

[171] Alex McDaniel, Marco Ajello, Christopher M. Karwin, Mattia Di Mauro, Alex Drlica-Wagner, and Miguel A. Sanchez-Conde. Legacy analysis of dark matter annihilation from the milky way dwarf spheroidal galaxies with 14 years of fermi-lat data, 2023. URL https://arxiv.org/abs/2311.04982.

[172] A. Albert et al. Search for dark matter towards the Galactic Centre with 11 years of ANTARES data. *Phys. Lett. B*, 805:135439, 2020. doi: 10.1016/j.physletb.2020.135439.

[173] Li-Wei Wei. Towards the first axion search results of the any light particle search ii experiment. In *Proceedings of XVIII International Conference on Topics in Astroparticle and Underground Physics — PoS(TAUP2023)*, TAUP2023, page 049. Sissa Medialab, January 2024. doi: 10.22323/1.441.0049. URL `http://dx.doi.org/10.22323/1.441.0049`.

[174] Y. Chikashige, Rabindra N. Mohapatra, and R. D. Peccei. Are There Real Goldstone Bosons Associated with Broken Lepton Number? *Phys. Lett. B*, 98: 265–268, 1981. doi: 10.1016/0370-2693(81)90011-3.

[175] G. B. Gelmini and M. Roncadelli. Left-Handed Neutrino Mass Scale and Spontaneously Broken Lepton Number. *Phys. Lett. B*, 99:411–415, 1981. doi: 10.1016/0370-2693(81)90559-1.

[176] Frank Wilczek. Axions and Family Symmetry Breaking. *Phys. Rev. Lett.*, 49: 1549–1552, 1982. doi: 10.1103/PhysRevLett.49.1549.

[177] Z. G. Berezhiani and M. Yu. Khlopov. The Theory of broken gauge symmetry of families. (In Russian). *Sov. J. Nucl. Phys.*, 51:739–746, 1990.

[178] Joerg Jaeckel. A family of wispy dark matter candidates. *Physics Letters B*, 732:1–7, May 2014. ISSN 0370-2693. doi: 10.1016/j.physletb.2014.03.005. URL `http://dx.doi.org/10.1016/j.physletb.2014.03.005`.

[179] Edward Witten. Some Properties of O(32) Superstrings. *Phys. Lett. B*, 149: 351–356, 1984. doi: 10.1016/0370-2693(84)90422-2.

[180] Joseph P Conlon. The qcd axion and moduli stabilisation. *Journal of High Energy Physics*, 2006(05):078–078, June 2006. ISSN 1029-8479. doi: 10.1088/1126-6708/2006/05/078. URL http://dx.doi.org/10.1088/1126-6708/2006/05/078.

[181] Michele Cicoli, Mark D. Goodsell, and Andreas Ringwald. The type iib string axiverse and its low-energy phenomenology. *Journal of High Energy Physics*, 2012(10), October 2012. ISSN 1029-8479. doi: 10.1007/jhep10(2012)146. URL http://dx.doi.org/10.1007/JHEP10(2012)146.

[182] E. Brezin and C. Itzykson. Polarization phenomena in vacuum nonlinear electrodynamics. *Phys. Rev. D*, 3:618–621, 1971. doi: 10.1103/PhysRevD.3.618.

[183] S. L. Adler. Photon splitting and photon dispersion in a strong magnetic field. *Annals of Physics*, 67:599–647, January 1971. doi: 10.1016/0003-4916(71)90154-0.

[184] B. KAYSER. Neutrino mass, mixing, and oscillation. In *Flavor Physics for the Millennium*, page 625–650. WORLD SCIENTIFIC, September 2001. doi: 10.1142/9789812811509_0017. URL http://dx.doi.org/10.1142/9789812811509_0017.

[185] Yuval Grossman. Tasi 2002 lectures on neutrinos, 2003. URL https://arxiv.org/abs/hep-ph/0305245.

[186] Andre de Gouvea. 2004 tasi lectures on neutrino physics, 2004. URL https://arxiv.org/abs/hep-ph/0411274.

[187] Jeff A. Dror, Hitoshi Murayama, and Nicholas L. Rodd. Cosmic axion background. *Physical Review D*, 103(11), June 2021. ISSN 2470-0029. doi:

10.1103/physrevd.103.115004. URL http://dx.doi.org/10.1103/PhysRevD.103.115004.

[188] Giorgio Galanti and Marco Roncadelli. Extragalactic photon–axion-like particle oscillations up to 1000 tev. *Journal of High Energy Astrophysics*, 20:1–17, November 2018. ISSN 2214-4048. doi: 10.1016/j.jheap.2018.07.002. URL http://dx.doi.org/10.1016/j.jheap.2018.07.002.

[189] Leo Stodolsky. Matter and Light Wave Interferometry in Gravitational Fields. *Gen. Rel. Grav.*, 11:391–405, 1979. doi: 10.1007/BF00759302.

[190] P. M. Alsing, J. C. Evans, and K. K. Nandi. The phase of a quantum mechanical particle in curved spacetime. *General Relativity and Gravitation*, 33(9): 1459–1487, September 2001. ISSN 1572-9532. doi: 10.1023/a:1012284625541. URL http://dx.doi.org/10.1023/A:1012284625541.

[191] H. Yoshino and H. Kodama. Bosenova collapse of axion cloud around a rotating black hole. *Progress of Theoretical Physics*, 128(1):153–190, July 2012. ISSN 1347-4081. doi: 10.1143/ptp.128.153. URL http://dx.doi.org/10.1143/PTP.128.153.

[192] Hirotaka Yoshino and Hideo Kodama. The bosenova and axiverse. *Classical and Quantum Gravity*, 32(21):214001, October 2015. ISSN 1361-6382. doi: 10.1088/0264-9381/32/21/214001. URL http://dx.doi.org/10.1088/0264-9381/32/21/214001.

[193] Stephon Alexander, Geoff Beck, Santiago Loane, and Tucker Manton. Detecting the π-axiverse through parametric resonance, 2025. URL https://arxiv.org/abs/2508.04784.

[194] Stephon Alexander and Nicolás Yunes. Chern–simons modified general relativity. *Physics Reports*, 480(1–2):1–55, August 2009. ISSN 0370-1573. doi: 10.1016/j.physrep.2009.07.002. URL http://dx.doi.org/10.1016/j.physrep.2009.07.002.

[195] Yacine Ali-Haïmoud and Yanbei Chen. Slowly rotating stars and black holes in dynamical chern-simons gravity. *Physical Review D*, 84(12), December 2011. ISSN 1550-2368. doi: 10.1103/physrevd.84.124033. URL http://dx.doi.org/10.1103/PhysRevD.84.124033.

[196] A.P. Prudnikov, Yury Brychkov, and O.I. Marichev. *Integrals and Series. Volume 3: More Special Functions*. 10 1989.

[197] RP Agarwal. An extension of meijer's g-function. In *Proc. Nat. Inst. Sci. India, Part A*, volume 13, pages 536–546, 1965.

[198] Bhagirath Lal Sharma. On generalised function of 2 variables (1). *ANNALES DE LA SOCIETE SCIENTIFIQUE DE BRUXELLES SERIES 1-SCIENCES MATHEMATIQUES ASTRONOMIQUES ET PHYSIQUES*, 79(1):26, 1965.

[199] Nguyen Hai and Semyon Yakubovich. *The Double Mellin-Barnes Type Integrals and Their Applications to Convolution Theory*. 01 1992. ISBN 978-981-02-0690-1. doi: 10.1142/1425.

[200] Manilal Shah. On generalizations of some results and their applications. *Collectanea Mathematica*, 24(3):249–265, 1973. URL http://eudml.org/doc/43876.